11-4-2016

The Influence of Oxygen Tension and Glycolytic and Citric Acid Cycle Substrates in Acrolein-induced Cellular Injury in the Differentiated H9c2 Cardiac Cell Model

Jayme Coyle
University of South Florida, jcoyle3@health.usf.edu

The Influence of Oxygen Tension and Glycolytic and Citric Acid Cycle Substrates in Acrolein-induced Cellular Injury in the Differentiated H9c2 Cardiac Cell Model

by

Jayme P. Coyle

A dissertation submitted in partial fulfillment
of the requirements for the degree of
Doctor of Philosophy
with a concentration in Toxicology and Risk Assessment
Department of Environmental and Occupational Health
College of Public Health
University of South Florida

Major Professor: Raymond D. Harbison, Ph.D.
Giffe T. Johnson, Ph.D.
Marie M. Bourgeois, Ph.D.
Nicholas Hall, Ph.D.

Date of Approval:
November 4, 2016

Keywords: Oxygen Tension, Citric Acid Cycle, Acrolein, Differentiated H9c2 Cells

ACKNOWLEDGEMENTS

I want to thank my committee members Drs. Raymond Harbison, Giffe Johnson, Marie Bourgeois, and Nicholas Hall for their guidance and constructive criticism. Also, I want to thank Dr. Robert Henning for his input and accommodation, Angela Salem for assisting in logistical support, and S.A.K. for permission to continue work with the low-oxygen incubator until the completion of the dissertation research. I am deeply gracious for the assistance in the laboratory from Amora Mayo-Perez, Daniel Mejia, Kristina Harand, and Robert Rinaldi for their unerring dedication and determination in the pursuit of science. Finally, I want to express unending gratitude to Dr. Bernard and the numerous members of the EOH department for logistical, funding, and training support during my education at USF. Finally, I want to thank family and friends, and J. E. Krüpp, for their support during this process.

TABLE OF CONTENTS

LIST OF TABLES

LIST OF FIGURES

ABSTRACT

Most in vitro systems employ the standard cell culture maintenance conditions of 95 % air with 5 % CO2 to balance medium pH, which translates to culture oxygen tensions of approximately 20 % - above the typical ≤ 6 % found in most tissues. The current investigation, therefore, aims to characterize the effect of maintenance and toxicant exposure with a particular focus on the α,β-unsaturated aldehyde, acrolein, in the presence of physiologically relevant oxygen tension using a differentiated H9c2 cardiomyoblast subclone. H9c2 cells were maintained separately in 20.1 and 5 % oxygen, after which cells were differentiated for five days, and then exposed to acrolein in media containing varying concentrations of tricarboxylic acid and glycolytic substrates. Cells were then assessed for viability and metabolism via the MTT conversion assay. H9c2 cells were assessed for mechanistic elucidation to characterize contributors to cellular death, including mitochondrial membrane potential ($\Delta\Psi_m$) reductions (JC-1), intracellular calcium influx (Fluo-4), and PARP activation. Exposure to acrolein in differing oxygen tensions revealed that standard culture cells are particularly sensitive to acrolein, but cells cultured in 5 % oxygen, depending on the medium pyruvate concentration, can be rescued significantly. Further, reductions in $\Delta\Psi_m$ were reversed by co-exposure of 5-10 mM EGTA for both culture conditions, while intracellular calcium transients were noted only for standard cultures. The results demonstrate significant metabolic reprogramming which desensitizes differentiated H9c2 to acrolein-induced cytotoxicity. Further, PARP and extracellular calcium contribute to the fate of these cells exposed to acrolein, though clotrimazole-associated TRPM2 channels may not be significantly involved. Conclusively, significant alteration of toxicogenic

response was noted in this cell line when cultured under physiologically relevant conditions, and may have a substantial impact on the reliability and predictive power and interpretive application of *in vitro*-based toxicity models cultured under standard culture conditions, depending on the parent tissue.

CHAPTER ONE:

INTRODUCTION

1.1 Cyclophosphamide and Acrolein

Cyclophosphamide is a DNA alkylating nitrogen mustard prodrug approved for the treatment of hematopoietic neoplasms, e.g., leukemias, lymphomas, multiple myeloma as well as ovarian adenocarcinoma and breast carcinoma. As cyclophosphamide can cross the blood-brain barrier, malignancies within the central nervous system, such as retinoblastoma and neuroblastoma, have also been treated using cyclophosphamide[1]. Cyclophosphamide is also utilized as a pre-treatment immunosuppressant agent in preparation for bone marrow transplant procedures due to the drug's significant bone marrow toxicity[2]. Treatment is, however, dose-limiting, as the major associated side-effect was traditionally acrolein-induced hemorrhagic cystitis[3]; a side effect largely attenuated with co-administration of the antioxidant mesna without negating the anti-neoplastic action of cyclophosphamide[4,5]. While the dose-limiting side effect of hemorrhagic cystitis has been largely reduced, a second, potentially fatal side-effect of cyclophosphamide, drug-induced cardiomyopathy, has been shown to afflict between 5 % and 22 % patients treated[6-8]; a higher incidence of cardiomyopathy is suggested in patients with a previous treatment history with anthracycline treatment[9]. Unlike anthracycline antineoplastic agents, e.g., doxorubicin, idarubicin, etc., the risk of cyclophosphamide-induced cardiomyopathy has not been associated with cumulative dose[10] nor has this effect been characterized as latent, i.e., several months to years post treatment, but rather may manifest as early as three weeks after

initializing treatment[11-13]. Goldberg and colleagues showed a possible dose threshold of 1.55 g cyclophosphamide/m² body surface/day, above which cardiotoxicity is associated with increased incidence[6]; however, case reports in the literature have demonstrated significant toxicity in patients below this value[14], particularly those with renal co-morbidities[15].

As of yet, no standard care for attenuating cyclophosphamide-induced cardiotoxicity exists[14]. While the mechanism of cardiomyopathy remains incompletely elucidated, a toxic, unsaturated α,β-aldehyde metabolite, acrolein, is among the most probable of implicated the species. Despite acrolein's high reactivity, the biological half-life of acrolein is expected to be substantially longer than other ROS species[16], especially when adducted to glutathione or endogenous biomolecules[17] (Reviewed in-depth in Kehrer and Biswal[18]). The blood concentration of acrolein after cyclophosphamide treatment, nonetheless, is not negligible. Measured unbound peak blood acrolein in five patients after a 1-hour infusion of 60 mg/kg i.v. for three consecutive days consistently registered between 6.2 μM and 10.2 μM, with no apparent difference in unbound blood concentration over the course of therapy[19]. The extent of protein-acrolein binding remains a significant determinant of free acrolein bioavailability, and routine fluorometric measures only detect the unbound fraction. For example, the peak unbound fraction of acrolein reported above was determined by Ren and colleagues[19], but fails to measure protein-bound acrolein, as the method for acrolein detection was performed by *m*-aminophenol derivatization of acrolein to a fluorescent 7-hydroxyquinoline (Max λ Emission/ Excitation: 350 nm/515 nm) in accordance with the method described by Alarcon in 1968[20]. Without rapid cross-sections of acrolein concentration determination, the peak concentration in blood may indeed be higher.

In the presence of microsomal metabolism, such as that found in the liver, and to a smaller extent the lung, rapid acrolein is rapidly degraded[17]. For example, an investigation by Baumann and colleagues[21] characterized the time- and protein-dependency of free acrolein in liver microsomal preparations, noting inverse proportionality of unbound acrolein with respect to microsomal protein preparation concentrations ranging from 0.25 and 2 mg/mL; acrolein concentration determination was performed in mouse liver microsomal isolates after a 20 minute incubation at 37°C and a pH of 7.4 when controlling for protein by simple dilution. The unbound acrolein fraction decreased substantially at initial acrolein concentrations below 62.44 μM compared to the unbound fraction (75.3 %) of the highest initial acrolein concentration of 89.20 μM. In the presence of 2.0 mg/mL protein, the unbound fraction was starkly reduced to 17.6 % of the initial 89.20 μM acrolein group. Baumann and colleagues[21] further exacted the time-dependency of acrolein within the same microsomal isolate system over a range of 120 minutes at 37°C, pH 7.4, and in the presence of 1 mg/mL protein. At initial acrolein concentrations of 1.0 μg/mL, 2.0 μg/mL and 5.0 μg/mL, the derived half-lives were estimated to be 3 minutes, 5 minutes, and 17 minutes, respectively; the half-life estimates were directly proportional to initial acrolein addition concentration, denoting metabolic capacity saturation (Zero-order kinetics) was not reached. Aside from microsomal systems, however, the physical property of the matrix contributes to acrolein degradation. The half-life of acrolein in acidic urine (pH 5.5) is approximately 20 minutes, and was reduced three-fold (approximately 6.7 minutes) with alkalization to a pH of 7.3[16]. These results, while not apparently comparable to blood or serum half-lives, characterize the influence of pH on acrolein degradation–a parameter crucial in performing deproteinization and derivatization of acrolein-containing media in preparation for the fluorometric measure of free acrolein concentrations[20]. *In vitro*, the contribution of acrolein

scavenging by metabolically inert proteinaceous components of fetal bovine serum has been shown to reduce peak unbound acrolein concentrations up to 65 % in M199 culture medium containing 10 % v/v serum[22]. In the same investigation, a negligible proportion of acrolein was bound in serum-free culture media, denoting serum-free media as a plausible solution for controlling bioavailability in *in vitro* systems. While circulating acrolein may result in systemic exposure, especially to cardiac tissue, an endogenous source within cardiomyocytes remains plausible. Clearance of cyclophosphamide via cardiac metabolism has not been well characterized, but is expected to be minimal due to the low CYP isoform presence (Reviewed in Chaudhary, Batchu, Seubert [23]) of primary contributors, such as CYP3A isoforms; nonetheless, the cytochrome isoform 2J2 has been denoted as the main implicated cytochrome isoform responsible for cyclophosphamide metabolism in cardiac tissue[24], and may produce localized elevations in acrolein within cardiomyocytes during and after cyclophosphamide treatment.

As previously mentioned, no standard of care is proposed for cyclophosphamide-induced cardiotoxicity. The use of antioxidants and radical scavengers has been shown effective *in vitro*[25], but little evidence of pharmacological intervention exists with regards to *in vivo* models[26]. Since genetic ablation of glutathione *S*-transferase sensitizes rodents to acrolein and cyclophosphamide metabolite cardiotoxicity[27], the importance of electrophilic detoxification in reducing adverse cardiac events seems expectedly paramount, despite little evidentiary efficacy when applying antioxidant intervention. Complexation of acrolein with glutathione forms GS-propionaldehyde with the potential for further aldehyde dehydrogenase- or xanthine oxidase-induced ROS generation[28], denoting glutathione adduction does not necessarily confer complete detoxification. With respect to DNA adduction, DNA replication by inhibited by 40 % in the

murine mammary carcinoma FM3A cell line after exposure to 15 μM acrolein[29]. Replication is a parameter closely associated with another *in vitro* phenomenon, which shall be discussed next.

1.2 Hyperoxic Culturing

The most important atmospheric constituent in cellular respiration, oxygen, is maintained at 140-150 mmHg, which is approximately 20.1 % mol/mol under standard culturing conditions, and corresponds to concentrations 5- to 10-fold higher than those found within most physiological niches[30]. Measurements of cardiac tissue reference oxygen tension in the canine[31] and rat[32] as falling within the range of 20 to 30 mmHg (2.6-3.9 %), and varies depending on the proximity to perfusion beds[32]. While the effects of high oxygen tension on *in vitro* systems remains primarily focused on stem cell and embryo systems, only scant research exists on the consequences of high oxygen tension on mechanistic characterization of cytotoxicity. Surprisingly, this is especially true of oxidative stress for which oxygen bioavailability is crucial for peroxynitrite formation-based stress[33]. Murine blastocysts cultured under 20 % oxygen demonstrate 5-fold increased levels of oxidative stress markers, such as γ-H2AX-positive staining, compared to blastocysts cultured in lower oxygen-containing atmospheres as well as *in vivo* parental tissue[34]. Additionally, rates of aneuploidy and general DNA instability are markedly reduced in stem cells cultures under physiologically relevant oxygen tension (5 %; 38 mmHg) when compared to typical culture conditions[35,36], likely the result of proliferating reactive oxygen species formed during hyperoxic culturing conditions[37,38]. ROS proliferation and genomic instability have been associated with enhanced senescence, the latter of which is closely associated with γ-H2AX-positivity in cell culture systems[39,40].

Oxygen tension *in vitro* has been shown as a critical factor in cellular respiration and adenine nucleotide formation. At oxygen partial pressures 30-100 mmHg, the lactate-to-pyruvate ratio in culture medium supporting MEFs exhibits a biphasic relationship, characterized by an initial negligible ratio increase at onset, followed by a rapid increase in lactate production at day three when oxygen partial pressure was fixed at 12 mmHg[41]. Neurons cultured under an atmosphere containing oxygen partial pressures below 35 mmHg typically exhibit lactic acidosis[42], similar to observations in stem cell cultures[43]; however, *in vitro* neurons adapt with time to such metabolic acidosis and demonstrate an approximately 25 % enhanced peak proliferative capacity compared to standard culture conditions[42], so long as respiration demand does not exceed the rate of dissolved oxygen permeation[44]. The induction of lactic acid production in cell culture is suggestive of a paradigmatic energy production shift towards glycolysis[43], and is found to be triggered by activation of hypoxia-inducible factor 1α (HIF-1α)[45,46]. Extracellular acidification was also observed in cardiac myoblast precursor cells, demonstrating a relatively applicable respiratory response to oxygen tension among heart progenitor cells[47]. Consequently, HIF-1α activation causes a fall in the rate of oxygen consumption and, thus, restricts the rate of oxidative phosphorylation kinetically to oxygen availability[48]. Basal and maximal oxygen respiration levels may depend on oxygen tension, though oxidative stress, e.g., hydrogen peroxide, may substantially modulate reserve oxygen consumption capacity[47]. Unfortunately, investigations directly linking high oxygen tension ROS production to such modulation are lacking. The work of Hoffman and colleagues offered some indirect evidence by demonstrating that endogenous hydrogen peroxide formation, which depends on superoxide, is reduced dramatically under low oxygen conditions[38], though metabolic capacity was not measured. Coincidently, superoxide leakage itself depends on the

rate of oxygen reduction via the ETC[45]. It, therefore, stands to reason that decreasing oxygen tension in cell culture to physiologically relevant oxygen tensions should ultimately reduce reactive oxygen species formation as a by-product of oxidative phosphorylation without deleteriously affecting cellular viability.

1.3 Poly(ADP-ribose) Polymerase

While poly(ADP-ribose) polymerase-mediated parthanatos has been recently characterized as an important mechanism of cellular death[49], the exact role of PARP overactivation in mediating cellular death remains partitioned between two general mechanisms: energy crisis or nuclear apoptosis-inducing factor (AIF) translocation. Oftentimes, neither mechanism occurs apparently with mutual exclusivity (Reviewed in Cregan and colleagues[50]). NAD^+ depletion is credited as an crucial outcome of PARP overactivation leading to eventual DNA fragmentation[51], for which competitive inhibition of PARP by small molecules, e.g., 3-aminobenzamide, PJ-34, and DIQ, has been shown to be efficacious in promoting a rescue phenotype[52]. Remarkably, results of *in vitro* studies of PARP overactivation-associated cytotoxicity amelioration with common citric acid cycle substrates, such as pyruvate, glutamine, and glutamate, among others, has been shown as effective as PARP inhibitors (PARPi) themselves[53-57], suggesting a unified mechanism of metabolic stress and energy crisis as attenuated by tricarboxylic acid (TCA) substrates. On the one hand, Alano and colleagues[58,59] credit cytosolic and nuclear NAD^+ depletion as both necessary and sufficient to induce cellular death; however, the role of reactive oxygen scavenging by antioxidants oftentimes cannot be separated from metabolic status rescue, as is the case for pyruvate - one of the most effective TCA cycle substrate in reducing PARP-induced NAD^+ depletion and cellular crisis. Pyruvate has

known antioxidant properties, which was corroborated by demonstrating a similar antioxidant capacity of a structural pyruvate analogue with no known TCA cycle metabolic pathway[60]. On the other hand, parthanatos has been shown to be dependent on AIF translocation, and operates independent of caspase-3 activity[57,61,62]. Interestingly, AIF-neutralizing antibodies do not abrogate cellular death under instances of PARP overactivation (Parthanatos), but partially attenuates reductions in cellular viability by approximately 40 %[63]. Therefore, AIF translocation and/or NAD^+/ATP depletion are not mutually exclusive mechanisms of cellular death, and may ultimately complement one another, resulting in cellular death. What is known, however, is that intracellular ROS formation and free cytosolic ADP-ribose (ADPr) polymers (Herein denoted simply as: PAR) induce a sharp increase in intracellular calcium levels; promote mitochondrial dysfunction, possibly through opening of the mPTP; and uncouple mitochondrial proton motive force driving oxidative ATP formation[64]. Combined with decreased glycolytic processing under hyperoxic conditions, some cell types may be artificially sensitized to PARP-mediated cellular crisis under atypical non-physiological conditions. As a result, discrepancies in the efficacy of *in vitro* pharmacological treatment versus *in vivo* for certain PARP-mediated pathologies may be explained by this phenomenon, and can detrimentally confound the mechanistic interpretation of *in vitro*-based cytotoxicity investigations.

1.4 H9c2 Cardiomyoblast Cell Line, Oxygen Tension, and TRPM2 Channels

The H9c2 rat cardiomyoblast cell line is a commercially available cell line which retains the potential for myogenic differentiation[65-67]. The value of the H9c2 model has been demonstrated by the ability to simulate *in vivo* hormone-specific responses. For example, antidiuretic hormone stimulation in both differentiated and non-differentiated H9c2

cardiomyoblasts recapitulates the hypertrophic response observed in isolated adult rat cardiomyocytes[68,69], thus demonstrating a tissue-specific receptor-mediated response[66]. While the undifferentiated H9c2 cell model is utilized as both a toxicological and a physiological cardiac model, interest in committing cultured H9c2 cells to a myogenic lineage, whereby further differentiation to skeletal muscle or cardiomyocytes can be promoted[67,70], and subsequent attainment of a cardiac-like phenotype more requisite representation for myocardial or skeletal muscle tissue has enhanced the discussion of potential models with high fidelity tissue responses. This becomes important when considering mechanistic elucidation, especially within a system where respiration may be important in elucidating tissue-specific toxicogenic responses.

Serum reduction to 1 %, with or without supplemented all trans-retinoic acid (RA), alters the expression profile of phase-specific mitogenic promoters[71] ultimately leading to cell-cycle arrest[72]. The determinant for commission to a cardiomyocyte-like phenotype, as opposed to skeletal muscle myotubes, requires culturing for a period of 5-7 days with supplemented RA at concentrations between 1.0 and 1,000 nM, after which significant alterations of mRNA expression are found[66,73]. As a result, differentiation was shown to significantly alter mitochondrial biogenesis and morphology. In addition to biogenesis and general morphological changes, e.g., mitochondrial size and mass, functional inter-mitochondrial networks are formed, i.e., highly enhances mitochondrial interconnected networks[74], with an increased propensity for both high- and low-potential mitochondrial membrane polarization, though the former is more favorably selected after differentiation[75]. While differentiation with RA without serum reduction neither directly alters succinate utilization within oxidative phosphorylation nor alters mitochondrial membrane polarization ($\Delta\Psi_m$), RA itself does seem to enhance oxidative phosphorylation via two central routes: increasing ATP synthase activity by intensifying F_0/F_1

ATPase assembly and coupling, and enhancing citrate synthase activity, resulting in accelerated pyruvate utilization for TCA adenine nucleotide production[75]. Differentiation, however, is not an H9c2-specific phenomenon. For example, differentiation of mouse C2C12 skeletal muscle myoblasts has been shown to significantly alter the sensitivity of the cells to oxidative stress, in particularly to PARP activity and oxygen consumption[76]. The influence of differentiation on toxicosis provides an attractive area of research, especially when considering metabolic stress after targeted oxidative stress. Despite the attraction, the wide utilization of differentiated models and physiologically relevant culture systems remains scant.

Most *in vitro* toxicological research utilizes standard culture conditions, i.e., humidified 95 % air mixed with 5 % CO2 under 37 °C. Only limited evidence of non-standard oxygen tension (Other than standard 19-20.1 % O_2) culturing of H9c2 cardioblasts is available, and less so for toxicological response modeling. Largely, the model has been utilized for the elucidation of ischemic pre-conditioning; otherwise, primary cell cultures from non-cardiac tissue have dominated the ischemic pre-conditioning literature, especially neuronal tissue. Furthermore, the assertion of physionormal oxygen tension remains contested. H9c2 cells cultured under an O_2 partial pressure of 13 % was described as “mild chronic hypoxia” and served as a protective factor against acute ischemia/reperfusion primarily mitigated through ERK/PI3K activation[77]. It was shown that HIF-1α was not induced, to which the authors credited chronic “hypoxia” as a protective factor against total hypoxia. While the induction of HIF-1α acutely does not necessarily confer HIF-1α involvement, exposure to a 13 % partial pressure of oxygen does not meet the criteria for hypoxia, especially when the baseline for comparison for typical culturing conditions is 20 %. Therefore, the appropriateness of denoting mild chronic hypoxia (13 %) as protective against acute ischemia comes into question, especially since the activity of key

glycolytic participants remained uncharacterized. Some information on acute toxicogenic cell death was obtained in hypoxia pre-conditioned neuronal cells that were exposed to an ischemia for 15 minutes, followed by reperfusion for 24 hours prior to treatment hypoxia or MNNG treatment[78]. Ischemic pre-conditioned PARP KO cells or exposed to a PARP inhibitor demonstrated significantly reduced neuronal death by 70 % or more. The implication of this investigation, therefore, denotes that the efficacy or potential for eventual neuronal death in response to DNA damage and/or metabolic crisis likely impinges upon an underlying oxygen-dependent factor. While HIF-1α mRNA constructs were not measured, the long-term effect of ischemic pre-conditioning on cellular rescue may serve as a preliminary representative model of HIF-1α-induced transcriptional adaptation to lower oxygen tension[79], similar to the recapitulation of endogenous cardiac HIF-1α induction under analogous conditions[80]. Therefore, cytoprotection of pre-conditioning may implicate an underlying metabolic shift by increasing pyruvate metabolism and glucose influx into cardiomyocytes (Reviewed by Martin-Puig and colleagues[81]), and subsequently incur resistance to reductions in oxygen bioavailability. Recent evidence of the role of Parkin and PINK1 in selective mitophagy after ischemic preconditioning support this notion, as pre-ischemic conditioning has been associated with increases in total $\Delta\Psi_m$[82,83] and seemingly operates in close association to increased oxidative maximal oxygen consumption rate and oxygen consumption reserve capacity offered by pyruvate influx[84]. Since excess reactive oxygen species formation is known to contribute to mitochondrial dysfunction[85], ischemic pre-conditioning studies indirectly implicate that hyperoxic culturing may sensitize cells to transient energy substrate depletion. In turn, pyruvate equivalents offered to the TCA cycle and subsequent ETC production yield is restricted to fixed capacity, ultimately resulting in an increased propensity for energy crisis and cellular metabolic collapse. The role of normoxic

culturing on cell fate, however, does not operate in isolation of differentiation state with the H9c2 cell line.

Evidence has shown that H9c2 differentiation to a cardiomyocyte-like phenotype significantly alters anthracycline and adrenergic agonist-induced cytotoxic response[73,86], suggesting retinoic acid supplementation with serum reduction induces not only differentiation, but also alters cellular machinery responsible for sensitization to toxicogenic injury[86]. While the exact specific mechanistic underpinnings leading to sensitization after differentiation remain unknown, alterations in mitochondrial metabolism, energy production, and calcium-influx response may be partially responsible. Basal ROS load of H9c2 cells under low-serum conditions increases[87] and may confer altered ROS sensitivity, though ROS loading may remain within physiological tolerance when coupled with up-regulation of SOD expression observed in differentiated H9c2 cells[73]; whether SOD up-regulation keeps pace with the basal increase in ROS is unknown and requires further investigation. However, it is definitively known that cardiac ROS generation is functionally linked with intracellular calcium concentrations[88] and mitochondrial integrity (Reviewed in Zorov and colleagues[89]). Within mitochondria, several TCA cycle enzymes are stimulated by calcium, thereby likely promoting increased ATP production, the effect of which may act as partially a compensatory mechanism independent of free-fatty acid metabolism[90,91] to fulfill energy demands during excitation-contraction coupling. Even still, evidence suggests that calcium serves as the factor responsible for coupling aerobic metabolism and myocardial work across the sarcoplasmic-mitochondrial interface[92]. When inhibiting the sarcoplasmic SERCA transporter in a mixed suspension of isolated SR and mitochondria, mitochondrial respiration is reduced by 88 %[92], likely suggesting the extra-SR calcium enrichment is mediated by SERCA, especially with novel evidence that microdomain at

the interface of the SR and mitochondria may facilitate calcium concentrations required for initiating intra-mitochondrial calcium influx and subsequent stimulation of F_0F_1-ATPase activity[93]. At high cytosolic calcium levels, e.g., greater than 700 nM, respiratory uncoupling occurs and proves cytotoxic when coupled to high concentrations of reduced adenine equivalents[94,95]. Overtly, extreme concentrations of intra-mitochondrial calcium seemingly promote mitochondrial membrane permeabilization transition pore (mPTP) formation, an event which has been implicated as a premier cytotoxic trigger leading to respiratory collapse[96]. The evidence for this association, paradoxically, is not directly discernable, as a simple correlation between calcium influx and mPTP formation does not fully explain mitochondrial sensitivity to calcium overload.

Reaching the mitochondrial calcium-loading maximum has not been shown sufficient to trigger mitochondrial failure[96], particularly when considering calcium-induced calcium release and the sodium-calcium exchanger. Mitochondrial calcium loading, as a supposed function of the low-affinity, high capacity mitochondrial calcium uniporter (MCU)[97], has been shown to provide acute facilitation of respiration support, e.g., OCR intensification, in response to stress-mediated myocardial contraction without altering basal respiratory function or maximal calcium influx [98,99], owing to a generalized mechanism of calcium-workload coupling via respiratory compensation. Since the MCU is voltage- and cytosolic calcium concentration-dependent, the MCU functions also acts as a mediator of cytosolic calcium buffering[97] and may also modulate mitochondrial ROS generation[100]. Pathologically, the MCU has been considered a possible indicative source of mitochondrial dysfunction, as some evidence suggests that mitochondrial calcium overload specifically through the MCU can lead to $\Delta\Psi_m$ reduction and eventual dysfunction[101,102]. Coupling with $\Delta\Psi_m$ dissipation, MCU calcium conductance has been shown to

undergo conductance reversal, mitochondrial matrix calcium efflux, and reduction in respiratory support, thus offering an explanation to the association between metabolic failure and MCU cycling, particularly under acute stress[103]. Paradoxically, lackluster rescue via MCU genetic ablation and specific pharmacological inhibition via ruthenium red 360 provides a paradigm, whereby MCU calcium loading does not ultimately decide cellular fate[104,105]. These results were in opposition to those utilizing ruthenium red; the difference may ultimately lay with the non-specific inhibitory nature of ruthenium red, especially at the concentrations required for MCU inhibition[106]. It is to be noted here that the MCU does not operate as the only calcium conductance channel. Under pathological conditions, $\Delta\Psi_m$ collapse occurs simultaneously with altered function of the cyclosporine A-sensitive, sodium-dependent calcium exchanger (NCX), which further intensifies the rate of mitochondrial matrix calcium influx in a cytosolic sodium-dependent manner[98,107]. Therefore, an increase in calcium influx rate is likely more important than maximal loading in leading to mPTP formation and eventual respiratory collapse[105,108]. Since undifferentiated H9c2 cells have been shown to express endogenously a similar cyclosporine A-sensitive NCX[109,110], the role of cytosolic calcium overload is of considerable interest.

Although cardiomyocytes have voltage-dependent calcium channels to facilitate electrogenic contraction, the non-specific cation-permeable, voltage-independent 2-aminoethoxydiphenyl borinate (2-APB)-sensitive[111-113] melastatin type-2 transient receptor potential (TRPM2) channel has received interest in its role in facilitating ROS-mediated cation influx from extracellular extracellular matrices[114-116]. Several inhibitors of the TRPM2 channel have been described, including 2-APB[117-121], anthranilic acid derivatives N-(p-amylcinnamoyl)anthranilic acid (ACA)[117,120-123] and flufenamic acid (FFA)[112,120,121,123,124], and

anti-fungal agents miconazole[112], econazole[125], and clotrimazole (CTZ)[119-121,125-127]. The activity of TRPM2 has been shown to be independent of ryanodine receptor activation[128], IP3 receptor activation[129], SERCA cycling[129], and intracellular kinase receptor signaling [130]. It is to be noted that each small molecule inhibitor aforementioned is not TRPM2-specific, and, in the case of 2-APB, may also lead to activation of vanilloid-type TRP channels[131] and allow calcium influx. 2-APB also inhibits TRPC channels[132], further complicating isolation of oxidative stress-related conductance. Further still, 2-APB inhibits calcium conductance via intracellular acidification[118], most implicated by inhibition of the IP3 receptor[133-135], while the anthranilic acid derivatives have been largely recognized as promoting reduction or inhibition of calcium conductance through extracellular acidification[136]. Interestingly, intracellular addition of 2-APB was less effective in abrogating enhanced calcium conductance in RB-1 cells[137], and, thus, may demonstrate cell-dependency. Hwang and colleagues[138] concluded, even in the absence of ACA, FFA, and 2-APB, that acidification does indeed alter intracellular calcium; the main stores affected by intracellular acidification seem to involve ER and sarcoplasmic reticulum and can occur independent of TRP channel activation and extracellular calcium influx[139]. Nonetheless, the presence of TRPM2 and TRPM8, particularly the former, is required for certain triggers of calcium conductance[130]. Therefore, CTZ, although as non-specific as anthranilic acid derivatives and 2-APB, does not induce compartmental or extracellular acidification, and is likely the most pertinent inhibitor to delineate TRPM2 channel conductance.

The exact contribution of TRPM2 activation on membrane excitability remains unknown, but ADP-ribose can activate the channel in as little as 1 μM of free ADP-ribose[140]; other adenine nucleotides do not interact significantly with the channel[140,141]. During gating, a proportion of the total TRPM2 conductance is carried by calcium, while approximately 50 % of the total charge is

carried by sodium[142,143]. Thereafter, not only does the TRPM2 induce a slight plasma membrane depolarization, but the increased calcium influx acts as a promoter of intracellular signaling, especially since TRPM2 channels allow relevant cationic conductance at physiologically relevant membrane potentials[144], i.e., conductance does not likely only occur under pathological conditions which likely result in obligate cell death. With calcium conductance, TRPM2 activation can promote cytosolic calcium transients, potentially leading to increasing mitochondrial calcium stores and respiratory support, particularly when TRPM2 activation has been associated with enhanced glucose metabolism *in vivo*[145]. The importance of extracellular calcium stores in facilitating metabolic response to cellular toxicity via TRPM2 conductance deserves further attention, as calcium conductance may be integral for cardiomyocyte metabolic compensation under acute metabolic insufficiency or after oxidative stress[146,147]. Nonetheless, the degree to which calcium loading becomes pathological is not clearly demarcated. Since extracellular calcium entrance is not confined to TRPM2 channels alone, the dependence of other calcium-permeable channels in membrane excitability, or direct co-dependence of TRPM2 channel activation, is similarly not yet delineated. Though, it must be noted that, when free PAR is fixed within the physiological range for TRPM2 activation, human TRPM2 channels expressed in *Xenopus* oocytes require a certain threshold concentration of intracellular calcium to induce gating and subsequent closure[148]. The reliance of the TRPM2 channel activation on parallel calcium store conductance mechanisms, e.g., L- and T-type calcium channels, has been demonstrated within only some tissue-specific models[149]. Nonetheless, the influence of TRPM2 channels in initiating or modulating cellular death programs remains ill-defined, but deserves further attention since PARP overactivation has been shown functionally linked to channel calcium conductance.

TRPM2 channels contain a c-terminus NUDT9 pyrophosphatase domain, which hydrolyzes ADP-ribose to AMP, and may also be implicated for TRPM2 activation[150,151]. Indeed, micromolar concentrations of intracellular ADP-ribose (10-100 μM) activate the channel with a Km of approximately 13 ± 1 μM[143,144,151-153]. ADP-ribose gating values as low as 1.1 μM were observed in patch-clamp readings[154], but this threshold may be dependent upon the cell type and ionic composition of the patch-clamp bath. Various adenine nucleotides have also been shown to gate TRPM2 channels, such as cyclic ADP-ribose [155], NAD^{+}[156,157], NAAD and NAADP[153,155]; however, none of these adenine nucleotides are effective in gating TRPM2 channels when contaminating ADP-ribose was removed [153,158]. Similarly, various glycosylated nucleotides also do not activate the channel[151], owing to the likely specificity of PAR in mediating TRPM2 channel opening with subsequent calcium influx. Nonetheless, TRPM2 gating, specifically due to high intracellular ADP-ribose concentrations, may act as an endogenous adaptive signal against oxidative stress and subsequent PARP activation, as the evolution of free PAR requires PARG[159]. Evidence suggests that redox alterations, i.e., hydrogen peroxide accumulation, though shown to activate TRPM2 channels, are not sufficient to induce specific TRPM2 gating[142,160], at least in non-cardiomyocyte cell types[149,161]. Alternately, high concentrations of hydrogen peroxide (≥ 500 μM) demonstrate non-specific conductance peaks, denoting a TRPM2-independent manner of cation conductance[162] likely via cell membrane permeation. Where redox stressors becomes particularly important is under a model, whereby ADP-ribose may actually synergize with redox and calcium sensors, i.e., through calmodulin, to activate TRPM2 channels and allow rapid, but sustained, cationic influx[130,143,156,163-166]. Others contest that oxidative stress is absolutely necessary for TRPM2 gating, and can occur irrespective of free PAR[123,167]. It must be noted that, indeed, oxidative stress purportedly can act

independently of PARP activation; however, these two phenomena are not mutually exclusive. Yang and colleagues[168] looked at PARP activation and TRPM2 activation by H_2O_2 treatment in primary rat ventricular cardiomyocytes. Within 20 minutes of treatment with 20-100 μM H_2O_2, marked intracellular PAR accumulation was noted which was expectedly reduced by PARPi. Characteristic of the non-specific cationic TRPM2 channel, intracellular concentrations of both sodium and calcium increased – an effect also ablated by exposure with a PARPi. Ultimately, cardiomyocytes eventually lost viability to a myriad of cellular death pathways, primarily apoptosis and necrosis. When having applied the PARPi in combination with the direct TRPM2 inhibitor CTZ, morphological and biochemical signs of cytotoxic endpoints were prevented. While the exact role of oxidative stress mediators in TRPM2 gating remains to be elucidated, the unequivocal role of ADP-ribose has been established.

1.5 Poly(ADP-ribose) Polymerase and Cytotoxicity

Pharmacological inhibition of PARP is known to reduce calcium transients during cytotoxic ischemia/reperfusion injury through reduction of free ADP-ribose[169]. Coincidently, TRPM2-mediated extracellular calcium transients during I/R injury are known to be sensitive to PARP inhibition[128,169,170], indicating free PAR as a functional link between calcium influx and I/R injury. Following, I/R injury returns a similar mechanistic pathway compared to oxidative injury, especially when considering the markers of calcium influx, PARP activation, and ROS generation. Therefore, PARP activity, under oxidative stress and electrophilic DNA damage, is a likely fundamental link between cellular injury and transient calcium influx via TRPM2 channels and would inevitably require intact PARG[171]; the role of ARH3 in TRPM2 activation has not been investigated[161], but may also contribute. As mentioned previously, the rate of calcium

influx may present an important factor in determining whether PAR-dependent TRPM2 gating would sufficiently induce a rapid calcium influx to the degree required to translate to a cytotoxic endpoint. Though little evidence has yet to imply a definitive answer, the rapid PAR transients typically observed may offer some circumstantial evidence of plausibility. The half-life of ADP-ribose polymers is short (< 30 seconds), and increases with increased branching[172]. Larger, more complex ADP-ribose polymers are considered more toxic than short-branching, low molecular weight polymers[173]. Since genetic ablation of PARG in neurons results in significant DNA instability and phenotypic lethality in mouse embryonic fibroblasts and stem cells[174], utilizing PARG knockout cell or animal models for characterizing PAR in toxicological assessment remains untenable. However, short-term gene knockdown studies have proved fruitful answers. PARG siRNA knockdowns were similarly effective in decreasing calcium influx as TRPM2 siRNA knockdowns[169], likely due to reduced long cytosolic PAR polymer accumulation[175,176]. These results implicate PARP, PARG, and TRPM2 constituting a single mechanistic unit, whereby significant PARP activity can result in modulating calcium-dependent intracellular signaling programs depending on the intensity of PAR formation. Conversely, Geistrikh, Visochek, Klein, Miller, Mittelman, Shainberg, Cohen-Armon [177] demonstrated significant calcium-dependent increases in PARP activity after cardiomyocyte angiotensin II administration. Unfortunately, though the role of calcium and underlying PKC/MEK/ERK activation in increasing PARP activity was the focus of this investigation, the notion of calcium-induced mitochondrial ROS promotion was left unresolved. Nonetheless, limited evidence of PARP activation perpetuation through cytosol-derived MCU channel mitochondrial calcium flux has been reported[100]. Hitherto, confirmation of a mechanistic unit among PARP activation, PARG hydrolysis, and TRPM2 activation remains quite tentative, and requires further investigation,

especially under faithful physiological conditions, but adequately lends insight into the mechanistic data culminated currently.

While free ADP-ribose is known to trigger TRPM2, PARP activity itself has been shown to consistently influence cellular energetics and mitochondrial integrity. Physiologically, high levels of endogenous PAR are associated with diminished $\Delta\Psi_m$[178], for which PARP inhibition has been shown ineffective in completely abrogating, but effective in merely delaying, such $\Delta\Psi_m$ dissipation[179]. Linking PARP activity mechanistically with mitochondrial permeabilization may be dependent upon the calcium-dependent cyclophilin D. Ppif -/- mouse MEFs and cardiomyocytes retain expression of *vdac1*, and *ant* isoforms 1 and 2, but are refractory to $\Delta\Psi_m$ dissipation caused by ischemia/reperfusion[180], thus implicating a calcium-dependent modality for determining mitochondrial fate. Previous *in vitro* models have confirmed these findings found *in vivo*[181]. In bridging *in vivo* and *in vitro* mechanisms, the cyclophilin-dependent AIF may be the prominent determinant in dictating cellular fate.

AIF was identified as part of the apoptotic machinery, leading to large-scale nucleic acid fragmentation and cell death[182], and associated with nuclear translocation in primary rat hippocampal neurons after ischemia/reperfusion-induced oxidative stress[183,184]. Since AIF knockouts result in an embryolethal phenotype, the genetic AIF knockdown Harlequin mouse, which produces approximately 80 % WT AIF expression levels[185], has assisted in resolving the link between neuronal oxidative stress and AIF translocation in triggering cellular death[63,173]. The AIF protein contains a putative PAR-binding domain[186], and, when complexed with PAR, is understood to be the effector whose mobilization ultimately results in DNA fragmentation and parthanatos. This is not surprising, since direct addition of complex PAR causes synthetic lethality[187]. Furthermore, the association between AIF translocation and $\Delta\Psi_m$ dissipation is

unequivocal; however, the temporal relationship of PARP-mobilized AIF translocation and mPTP formation or vice versa is still debated[182,188,189]. Likewise, the dependence of $\Delta\Psi_m$ dissipation upon mPTP formation remains in question, and undermines the dependence of AIF mobilization in promoting mPTP formation. This becomes apparent when both cyclosporine-A sensitive cyclophilin isoforms (A and D) are implicated in AIF execution and mPTP formation[190]. In a mouse model of cerebral ischemia, cyclophilin A was co-localized with AIF nuclear translocation after ischemia/reperfusion, an observation previously uncharacterized in neuronal tissue[191]. In the same investigation, a CypA (-/-) knockdown model caused a significant reduction in the volume of reperfusion tissue necrosis by 33.8 % compared to WT controls, offering at least some neuroprotection. Unfortunately, the effect of CypA KO on mitochondrial integrity was not directly explored, though the dependency of calcium in determining mitochondrial integrity was characterized. These results tentatively confer evidence of universal calcium sensitization of mPTP formation, which may be cyclophilin-dependent, after reperfusion injury in heart tissue[192].

When considering *in vitro* investigations of parthanatos, the functional isolation of the outer membrane-associated AIF, intramembranous mitochondrial AIF, and mPTP formation cannot be segregated sufficiently to explain the contributory role of metabolic crisis simultaneously with other mechanisms. Given some evidence of AIF localization to the mitochondrial membrane outer leaf[193], the necessity of mitochondrial function in determining cellular fate with respect to parthanatos seems mechanistically unresolved. Were this true, and the outer leaf isoform of AIF contributed to cell execution, mitochondrial dysfunction may ultimately be irrelevant in determining cell fate. This interpretation would stand in juxtaposition to those focusing primarily on metabolic failure, despite *in vitro* investigations having shown the

efficacy of pyruvate in attenuating MNNG or H_2O_2 toxicosis similar to that of PARPi[54]. While these results may indicate a plausible metabolic rescue by supplementation of pyruvate to the TCA cycle[56], the antioxidant potential of pyruvate may confound the mechanistic interpretation of pyruvate rescue. Indeed, even pyruvate at levels typically found in standard DMEM (1 mM), a level approximately 10-fold found in rodent whole blood[194-196], has been shown to significantly alter toxicogenic response under oxidative stress[197]. Therefore, whether pyruvate actually results in a rescue phenotype or merely reduces ROS, particularly that of H_2O_2, load remains unelucidated.

Respiratory support under cytotoxic stress by certain glycolytic and TCA substrates has been, nonetheless, shown under similar circumstances, i.e., standard culturing conditions, albeit neuronal rescue by glucose has proven inconsistent[54,198]. These results are not surprising, since neurons are highly dependent upon glucose metabolism for producing reducing equivalents required for energy production, but whose glycolytic capacity is likely reduced under standard culturing conditions. For example, rotenone sensitivity is reduced under hyperoxic standard culturing conditions compared to reduced (5.0 %) oxygen conditions in the neuroblastoma SH-SY5Y cell line[199] – evidence that reducing equivalent through complex I of the ETC becomes blunted under an oxygen-rich environment. The ED_{50} for complex I inhibition by rotenone was reduced to 1.98 ± 0.04 μM at 5 % oxygen, compared to 49.8 ± 0.03 μM at 20 % oxygen, denoting significant oxygen-dependent protection under 20 % oxygen culturing. Further still, under hypoxia (0.1-0.5 % oxygen), cells require glycolysis in order to support ATP production via complex I reduction, and represents a functional proteomic shift from partial reliance of complex II reduction for promoting F_0F_1-ATPase support[200]. ATP production under hypoxia depends upon functional pyruvate dehydrogenase, implicating a respiratory model whereby

metabolic contribution by fermentation is rather negligible[45]. Since the other TCA substrates used in metabolic rescue after PARP activation, except pyruvate, operate downstream of pyruvate dehydrogenase and citrate synthase, the weight of shunting glycolytic pyruvate on metabolic rescue thus remains unknown, but is of critical consideration for the interpretation of *in vitro* findings with respect to toxicodynamic effects which imping upon metabolic disruption. When considering the significantly increased citrate synthase production in differentiated H9c2 cardiomyoblast, the role of glycolysis-derived pyruvate production coupled to increased citrate synthase activity in reducing or abrogating metabolic crisis requires attention both *in vitro* and *in vivo*.

In summation, two fundamentally competing mechanisms are obviously tantamount in the current literature: One characterized by AIF translocation, which likely relies upon $\Delta\Psi_m$ reduction, and a second which describes metabolic failure which may act independently of AIF translocation, though co-dependence later in the mechanistic pathway, e.g., ETC respiratory failure after AIF-dependent potential dissipation, cannot substitute for the underlying acute mechanisms which effectively commit the cell to death. This investigation focuses on the latter of the two in an effort to indirectly implicate the role of oxygen in determining cellular fate by altering respiratory capacity derived from functional TCA and glycolytic pathways

1.6 Problem Statement

In considering the potential sensitization of cardiomyoblast H9c2 cells to metabolic crisis when cultured under hyperoxic conditions (20 % oxygen), confounders of mechanistic elucidation undermine the interpretation of studies, and cast doubt upon the *in vitro* model to recapitulate the circumstances under which cell-specific toxicodynamics may actually differ.

Since parthanatos involves the nuclear translocation of AIF: a translocation which occurs generally concomitantly with ATP-dependent mitochondrial membrane dissipation[108,201,202], respiratory rescue either through PARP inhibition or TCA substrate supplementation provides a strong case for implicating NAD^+ and ATP depletion as sufficient for determining cellular fate under the pretenses where respiratory capacity cannot be sustained directly from alteration of respiratory machinery. The influence of metabolic rescue for *in vitro* cardiomyoblasts under representative physiological conditions has not been completely investigated with an appropriate model. In this investigation, differentiated H9c2 cells were cultured under normoxic conditions (5 % O_2) prior to exposure to an electrophilic compound known to induce cardiomyopathy, acrolein. The purpose was to characterize the role of poly(ADP-ribose) polymerase in determining cellular fate under the conditions of normoxia in order to characterize the toxicological and mechanistic effect of normoxia on determining cellular fate under term of metabolic stress. Since a majority of *in vitro* toxicological studies involve the utilization of physiologically non-relevant oxygen conditions, the discordant efficacy of *in vitro* to *in vivo* translational research requires further investigation.

1.7 Hypotheses

The current investigation aims at examining the influence of oxygen tension in modulating acrolein-induced cytotoxicity in the differentiated H9c2 cardiomyoblast model, along with a mechanistic characterization of cytotoxicity. As such, three hypotheses are proposed.

Hypothesis One. Since several TCA and glycolytic substrate have been shown to attenuate toxicosis in several cell models. Therefore, supplementation of such TCA and glycolytic substrates will have a differential capacity for attenuating cell death among

differentiated H9c2 under physiologically relevant oxygen tension (5 %) compared to standard culturing after acrolein exposure:

a) L-pyruvate will attenuate acrolein-induced reductions in cell viability;

b) L-glutamine will attenuate acrolein-induced reductions in cell viability;

c) α-ketoglutarate will attenuate acrolein-induced reductions in cell viability;

d) D-glucose will attenuate acrolein-induced reductions in cell viability; and

e) L-glutamate will not attenuate acrolein-induced reductions in cell viability, and will demonstrate similar sensitivity compared to standard condition cultured cells.

Hypothesis Two. Depletion of adenine nucleotides has been shown effective in mitigating cytotoxic stress with various toxicants. Therefore, inhibition of PARP by co-exposure with olaparib will significantly attenuate acrolein-induce cytotoxicity compared to exposure-only cells cultured under physiologically relevant oxygen conditions.

Hypothesis Three. Overactivation of PARP under oxidative stress is associated with induction of calcium transients; the latter of which is associated with pathological reduction of mitochondrial membrane potential. Therefore, inhibition of PARP by olaparib among differentiated H9c2 cells cultured under physiologically relevant oxygen conditions will:

a. result in attenuation of clotrimazole-sensitive extracellular calcium conductance in H9c2 cardiomyoblasts, and

b. retain mitochondrial membrane potential polarization to acrolein-unexposed cell levels

CHAPTER TWO:

METHODS

2.1 H9c2 (2-1) Cardiomyoblast Culturing and Treatment

A subclone (2-1) of the commercially available H9c2 cardiomyoblast cell line derived from the rat (*Rattus novegicus*) was purchased from the American Type Culture Collection (ATCC; Manassa, VA) and utilized as the cardiac model for this investigation. H9c2 cells were cultured and maintained under standard culturing conditions (37 °C humidified 5 % CO_2/ balance air atmosphere) with Dulbecco's Modified Eagle's Medium (Abbr. DMEM; Sigma-Aldrich; St. Louis, MO) + 10 % FBS (ATCC) in 100 mm glass Petri dishes with a rotating use of 100 IU/mL penicillin/100 µg/mL streptomycin (ATCC). Medium was changed every 2-3 days, until cells were passaged with pH-balanced 0.25 % trypsin/2.21 mM EDTA Hank's buffered saline solution (Corning; Manassa, VA) when reaching 75- 80 % confluency after a brief wash with calcium- and magnesium-deficient Dulbecco's phosphate buffered saline (D-PBS; Sigma-Aldrich), and seeded at a ratio of 1:3 or 1:4. All manipulations were performed within a standard Class II biological safety cabinet.

H9c2 cells maintained under reduced oxygen, e.g., 5 % denoted as physiologically relevant oxygen tension, were supplied an air mixture of 5 % O_2/5 % CO_2/ Balance N_2 in order to attain normal oxygen tension roughly equivalent to that of *in situ* cardiomyocytes[31]. Culture and maintenance medium was analogous to 20.1 % oxygen cultures (DMEM + 10 % FBS in 100 mm glass Petri dishes with a rotating use of 100 IU/mL penicillin/100 µg/mL streptomycin),

though the DMEM was pre-equilibrated within culture flasks with affixed 0.22 μm filter-containing venting caps to ensure microbial exclusion. Cell passaging was performed similarly to standard culture H9c2 cells, except with the use of 5 % oxygen pre-equilibrated medium. For all procedures with a duration longer than 10 minutes, e.g., microplate seeding, maintenance, and treatment in 96-well plates, such procedures were executed within a custom-built transparent acrylic chamber (*Appendix 3*), wherein the intra-chamber oxygen concentration was reduced to, and maintained at, 5 % via nitrogen gas displacement. Nitrogen gas was supplied via 125-pound nitrogen tank (Purity 99.99 %; Airgas; Radnor, PA) with purge flow regulation at 5-10 L/min using a Coplay-Norstar heavy-duty inert gas flow-meter (Model N302014; Coplay, PA); nitrogen gas was further purified via a 0.22 μm in-line filter prior to entry. Intra-chamber oxygen was monitored in real-time via the Traceable® Digital Oxygen Meter during and after purging to ensure optimal 5.0 ± 0.5 % oxygen partial pressure within the main chamber along the duration of procedure execution.

In preparation for experimentation, passaged H9c2 cells were resuspended in DMEM + 10 % FBS, counted via trypan blue (Corning) exclusion using a hemocytometer, and then plated in 96-well tissue culture-treated plates (5,000 or 10,000 cells/well), in Corning Costar 12-well tissue culture-treated plates (80,000 cells per well), or on 22 x 22 mm coverslips (7,500 cells/cover slip), and allowed 24-48 hours to adhere. For live cell imaging, H9c2 cells were seeded on coverslips. At least two days prior to seeding, 30 mL or more of a 2M NaOH in reverse osmosis water solution was prepared. Fresh coverslips were initially cleaned with mild detergent, rinsed copiously with dH_2O, and submerged in the 2 M NaOH for 2 hours on a rocker platform to remove contaminants from the glass. After the two-hour wash period, coverslips were soaked in the same 2 M NaOH solution overnight. The following day, the coverslips were

rinsed copiously with dH_2O and stored in 70 % reagent alcohol until the day of use. Immediately prior to use, coverslips were sterilized by autoclaving for 30 minutes at 121 °C in a glass 100 mm Petri dish. One sterile coverslip was placed per single well of a 6-well plate and coated with 200 µL of 100 µg/mL sterile poly-*l*-lysine (MW > 150,000 Da; Sigma-Aldrich) in dH_2O for 10 minutes at room temperature, followed by copious rinsing with sterile dH_2O, and air drying. After drying, 200 µL of cell suspension (37,500 cells/mL) were placed onto the center of each coverslip. Cells were allowed to adhere and attach for two days under the desired culture condition; thereupon, seeded cells were treated analogously to microplate-seeded cells.

2.1.1 H9c2 Cardiomyoblast Differentiation

The H9c2 cardiomyoblast model is a widely utilized *in vitro* cardiotoxicity and mechanistic elucidation model, as the cells can recapitulate the electrophysiological and biochemical nuances of cardiac muscle[203]. Despite the ability to differentiate, however, most studies utilize the stock undifferentiated H9c2 cardiomyoblast model for toxicity testing[204]. In order to promote differentiation, the culture medium was replaced with fresh DMEM + 1 % FBS with 10 nM retinoic acid (Stock 50 mM retinoic acid (Sigma-Aldrich) in sterile DMSO (ATCC) under 100 % nitrogen) on the second day post-seeding; medium was changed as described in *Figure 1* for the five days prior to experimentation[65,66,86]. The prevalence of differentiation among H9c2 cardiomyoblasts is expected to be approximately 25-27 %[73], and was checked visually via light microscopy in order to confirm morphological changes and general cell health.

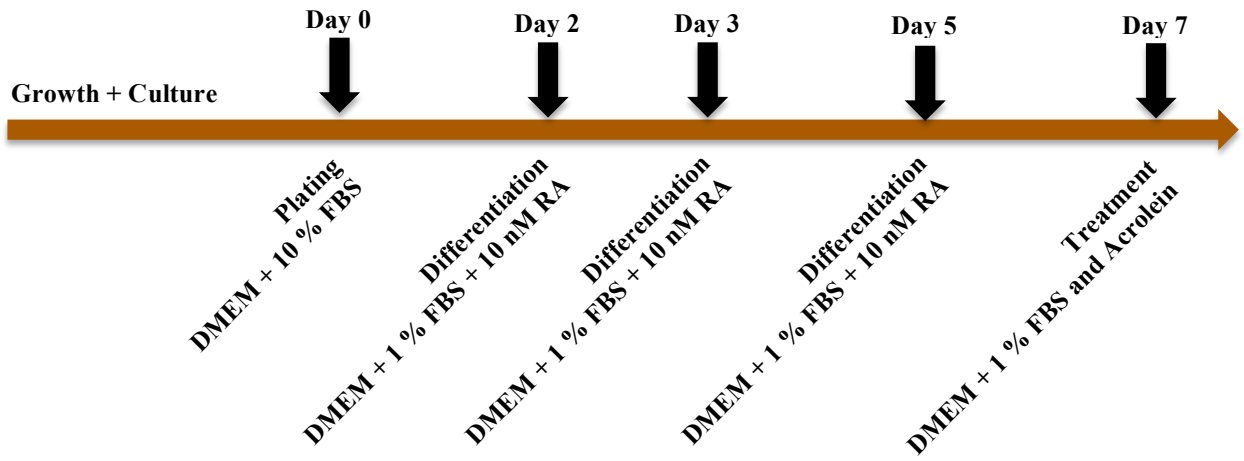

Figure 1. H9c2 Differentiation Scheme. Cultured cells were subdivided at 75-80 % confluency and plated at specific densities, depending on plate geometry or if on coverslips (See specific Methods). Thereafter, cells were differentiated according to the scheme above while maintained within their respective oxygen tension, e.g., 20.1 or 5 %, either under open atmosphere or under an oxygen-controlled environment.

2.1.2 TCA and Glycolytic Substrate Media

From a stock powder DMEM (Sigma-Aldrich) without D-glucose, L-glutamine, sodium L-pyruvate, sodium bicarbonate, and phenol red, a 1.11 X medium, denoted pre-basal medium, was made containing (In mM): 1.0 glucose, 0.12 pyruvate, 0.6 glutamine, and 0.25 glutamate (All Purchased from Sigma-Aldrich), when diluted to 1X strength using sterile ddH_2O. The pre-basal medium was sterilized via vacuum filtration through a 47 mm polyethersulfone (0.2 μm pore; ≥ 150 μm to < 200 μm thickness; Millipore; Billerica, MA) membrane; the solubilized medium was then be supplemented with 1 % (v/v) fetal bovine serum up to the working pre-basal medium with a concentration of ≈ 1.05 X. Individual substrate media were formulated from the working pre-basal medium by aliquoting aseptically 95 mL into sterile 100 mL media culture bottles, followed by addition of required substrate volume/weight in order to attain the desired TCA/glycolytic substrate concentration denoted in *Table 1*; the remaining portion of the 5 mL volume was composed of sterile ddH_2O and added to the original 95 mL working pre-basal

medium via a 10 mL syringe filtered through a syringe-driven 0.22 μm PES filter (33 mm diameter; Millipore), bringing the final substrate-specific medium to 1X strength at 100 mL. The exact concentrations of TCA and glycolytic substrates in each respective substrate medium are shown explicitly in *Table 1*. The medium closest in concentration to rat blood for TCA substrates and glucose was supplemented with 5.0 mM glucose in addition to standard concentrations of TCA substrates found in blood. For the purpose of standardizing labeling, the 5.0 mM glucose group were henceforth designated as "rat physiological" and abbreviated as "RP". Basal RP medium substrate components were determined as approximately 0.12 mM for pyruvate[194-196], 0.6 mM for L-glutamine, 0.25 mM for L-glutamate, and 5.0 mM for glucose[54].

2.1.3 Acrolein Treatment

Acrolein (90 % w/v acrolein with 0.3 % w/v hydroquinone in sterile ddH_2O) and pure hydroquinone were purchased from Sigma-Aldrich. Acrolein was diluted in either low-serum differentiation DMEM or TCA/glycolytic substrate medium immediately prior to use. Controls received a similar dilution of freshly prepared hydroquinone (0.3 % w/v stock solution in sterile ddH_2O water) in order to adjust for hydroquinone stabilizer (0.25-0.35 % w/v). Unless otherwise stated, cells were exposed to concentrations of acrolein ranging from 0.5 to 250 μM for thirty minutes, after which the complete medium volume was aspirated and replaced with acrolein-deficient medium (Washout) or protocol specific buffers/reagents.

Table 1: DMEM Composition and TCA Substrate and Glucose Supplementation

	Medium Designation								
	Rat Physiological	Glucose-Deficient	Glucose 10 mM	Pyruvate 1.0 mM	Pyruvate 2.5 mM	Glutamine 5.0 mM	Glutamate 1.0 mM	α-Keto-glutarate 5.0 mM	Low-Serum DMEM
Minerals/amino acids/vitamins	*See Appendix 2: Dulbecco's Modified Eagle's Medium*								
FBS	1.0 % v/v Fetal Bovine Serum								
Penicillin-streptomycin	100 I.U./mL Penicillin, 100 (µg/mL) Streptomycin								
d-Glucose	5.0 mM	*1.0 mM*	*10 mM*	5.0 mM	5.0 mM	5.0 mM	5.0 mM	5.0 mM	25 mM
Pyruvate	0.12 mM	0.12 mM	0.12 mM	*1.0 mM*	*2.5 mM*	0.12 mM	0.12 mM	0.12 mM	1.0 mM
L-Glutamine	0.6 mM	0.6 mM	0.6 mM	0.6 mM	0.6 mM	*5.0 mM*	0.6 mM	0.6 mM	2.0 mM
L-Glutamate	0.25 mM	0.25 mM	0.25 mM	0.25 mM	0.25 mM	0.25 mM	*1.0 mM*	0.25 mM	-
α-Ketoglutarate	-*	-*	-*	-*	-*	-*	-*	*5.0 mM*	-

**α-Ketoglutarate is not a typical constituent of DMEM, nor found in significant quantities (< 0.1 mM in human serum)[205]. At the selected concentration of 5.0 mM, α-ketoglutarate was subsequently found to interact with MTT reactivity, as described below. Therefore, media composites do not contain basal concentrations of α-ketoglutarate.*

2.2 Endpoint Analysis and Quantitation

2.2.1 Unbound Acrolein Determination

All reagents utilized for derivatization and protein precipitation were purchased from Fisher (Pittsburg, PA). Unbound acrolein concentration determination was performed in accordance with Baumann and colleagues [21]. Low serum DMEM (DMEM + 1 % FBS) supplemented with acrolein or hydroquinone was combined with one volume equivalent of derivatization solution containing 6 mg/mL m-aminophenol and 6 mg/mL hydroxylamine HCl in 1 MCl, and boiled for 30 minutes at 95 °C protected from light. Thereafter, samples were vortexed briefly and allowed to come to room temperature for 10 minutes. Upon cooling, 200 µL of derivatized sample were abstracted and sequentially combined with 0.4 volume ice-cold 2 % w/v $ZnSO_4$ (Fisher) in ddH_2O, 0.4 volume room temperature saturated barium hydroxide in ddH_2O, and 0.2 volume ice-cold hydrochloric acid; insoluble protein and barium sulfate complexes were cleared by

centrifugation (16,000 x g; 5 minutes; room temperature) followed by supernatant recovery. Finally, sample supernatants were assayed for fluorescence (Emission λ 328/40; Excitation λ 528/20) in microplate format using the Synergy HT fluorescent microplate reader (BioTek; Winooski, VT) integrated with the KC4 data acquisition software (BioTek). Known concentrations of acrolein were diluted in medium to serve as calibration standards in calculating sample acrolein concentrations.

2.2.2 MTT Metabolism and Cell Viability

The reduction of 3-(4,5-dimethylthiazol-2-yl)-2,5-diphenyltetrazolium bromide (MTT) to an insoluble blue formazan salt was first described by Mosmann[206], and will serve as a measure of metabolism and viability. While the exact composition and partition of metabolic system(s) responsible for MTT reduction remains elusive [207], the proportional reduction of MTT to formazan as a function of viable cells confers the method's value to assessing both viability and general cell metabolic capacity. The MTT reagent is prepared by solubilizing pure MTT powder (Sigma-Aldrich) in 1X D-PBS to a concentration of 5 mg/mL; non-solubilized MTT powder was removed by sedimentation. Solubilized MTT reagent may be stored for up to one year in aliquots frozen at -20°C, when protected from light.

H9c2 cells were passaged, and diluted in order to seed 96-well microplate(s) at 5,000 cells/well for samples; a simultaneous standard curve of varying H9c2 cell densities (0 cells to 7,500 cells per well) was established in order to assess for viability in preparation for differentiation up to the point of treatment. Thereupon, the medium was completely aspirated and replaced with 100 μL of acrolein-containing or vehicle (Hydroquinone-containing) medium for 30 minutes, followed with or without a washout period in respective acrolein- and

hydroquinone-deficient medium. In trials without a washout period, MTT reduction was initiated directly after treatment. In trials with a washout period, each well was aspirated of acrolein-containing medium, washed with 150 µL D-PBS, and replaced with respective medium for 2 hours. Viability assessment was performed by incubating cells in 100 µL of a 1:9 MTT reagent:respective acrolein-deficient medium for 2.5-3 hours at 37 °C. Formazan crystal development was checked via brightfield microscopy to ensure assay compliance. If sufficiently developed, wells were completely aspirated of medium and dried via inversion, followed by solubilization of formazan crystals in 100 µL DMSO (Fisher). Thereafter, homogenization was ensured via gentle mixing for ten minutes and quantified at 570 nm using a microplate spectrophotometer.

2.2.3 Poly(ADP-ribose) Polymerase Activity

H9c2 cells were maintained and subdivided as described above. After passaging, H9c2 cells were seeded at 80,000 cells per well in 12-well tissue culture-treated plates and allowed 48 hours for attachment prior to differentiation. On the day of treatment, 25 µM dilutions of acrolein or hydroquinone controls in RP medium were made to accommodate a 800 µL per well treatment volume. After 5 or 15 minutes of exposure (*See Results*), wells was aspirated of medium, washed with 1,000 µL of ice-cold 1X D-PBS, and lysed in 100 µL of PARP lysis buffer containing; 50 mM Tris-HCl (pH 8.0; Fisher), 1.0 % Triton X-100 (Sigma-Aldrich), 400 mM NaCl, 2 mM $MgCl_2$ (Fisher), 100 ng/µL BSA (Pierce; Rockford, IL), 1 mM D-*l*-1,4-dithiothreitol (Fisher). Lysed cells were incubated for 25 minutes on ice. Thereafter, the total volume lysate was moved into sterile 0.6 mL microcentrifuge tubes, from which a 5 µL sample was removed and combined with 45 µL 0.9 % (w/v) saline in order to quantify total protein via the Bradford method[208].

96-well high-binding microplates (Perkin Elmer; Waltham, MA) used for PARP activity detection were prepared in-house. Microplates were coated with 25 μg of fraction V histones (MP Biologicals; Santa Ana, CA) in a bicarbonate/carbonate buffer (pH = 10.5) per well, and allowed to attach overnight at 4 °C. The following day, wells were washed twice with 1X Dulbecco's modified phosphate buffer saline (Without calcium or magnesium) supplemented with 0.05 % v/v Tween-20 (D-PBSTw; Fisher), followed by two washes with 1X D-PBS without Tween-20. Wells were then blocked overnight at 4 °C with a 3 % w/v solution of bovine serum albumin composed of 3 parts pre-made 10 % BSA blocking solution (Pierce) and seven parts 1X D-PBS without calcium or magnesium.

On the day of PARP activity detection, the blocking solution was dispensed from wells via inversion, followed by gentle tapping on Kim-Wipe, and washed twice each with D-PBSTw and D-PBS consecutively. An eight-point calibration curve composed of purified high-specific activity PARP enzyme (Trevigen, Gaithersburg, MD) from 10 mU to 5 U per well in a buffer containing 50 mM Tris, 10 mM $MgCl_2$, 100 μg/mL bovine serum albumin, 0.1 % Triton-X100, pH adjusted with HCl to 8.00, allowed quantification of samples. 25 μL of whole-cell lysate or PARP activity standard were plated per well in triplicates, to which an equal volume of the reaction buffer containing 50 mM Tris, 10 mM MgCl2, 100 μg/mL, 0.1 % Triton-X100, 4 ng/μL sheared herring sperm DNA (Promega; Madison, WI), 4 mM biotinylated NAD^+ (Trevigen), pH 8.00, was added, followed by a two hour incubation at room temperature. Wells were then washed thrice with each D-PBSTw and cleared with three washes D-PBS. Stock streptavidin-conjugated horseradish peroxidase (Pierce) was diluted to 25 ng/mL in a D-PBSTw buffer containing 100 μg/mL bovine serum albumin immediately prior to completion of washes. After completion of washes, 100 μL of diluted streptavidin-conjugated horseradish peroxidase were

added per well, and incubated for 1 hour at room temperature. Wells were again washed and cleared in D-PBSTw and D-PBS trice, respectively, prior to addition of 50 µL of Turbo-3,3',5,5'-tetramethylbenzidine ELISA solution (Pierce) per well and incubation for 25 minutes at room temperature protected from light. The reaction was stopped with 75 µL of 0.2M HCl and read on microplate reader (µQuant; BioTek) at 450 nm with data acquisition using the KC Junior software platform (BioTek). Results are expressed as control-normalized PARP activity derived from PARP activity per µg whole-cell lysate.

2.2.4 Mitochondrial Membrane Potential

JC-1 (5,5',6,6'-tetrachloro-1,1',3,3'-tetramethylbentimidazolylcarbocyanine iodide) dye use as a fluorometric probe to monitor mitochondrial potential was described by Lan Bo Chen and colleagues[209]. JC-1 is a delocalized lipophilic cation that distributes within the mitochondrion and forms aggregates in a voltage potential-dependent manner. Because potential measures can be performed on a ratiometric basis of the J-aggregate to the monomer, potential measurement remains independent of the individual mitochondrion's size, shape, or density. Evidence suggests that neither rhodamine 123 nor DiOC6(3) are sensitive markers of mitochondria membrane potential changes, especially under apoptosis or mitochondrial uncoupling[210]. The monomeric dye form has an emission maximum of ≈526 nm. The dye, at higher concentrations or potential, forms red fluorescent J-aggregates with an emission maximum at 590 nm (*Table 2*).

JC-1 powder (Adipogene; San Diego, CA) was solubilized in anhydrous neat DMSO to a concentration of 10 mM immediately prior to experimentation, and stored in aliquots at -20°C until use. Immediately prior to labeling, a working solution of 20 µM JC-1 labeling solution was

prepared in low-serum DMEM. The incubation medium was combined with an equal volume of JC-1 labeling solution for 15 minutes at 37 °C; as a positive control of $\Delta\Psi_m$ dissipation, a solution containing 200 μM carbonyl cyanide m-chlorophenyl hydrazine (CCCP; Sigma-Aldrich) was combined in equal parts with the 20 μM JC-1 labeling solution (Final CCCP concentration 100 μM). For qualitative measurements, cells were cultured and differentiated on coverslips. After preparation of labeling reagents and CCCP, slides were incubated with the labeling solution after copious washing with D-PBS as noted above. Thereafter, coverslips were washed with cell culture medium lacking JC-1, and mounted in an aqueous medium for fluorescent microscopy.

Table 2. JC-1 Label Parameters

Dye Form	Excitation Maximum (nm)	Emission Maximum (nm)	Filter Set[a]
Monomeric JC-1 Dye	514	529	FITC
J-aggregate form of JC-1	≈485-585	≈590	Cy5

[a]Alternative filter set: Both monomer and aggregate can be viewed simultaneously with a standard LP fluorescein filter set.

For quantitative analysis of $\Delta\Psi_m$, CCCP and JC-1 were prepared as above; however, H9c2 cells were plated at 10,000 cells/well prior to differentiation. On the day of examination, wells were aspirated completely of medium and promptly replaced with 200 μL of D-PBS containing calcium and magnesium. 150 μL of D-PBS was then aspirated, and 50 μL of 2X JC-1 labeling solution added, followed by a 15-minute incubation at 37 °C. Each well was then washed with 150 μL culture medium twice, ensuring wells retained 50 μL medium to avoid drying out. The final wash was aspirated leaving 50 μL, to which and equal volume of 2X

hydroquinone-only (Controls) or 2X acrolein (50 μM)-supplemented medium. With co-exposure to small molecules, acrolein- or hydroquinone-supplemented treatment media were supplemented with either 2X small molecule (200 μM olaparib; 10 μM CTZ, 10 mM EGTA) or respective small molecule vehicle prior to incubation at 37 °C. At one, two, and four hours post-treatment, cells were analyzed for J-aggregates and monomers with the Synergy HT microplate reader with filter sets composed of two narrow-band filters: J-aggregate fluorometric measurements (Ex/Em 535/20 nm and 590/35 nm) and JC-1 monomers (Ex/Em 485/20 nm and 528/20 nm). Results are presented as the ratio of J-aggregate-to-monomer fluorescence normalized against the respective time-matched controls.

Olaparib and CTZ were purchased from APExBio (Houston, TX) and EGTA was purchased from Sigma-Aldrich. Stock solutions of olaparib and CTZ were made by solubilizing in sterile DMSO, while EGTA was solubilized in sterile ddH2O with pH adjustment to 7.4 using NaOH.

2.2.5 Calcium Conductance

Fluo-4AM incorporates the more intense fluorescein fluorophore, which operates at visible wavelengths resulting in decreased cellular autofluorescence than UV excitation fluorophores. All long-wavelength Ca^{2+} indicators use Ca^{2+} coupling chelation to inhibit intramolecular fluoroquenching via electron transfer, resulting in emission intensity changes with negligible excitation/emission shifts. Acetoxymethyl ester conjugation of the calcium fluorophore indicator, while increasing permeabilization and specific intracellular localization, decreases dye solubility. Pluronic F-127 allows for homogenous dispersion of large ester-

containing molecule dyes which subsequently increases fluorescent amplitude and a more rapid esterase hydrolysis[211,212].

A stock 2.5 mM solution of Fluo-4AM (Molecular Probes; Waltham, MA) in sterile DMSO (ATCC) was prepared and stored in aliquots at -20 °C. Immediately prior to use, Fluo-4AM in DMSO was combined in an equal volume of 20 % Pluronic F-127 (Pierce), and subsequently diluted to 5 μM in D-PBS containing calcium and magnesium. Cells were loaded with Fluo-4AM for 30 minutes, and then be cleared of Fluo-4AM-containing D-PBS with triplicate washes with 1X D-PBS, and allowed to de-esterify for 30 minutes at 37 °C prior to treatment with acrolein in RP medium. For qualitative assessment, the cells were washed with 1X PBS, inverted upon two pieces of paraffin, sealed with melted VALAP, and imaged live. In order to determine the origin of calcium influx, dosing media contained either CTZ (5 μM)[113] or EGTA (20 mM) to determine the role of extracellular calcium influx.

For quantitative measures, cells were exposed analogously to those described above, except cells were plated in 96-well microplates at 10,000 cells/well prior to Fluo-4AM assessment. Directly after Fluo-4AM de-esterification and subsequent treatment, cells were assessed quantitatively every thirty seconds, for a total of thirty minutes using the Synergy HT fluorescent microplate reader with excitation/emission filters 485/20 nm and 528/20 nm, respectively. In quantitating each well, the lowest RFU value served as the respective blank, followed by normalization against small-molecule exposed cells devoid of acrolein at each respective time point; quantitated as a percent of maximal response for which the ionomycin control served as the 100 % response; and normalized against vehicle-only containing hydroquinone-exposed cells.

2.3 Equipment

2.3.1 H9c2 Cardiomyoblast Culturing

H9c2 cells were maintained under standard culture conditions in the Forma™ Series II 3010 water-jacketed CO_2 incubator (Thermo Fisher; Waltham, MA) with a pressure-regulated (15 psig) CO_2 supply. Ambient conditions of standard culture conditions included a humidified 37 °C, 5 % CO_2/95 % atmosphere (Standard culturing conditions). For culturing under reduced oxygen conditions (Physiologically relevant), cells were incubated in the Forma™ Series II 3030 water-jacketed oxygen-controlled CO_2 incubator, linked to a pressure regulated (15 psig) nitrogen (99.99 % pure; Airgas) tank and to a similarly regulated (15 psig) CO_2 tank. The ambient conditions for H9c2 maintenance was a humidified 5 %/5 % oxygen/CO_2 balance nitrogen 37°C atmosphere, and verified using the Traceable® Digital Oxygen Meter system (Control Company; Friendswood, TX). The oxygen content under standard culture conditions was verified at 20.1 ± 0.1 % using the Traceable® Digital Oxygen Meter system. Similarly, the oxygen tension of the acrylic exposure chamber described in *Table 3* and *Appendix 3* was measured and verified at 5 % during complex procedures in real-time in order to allow oxygen concentration modulation via nitrogen purging when necessary to maintain the desired 5 % oxygen atmosphere.

Prior to execution of procedures in the acrylic exposure chamber, the main chamber was purged with nitrogen to offset atmospheric oxygen. However, since the ante-chamber provided the only access to the main chamber when passing cells/materials between the main chamber and the maintenance incubator, the oxygen concentration displacement in the main chamber with air

trapped within the ante-chamber required quantification. Given the parameters estimated, a rudimentary estimation of percent oxygen offset of the main chamber upon item passage, and

Table 3. Acrylic Exposure Chamber Parameters

	Width	Depth	Height	Approximate Volume	Percent Controlled Volume*
*Main Chamber***	89.54 cm	60.33 cm	44.45 cm	240,100 cm^3	-
Ante-chamber	20.32 cm	20.32 cm	15.24 cm	6,300 cm^3	2.6 %
*Main Chamber Less Ante-chamber***	-	-	-	235,800 cm^3	97.4 %
Total Controlled Volume†	-	-	-	242,100 cm^3	100 %

*Control Volume pertains to the volume enclosed within the main chamber or ante-chamber.
**The Main Chamber measurements include those of the core height, width, depth measurements. Since the ante-chamber protrudes into the main chamber (Approximately 4,300 cm^3), no associated Percent Controlled Volume was attributed to this measurement. Thus, the estimated volume of the main chamber considering the ante-chamber displacement is exacted by subtracting the protruding ante-chamber from the core main chamber volume, denoted by Main Chamber Less Ante-chamber.
† Sum of Main Chamber Less Ante-chamber and Ante-chamber.

subsequent ante-chamber atmosphere introduction into the main chamber, may be summarized by the following equation:

$$\%O_{2C}\ Offset = ((\%O_{2C} * V_C) + (\%O_{2A} * V_A)) - \%O_{2C}$$

Where:

$\%O_{2C}$ = Initial Main Chamber O_2 Percent

V_C = Percent volume of Main Chamber

$\%O_{2A}$ = Initial Ante-chamber O_2 Percent

V_A = Percent volume of Ante-chamber

Assuming ante-chamber oxygen percent as 20.9-21.0 % typical of standard oxygen percent at sea level, and the ideal main chamber oxygen percent during testing as 5.0 %, the theoretical oxygen percent offset is equal to 0.4 %. Validity of the theoretical offset oxygen percent was assessed by an experimental derivation of this parameter prior to experimentation. Additionally, the oxygen infiltration rate (Oxygen retention decay) into the main chamber, expressed as percent oxygen increased per hour, required experimental derivation, in order to assess whether long-duration procedures (> 1 hour) could be performed without maintenance purging. Experiments measuring ambient oxygen concentration were performed utilizing the using the Traceable® Digital Oxygen Meter.

2.3.2 Spectroscopy

For all UV/Visible spectrophotometric quantification, the BioTek μQuant spectrophotometer with 96-well carrier was utilized. Similarly, the KCJunior data reduction software was utilized in order to interface with the μQuant. For methods not requiring tissue culture-treated plates (Bradford protein quantification and acrolein concentration determination), high binding Grainger 96-well plates or, for the PARP activity assay, 96-well high binding microplates were used. For fluorescent spectroscopy, the BioTek Synergy HT interfaced with the KC4 data reduction software was utilized. The Synergy HT is affixed with eight individual narrow bandwidth filters: four excitation and four emission filters. The excitation filters are as follows: 360/40 nm, 485/20 nm, 530/25 nm, and 590/20 nm. The emission filters are as follows: 460/40 nm, 528/20 nm, 590/35 nm, and 645/40 nm. The appropriate combination of excitation and emission filter sets was selected based on the specific wavelengths required for each respective fluorescence application.

2.3.3 Microscopy

A combination of brightfield and fluorescent microscopy was utilized in the completion of this project. For brightfield microscopy, a Leitz Labovert FS (Leica; Wetzler, Deutschland) inverted microscope was utilized, supporting a 6V, 20W Xenon lamp housing. The microscope is affixed with the following objectives: Leitz Wetzlar 4X/0.12NA 160/- (519759); Leitz Wetzlar 10X/0.25NA EF L Phaco 1a 160/-; and Leitz Wetzlar 20X/0.30NA EF L Phaco 1a 160/-. The Leitz Labovert FS inverted microscope was used for tasks within routine culture and cell isolation counting.

For fluorescent microscopy, a Leitz LaborLux S (Leica) affixed with the 3-λ Ploemopak fluorescent microscopy tube (Factor 1X) and the Leitz Wetzlar Type 307-148.002 mercury arc lamp housing. A LEP^{LTD} # 990002 50W Arc Lamp HBO AC power supply provides power to the Osram 50W HBO mercury arc lamp (L2 voltage group; 34-39V/1.45A) for fluorophore excitation. The LaborLux S is fitted with the following objectives: Leitz Wetzlar 10X/0.25NA PLAN 160/-; Leitz Wetzlar 25X/0.50NA Phaco 2 EF 160/0.17; Leitz Wetzlar 40X/0.65NA Phaco 2 EF 160/0.17; and Leitz Wetzlar 100X/1.25NA Phaco 3 EF 160/0.17. Supplied with the 3-λ Ploemopak, the following filter cube assemblies allow illumination of fluorophores (*Table 4*).

2.4 Statistical Analyses

All estimates were reported as the arithmetic mean. Except where noted, all uncertainty measures correspond to the respective standard error of the mean. Statistical analyses were performed using SPSS version 22 (IBM Corporation; Armonk, NY) and R version 3.3.1 (R Foundation for Statistical Computing; Wien, Österreich) software platforms. Prior to statistical

Table 4. Filter Sets for LaborLux S Microscope Affixed with 3-λ Ploemopak Binocular Incident Light Fluorescence Illuminator

Filter Set	Cube ID	$\lambda_{excitation}$ (nm)	Dichroic Mirror	Suppression Filter	Filter Set†	Dyes
A/DAPI	1582	340-380	400	425 LP	DAPI	**Hoechst 33342**
I3	513719	450-490	510	515 LP	FITC	**Fluo-4, JC-1**
N2	513609	515-560	580 LP	590 LP	Cy5	**JC-1**

†General equivalency to associated cube.

analyses, pertinent assumptions for parametric statistical comparisons were made regarding normality about the mean, using the Shapiro-Wilk's test[213], and for homogeneity of distribution variance, using the Levene's equivalence of variance (Homoscedasticity) test [214]. When both statistical assumptions were valid, parametric tests were performed, e.g., one-way ANOVA coupled with Student's t-test comparisons. Otherwise, equivalent Mann-Whitney U tests under the violation of parametric distribution assumptions, e.g., heteroscedasticity of variance and/or non-normality, were performed. Significance was assumed to be based on the statistical difference of arithmetic mean scores, and must meet a probability of observation difference level less than 0.05, i.e., 5 %. Similarly, non-normality and heteroscedasticity were presumed when a statistical difference less than 5 % ($p < 0.05$) was observed for individual Shapiro-Wilk's or Levene's tests, respectively.

For acrolein-dependent IC_{50} value derivations across substrate-enriched media, the statistical program R version 3.3.1 (R Foundation for Statistical Computing; Wien, Österreich) with the statistical Package "drc"[215] was utilized for distribution-specific estimate derivations. Initially, a model selection algorithm was performed in order to characterize curve parameters of

the acrolein concentration-response in H9c2 cells among curve parameters accepted within the toxicological literature, e.g., Log-linear, Weibull, etc., based on residual error minimization and Akaike information criterion (AIC) maximization for final IC_{50} derivation and associated standard error estimates. In order to make comparisons viable, the distribution type, for which residual error was most adequately explained for both oxygen tension cultures simultaneously, was selected for estimate modeling; where necessary, single substrate groups were modeled independently using the three-parameter Weibull distribution parameters when standard error estimates were returned as "N/A", denoting residua were infinitely large or zero. Thereafter, statistical comparisons of substrate-specific IC_{50} values were performed in R via a Student's t-test or Mann-Whitney U test.

The K_i value derivation for 3-aminobenzamide competitive inhibition of PARP was also performed utilizing the "drc" Package in R version 3.3.1. Given the simple system and competitive binding, the three-parameter log-logistic distribution was pre-selected for parameter estimation. Results of K_i estimation are presented in *Appendix 4*.

CHAPTER THREE:

RESULTS

3.1 Method Validation

Prior to data generation, validation of specific methods must be attained in order to demonstrate analyte representation and applicability for the model system. Firstly, analyte specificity with respect to acrolein determination must be ensured. The spectrophotometric absorption signature of the derivatization product, 7-hydroxyquinoline, must be demonstrated, as well as assurance of precise acrolein quantitation within a dynamic range. Further, the oxygen concentration infiltration rate into the constructed acrylic exposure chamber must be performed in order to determine whether retention and stability of reduced oxygen conditions will suffice for routine maintenance procedures and for *in vitro* treatment regimens. Since the MTT assay is not routinely performed in differentiated H9c2 cultures, the method must be validated for use within this model under the experimental parameters. Finally, detection and quantitation of intracellular calcium conductance, as well as qualitative assessment of $\Delta\Psi_m$, must be validated in the differentiated H9c2 model prior to quantitative measurement and analysis with respect to acrolein treatment and proposed intervention strategies.

3.1.1 Acrolein Determination and Decay in Aqueous Medium

In order to ensure repeatable exposure metrics with respect to acrolein concentrations, the time-dependent decay rate in low serum medium establishment was imperative to minimize

inter-trial heterogeneity, should decay outpace treatment preparation. Prior to temporal acrolein decay determination, the fluorometric derivatization of acrolein to 7-hydroxyquinoline described by Alarcon[20] using 3-aminophenol in the presence of hydroxylamine must be validated in the current system, and the limit of detection/quantification determined. The method by Alarcon was modified in order to account for measurement in low-serum DMEM and for protein precipitation via zinc sulfate/saturated barium hydroxide as per Baumann and colleagues[21]. Additionally, protein concentration of low-serum medium was quantified to demonstrate the efficacy of protein precipitation via the chosen method and to resolve heterogeneities in acrolein degradation trends with respect to initial acrolein concentrations.

Protein quantitation of low-serum DMEM revealed an approximate concentration of 1,600 ng/μL (SD: 320 ng/μL) as reported by the BCA protein quantification method; protein precipitation via the zinc sulfate-barium hydroxide method resulted in removal of 63 % as reported by the BCA method; incubations with zinc sulfate exceeding 30 seconds on ice did not produce higher efficacy in protein removal (Data not shown). Protein precipitation by this method was presumed to remove 63 % of protein, despite ≥ 90 % removal efficiency among standards containing 2,000 ng/μL purified bovine serum albumin containing used for calibration curve composition.

Methodological validation for acrolein determination was established for the instrument system available in our laboratory based on the recommendations outlined in the 1996 International Council for Harmonisation of Technical Requirements for Pharmaceuticals for Human Use (ICH) *Validation of Analytical Procedures: Methodology*[216]. In order to assure specificity of derivatization, a spectral scan of the resultant derivatized acrolein in D-PBS (pH 7.4) was performed and matched to those described in Alarcon[20]. Spectral signatures taken

demonstrate an absorption maximum between 344-352 nm, with a lesser secondary peak centered about 303-305 nm (*Figure 2*); this absorption pattern is consistent with the results published by Alacron[20] with respect to acrolein derivatization at pH 7.0, denoting successful derivatization of acrolein to 7-hydroxyquinoline in the current system. The magnitude of the peak decreased with decreasing initial acrolein concentrations (A → G) as expected for transmission spectroscopic measurements.

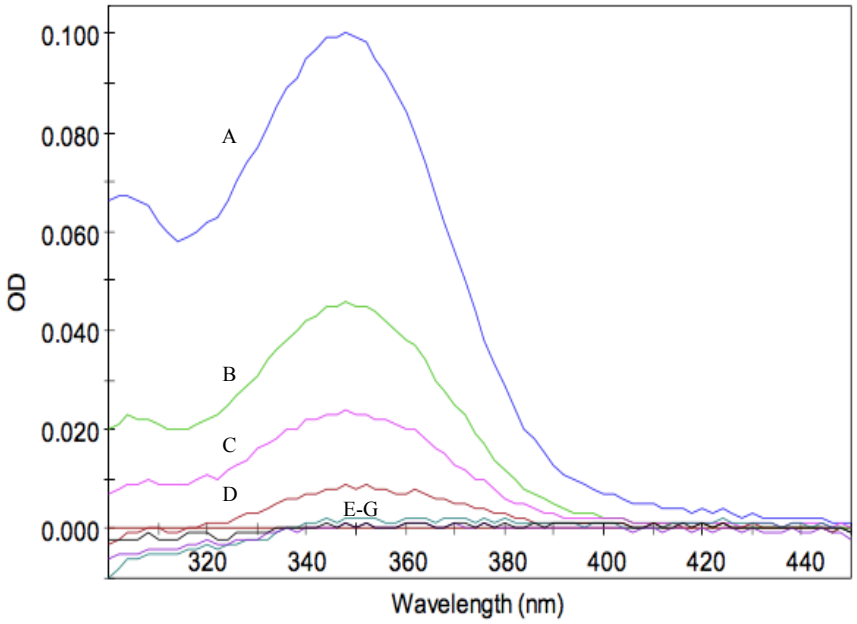

Figure 2. Spectral Scan of Derivatized Acrolein. D-PBS was spiked with seven concentrations of acrolein, in addition to a vehicle-only blank, prior to derivatization with 3-aminophenol in the presence of hydroxylamine HCl. Thereafter, 200 µL of derivatized solution were dispensed per well of a 96-well microplate and scanned from 300-450 nm at 2 nm increments using the µQuant spectrophotometer. The resultant scans are blanked from the D-PBS-only vehicle, and presented above with the following designations: A) 100 µM; B) 50 µM; C) 25 µM; D) 12.5 µM; E-G) in order: 6.25 µM, 3.125 µM, and 1.5623 µM (These three concentrations proved BDL in later testing, and were combined in designation here for clarity). The blank, D-PBS only sample is designated as the 0.000 OD horizontal axis. Each scan is composed of data from a single well.

Approximate linearity was shown up to the highest concentration of 250 µM along a seven-point standard curve (*Figure 3*). Blanked RFU fluorescence was highly correlated with acrolein concentration (R = 0.9998) with an equally high coefficient of determination (R^2 =

0.9997). To confirm hydroquinone contained within the stock solution did not apparently interfere with the acrolein-associated fluorescent signal, a separate test was performed whereby LS medium was spiked with a high concentration of hydroquinone above the analogous 250 µM acrolein dilution. At such a high concentration, hydroquinone did not produce a detectable fluorescent signal different than the low-serum DMEM blank (Data not shown), indicating adjustment for hydroquinone content was not necessary.

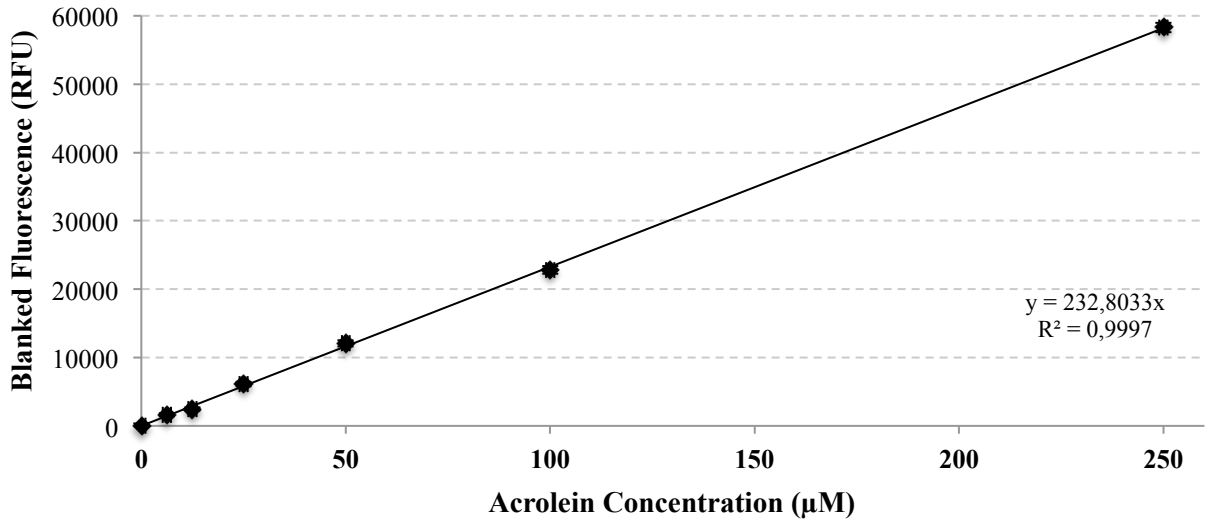

Figure 3. Representative Acrolein Quantification Calibration Curve. Low-serum DMEM was spiked with 250 µM of acrolein, and diluted serially prior to derivatization by 3 mg/mL 3-aminophenol in the presence of 3 mg/mL hydroxylamine HCl at 95 °C for 30 minutes. The standards were then deproteinated with 9.8 % w/v ice-cold zinc sulfate octahydrate, followed by barium hydroxide saturation to promote precipitation. Precipitates were removed by centrifugation at 16,000 x g for 5 minutes at room temperature. Samples from the supernatant were plated in 96-well assay plates, and quantified using the Synergy HT microplate reader via fluorescent capture using an excitation and emission filter set of 328/40 and 528/20, respectively. Each point consists of duplicate technical replicates with associated SD denoted by error bars (Too small to see visually).

The limit of detection and quantification for acrolein determination was established based on the standard deviation and slope of the response method aggregated across four independent 0-100 µM calibration curves for the purposes of LOD/LOQ derivations, as not all curves produced linearity up to 250 µM as clearly as presented in *Figure 3*. The detection limit was

determined as 3.3-fold the ratio of the standard deviation of the y-intercept and slope of the response derived from the calibration curve regression function.

$$LOD = \frac{3.3 * \sigma_{y-intercept}}{Slope}$$

The limit of quantitation was derived analogously to the LOD, except the multiplier of the standard deviation of the y-intercept and slope of the response was 10:

$$LOQ = \frac{10 * \sigma_{y-intercept}}{Slope}$$

Aggregated from four calibration curves, the LOD and LOQ of fluorometric acrolein determination via the derivatization method by Alarcon for our system were established as 2.2 ± 0.4 μM and 6.7 ± 1.2 μM (Mean ± SD), respectively. Validation of the LOD was performed during temporal acrolein decay measurements with a battery of low-serum DMEM samples supplemented with an initial acrolein concentration of 6.25 μM. Over the course of eight hours (Three independent trials), reduction in acrolein concentration medium samples initially spiked with 6.25 μM was not well-correlated with respect to time (Pearson Correlation Coefficient = 67.2 %) and concentration determinations were greater than the initial acrolein measurement at time zero, i.e., > 100 % initial, denoting high uncertainty in resolute acrolein concentration measurement below the derived LOQ. Therefore, the LOQ determination as 6.7 μM was presumed the valid LOQ for the system available, and values at or below 6.7 μM were henceforth denoted as below the limit of quantitation (≤ LOQ) for presentation purposes. For

samples below this value, for which numeric incorporation to quantitative data would be required, the replacement value was quantified as the LOQ divided by the square root of two.

Over the course of 24 hours, seven time-points spanning from 30 minutes to 24 hours, including the baseline time zero, were selected for determining the rate of acrolein decay in low-serum medium. Initial testing included measures only up to 8 hours, as acrolein in aqueous medium was expected to decay rapidly; later experimental protocols integrated an additional time-point measure to include 24-hour sampling. Therefore, only few measures were taken at the 24-hour time point (n =3); the results are summarized in the table below (*Table 5*). With respect to time, acrolein concentration did reduce incrementally up to 24 hours and demonstrated a slight dependency of decay magnitude on the initial acrolein concentration, i.e., depletion was inversely correlated with initial concentration, though this trend was not statistically significant ($F_{2,6}$ = 4.135; p = 0.074). Incidentally, the most rapid decay occurred within the first 30 minutes, after which the rate of decay decelerated. While degradations to 81-85 % of initial concentrations within 30 minutes were observed, the decay fraction did not differ with respect to the initial concentration; measures to 4 hours after addition to low-serum medium between low-serum media containing differing initial concentrations were not different ($F_{2,6}$ = 0.090; p = 0.915), denoting that resultant MTT reduction results after a 30-minute acute exposure should not be substantially confounded by differential decay across the proposed concentrations in low-serum DMEM below. At 24 hours, the remaining fraction of acrolein was 56.7 ± 3.8 %, 45.9 ± 1.8 %, and 41.0 ± 5.4 % for the initial concentrations of 250 μM, 50 μM, and 25 μM, respectively. The half-life in low-serum DMEM was greater than 8 hours, and greater than 24 hours at the high initial acrolein concentration of 250 μM. No values fell on or below the limit of quantitation during testing.

Table 5. Time-dependent Acrolein Degradation In Low-serum Medium at 20 °C

Initial Acrolein	Acrolein Remaining	0.5 Hour	1 Hour	2 Hours	4 Hours	8 Hours	24 Hours
250 µM	250 µM	210.3 ± 12.5 µM	215.6 ± 7.7 µM	197.7 ± 9.6 µM	168.4 ± 10.9 µM	148.8 ± 13.3 µM	147.4 ± 8.8 µM
	100.0 %	84.1 ± 5.0 %	86.2 ± 3.1 %	79.1 ± 3.8 %	67.4 ± 4.4 %	59.5 ± 5.3 %	56.7 ± 3.8 %
50 µM	50 µM	42.4 ± 2.5 µM	42.3 ± 2.1 µM	41.2 ± 2.6 µM	31.2 ± 1.2 µM	29.9 ± 1.2 µM	25.9 ± 3.0 µM
	100.0 %	84.8 ± 5.0 %	84.5 ± 4.3 %	82.5 ± 5.2 %	62.5 ± 2.4 %	59.7 ± 2.4 %	45.9 ± 1.8 %
25 µM	25 µM	20.3 ± 1.4 µM	19.3 ± 1.1 µM	18.6 ± 1.9 µM	15.3 ± 4.6 µM	13 ± 1.3 µM	12.3 ± 2.2 µM
	100.0 %	81.2 ± 5.7 %	77.3 ± 4.3 %	74.2 ± 7.8 %	61.1 ± 18.4 %	51.9 ± 5.2 %	41.0 ± 5.4 %

Each data point is composed of 3-5 replicates, depending on the time-point. Values are mean and percent remaining with associated SEM.

3.1.2 Acrylic Exposure Chamber Validation

Exposure chamber purge with 99.99 % pure nitrogen resulted in a reduction of internal oxygen concentration to 5.4 %, as the tank utilized was depleted in the process of purging. For the purposes of initial validation, the baseline oxygen concentration was established at 5.4 % for the retention decay with respect to time. Simultaneously, chamber temperature was recorded using the Traceable® Digital Oxygen Meter which has a built-in temperature probe. Oxygen measurements for the initial 3.5 hours demonstrated complete retention of established oxygen (5.4 %) over this time (*Figure 4)*, suggesting insignificant diffusion of oxygen into the main chamber through the environment interface seals. At time point 3 hours 40 minutes, the internally-facing ante-chamber door was opened, and then re-sealed to allow ambient air trapped within the ante-chamber to infiltrate and equilibrate with that of the main chamber; oxygen concentration measurements at time point 3 hours 50 minutes revealed an expected increase in oxygen concentration, which stabilized at 5.7 % - an increase of 0.3 % from the 5.4 % pre-ante-chamber opening. Therefore, the experimentally-derived oxygen concentration offset was determined to be 0.3 % when the main chamber was mixed with one volume of ambient air

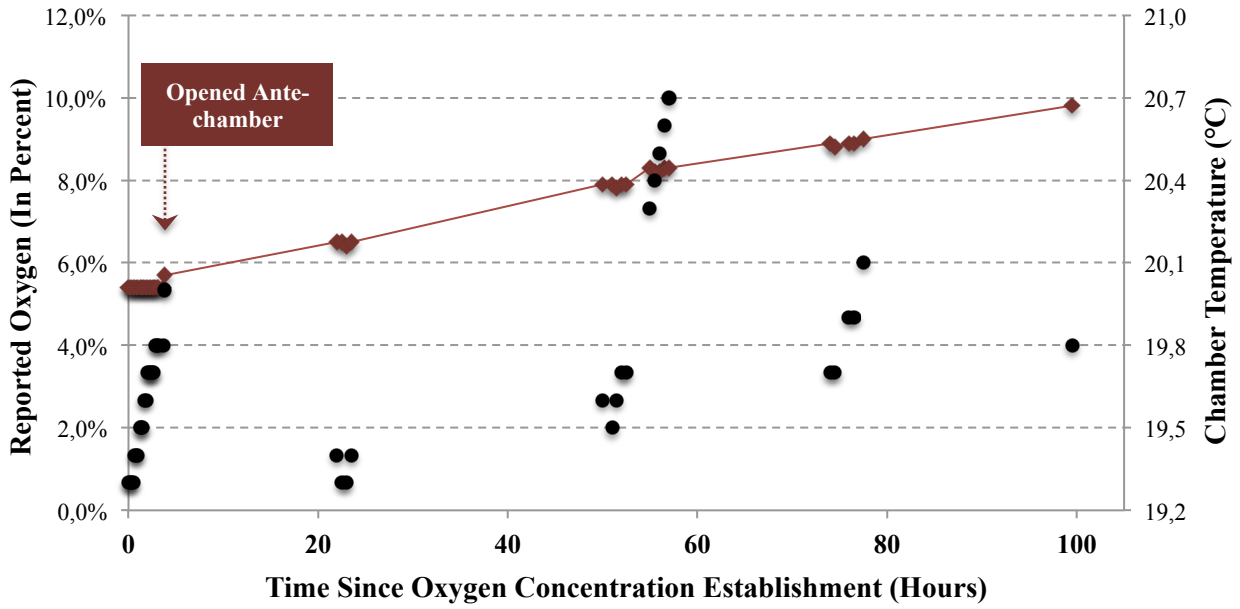

Figure 4. Acrylic Exposure Chamber Oxygen Retention Over Time. Initial validation of oxygen concentration retention over time was performed by purging the main chamber with nitrogen to a final concentration of 5.4 % mol/mol; real-time recordings of oxygen were taken via hand-held oximeter placed within the chamber and reported over 99.5 hours post-purging (Red Diamonds with Point-to-point Line). Simultaneously, the oximeter also reported ambient temperature and are presented here (Black Circles). Opening of the ante-chamber door leading into the main chamber resulted in an expected increase in main chamber oxygen concentration, as denoted above, after which a steady increase over time was observed.

(20.9-21.0 % oxygen-containing) contained within the ante-chamber, as opposed to the theoretical value of 0.4 % calculated using the $\%O_{2C}$ Offset equation presented above (*See Methods*). Repeated measurements resumed over 99.5 hours at sporadic intervals to determine the long-term low-oxygen concentration retention capacity and rate of decay. As seen in *Figure 4*, internal main chamber oxygen concentration increased approximately linearly over the duration of measurement with a final measurement of 9.8 % approaching 100 hours. Regressing the function of reported oxygen concentration against time beginning at the 3 hours and 50 minute time point (The time-point measurement after ante-chamber opening and internal oxygen concentration stabilization), the rate of low-oxygen retention decay with respect to time was estimated to be 0.045 % per hour (R^2 = 0.9847). These results denote adequate retention of a low-oxygen environment during the 1-4 hours required to complete medium changes, microplate

seeding, acrolein treatment, and MTT viability testing. Continuous, real-time oxygen measurements were taken during testing, as maintenance purging was required during procedures, particularly when samples and materials were passed through the ante-chamber at regular intervals during the testing period in order to ensure oxygen concentrations close to 5.0 % (Tolerance ± 0.5 %).

3.1.3 MTT Reduction Assay

In order to assess cellular viability using the MTT formazan reduction method developed by Mosman[206], the predictive power of the MTT assay in measuring the endpoint of interest must be validated for experimental conditions. Each set of seeded cells intended for acrolein treatment and metabolism/viability measurement was accompanied by an 8-point standard curve of known cell seeding densities plated in triplicate. As presented (*Figure 4*), the plating procedure results in a stable estimator of cells per well, even after the five-day differentiation period. While most investigations normalize treatment samples against the control proportionally with optical density, the presented quantification method allows derivation of sample cell counts over a range, which, for our system, departs from linearity above 2,500 cells per well. As such, measurements of minor cytotoxic insults resulting in low-magnitude alterations in MTT reduction metabolic competency would be underestimated should a two-point linear extrapolation be performed. These results denote the validity of utilizing the initial plating seeding method as a valid methodological approach for assessing number of MTT reducing-metabolically competent cells per well for the differentiated H9c2 cardiomyoblast cell line, and the use of a polynomial-derived regression function for quantification of cells over the range of

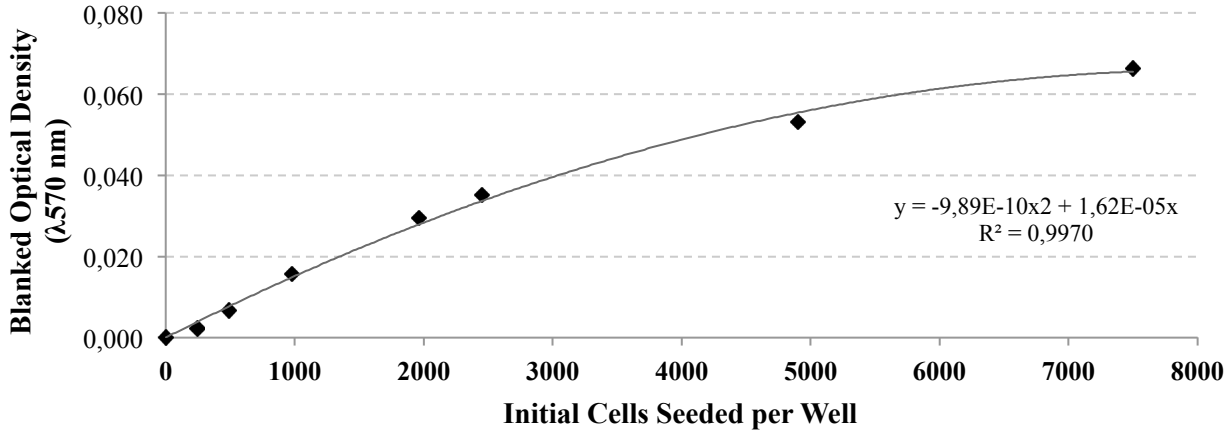

Figure 5. Representative Standard Curve of MTT Reduction Assay. H9c2 cells cultured under standard conditions were subdivided, counted via hemocytometer, and plated in a tissue culture-treated 96-well microplate at specified cell densities. On day two, cells were differentiated for five days as mentioned Methods section, prior to exposure to MTT tetrazolium salt for 3 hours at 37 °C under standard cell culture conditions. Thereafter, medium was aspirated and well allowed to dry for 10 minutes. Thereafter, 100 µL DMSO were dispensed per well and mixed for 10 minutes prior to absorbance reading on µQuant spectrophotometer.

0-7,500 cells per well provides higher fidelity in ascertaining low-magnitude toxicity in our system. With measurements of the 24-hour post-treatment washout period groups, an eight-point standard calibration curve was derived with a maximum of 8,000 cells per well. The resultant calibration curve was similar as presented above (Data not shown).

3.1.4 Intracellular Calcium Conductance

In validating the method Fluo-4 staining, differentiated H92c cells were exposed to 20 mM EGTA or 5 µM ionomycin – a well known intracellular calcium modulatory ionophore (*Figure 6*). As expected, ionomycin induced a rapid increase in Fluo-4 fluorescence associated with ionophore-mediated intracellular calcium influx; individual time points were blanked from fluorescent signals of EGTA-exposed (Baseline) wells. Generally, differentiated H9c2 cultures under standard oxygen conditions tended to result in higher peak fluorescence. Furthermore, 25 µM acrolein did not alter substantially the fluorescent signal magnitude or time-to-peak reported

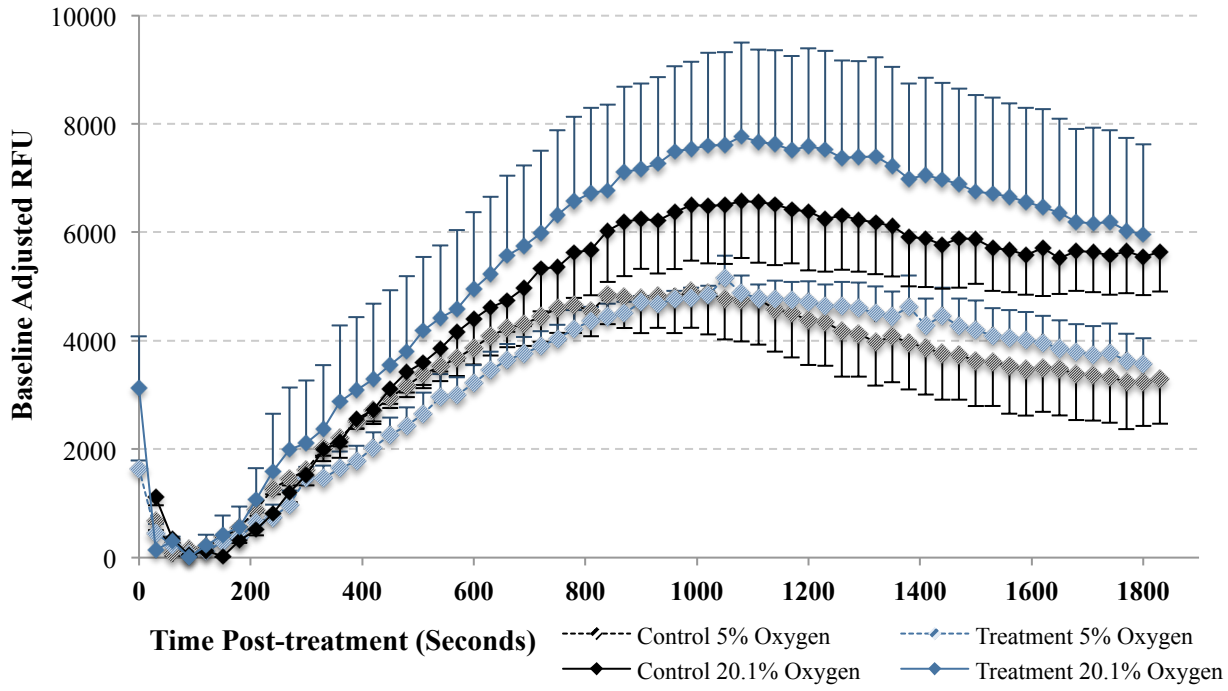

Figure 6. Baseline Adjusted Calcium/Fluo-4 Complex Fluorescence in the presence of Ionomycin. After a 30-minute Fluo-4AM loading time, and equivalent de-esterification period, differentiated H9c2 cells cultured at either 5 % or 20.1 % oxygen were exposed to 5 µM ionomycin either in the presence (Treatment; Blue Diamonds) or absence (Control; Black Diamonds) of 25 µM acrolein, and quantitated every thirty seconds for a period of thirty minutes using the Synergy HT microplate reader pre-heated to 37 °C; the filter set utilized consisted of excitation/emission spectra of 485/20 nm and 528/20 nm, respectively. Each point along the curve corresponds to the mean baseline-adjusted RFU of triplicate technical replicates per trial over four independent trials with SEM denoted by error bars.

by Fluo-4. Within the initial 90 seconds of fluorometric readings, a consistent, rapid reduction in RFU was observed, followed by a nadir; this nadir was presumed the baseline for ionomycin measurements. The results presented in *Figure 6* do not include a 60-second delay in fluorometric reading after exposure to ionomycin which includes the physical period between exposure and initiation of microplate reading; the results here merely demonstrate the positive control as a proxy of assay validation irrespective of time-to-efficacious calcium transient induction. Results from calcium transient due to acrolein below include a 60-second delay in order to align PARP-activity increases temporally with calcium transient data. As presented with the ionomycin-exposed wells, the initial 90 seconds, corresponding to time-points 60-150

seconds in acrolein-exposed samples, of initial calcium fluorometric readings were reported, but disregarded for mechanistic purposes due to the erroneous readings consistently resultant of this initial time period.

3.1.5 Mitochondrial Membrane Potential

In qualitatively validating JC-1 labeling for measurements of $\Delta\Psi_m$, H9c2 cells were plated on poly-l-lysine-coated coverslips, and differentiated as described previously under standard culture conditions. Thereafter, the H9c2 cells were washed with D-PBS and labeled for 10 minutes with 20 μM JC-1 at 37 °C prior to treatment with 100 μM CCCP or CCCP vehicle (DMSO) in D-PBS in preparation for live fluorescent microscopy (*Figure 7*). Vehicle controls demonstrate strong punctate fluorescence associated with J-aggregate signaling, whilst diffuse, low-level JC-1 monomer fluorescence was observed. Cells exposed to CCCP showed an absence of J-aggregate fluorescent signaling, and consistent monomer signals.

Extension of the JC-1 staining duration to 15 minutes enhanced the intensity of J-aggregate signal (*Figure 8*), while the monomer signal remained relatively constant (Not shown). Therefore, subsequent quantitative analyses were executed with a 15-minute labeling period, rather than the initial 10-minute labeling procedure. Of note, since image capture within the system in the current investigation was not processed via software, a typical exposure balance, which reduces the "background noise" associated with subsequent isolation of the signal of interest, was not available; thus, the images contain a certain level of non-specific background.

3.2 Endpoint Analyses and Quantitation

Proxies of both cell metabolism (2-hour washout period) and cellular viability (24-hour

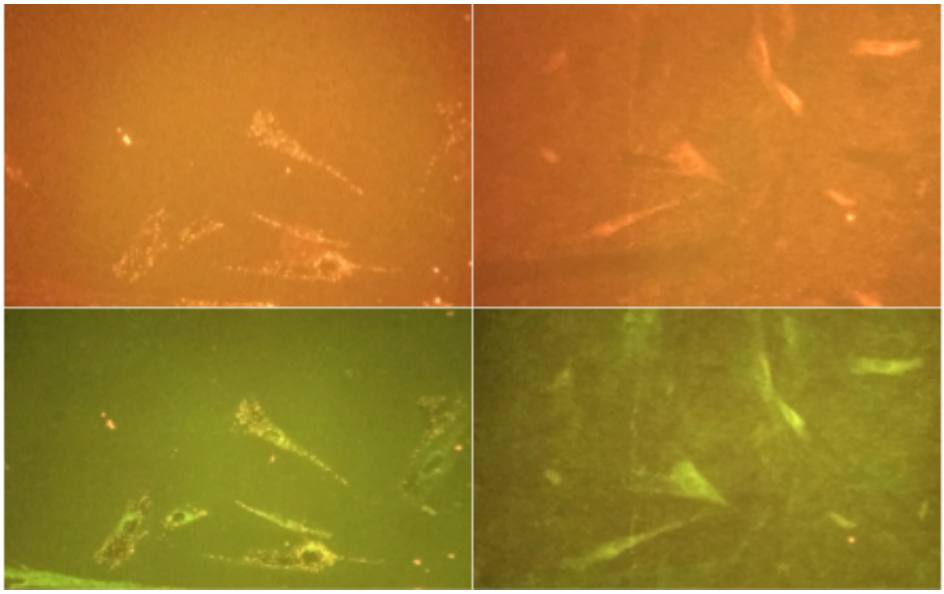

Figure 7. JC-1 Visualization via Fluorescent Microscopy. H9c2 cells under standard culture were seeded on coverslips, and differentiated prior to JC-1 labeling and exposure to 100 µM CCCP. Immediately after CCCP addition and slide mount, H9c2 cells were visualized via fluorescent microscopy. Images were taken using a hand-held cellular device through objective eyepiece. (**Top**) Control (**Left)** and 100 µM CCCP-exposed (**Right**) H9c2 cells labeled with JC-1 were visualized with the N2 filter cube which specifically detects JC-1 aggregates, indicating polarized mitochondria. Cells on the left exhibit punctate monomer signals, indicating detectable polarization, which is absent in the CCCP-exposed cells (Right). (**Bottom**) Control (**Left**) and 100 µM CCCP-exposed (**Right**) H9c2 cells labeled with JC-1 were visualized with the I3 filter cube that detects both JC-1 aggregates (*Red*) and JC-1 monomers (*Green*). Cells exposed to CCCP (Right) demonstrate diffuse green labeling with negligible monomer detection, whist control cells (Left) demonstrate diffuse JC-1 monomer labeling, but with strong monomer signals.

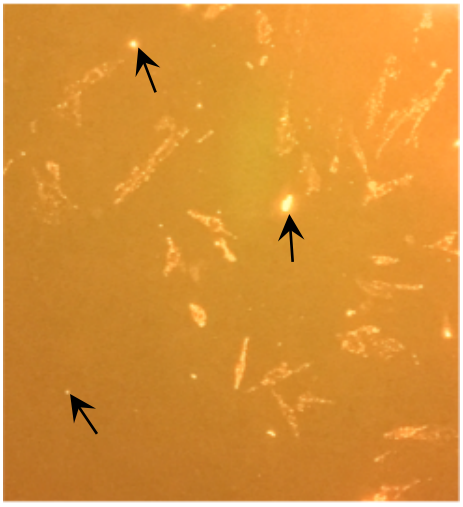

Figure 8. J-aggregate Visualization Among Controls After Extended Staining. A second coverslip of H9c2 cells was labeled with JC-1 for 15 minutes. J-aggregate signaling was starkly enhanced with the addition of 5 minutes. The poor solubility of JC-1 in D-PBS is exemplified by the numerous fluorescent particulate flakes observed in the image (Black Arrows); these were also observed visually without the facilitation of a microscope. Solubalization in low-serum DMEM in preparation for quantitative analyses greatly reduced the amount of particulate flakes observed.

washout period) were assessed via the MTT reduction assay on all substrate groups. With discovery of interference of the MTT assay with 5.0 mM α-ketoglutarate, this particular group was assessed for metabolism via trypan blue exclusion, and subsequently eliminated from further testing; exposure with acrolein in standard low-serum DMEM replaced the α-ketoglutarate substrate group for further analyses.

After viability and metabolism assessments, mechanistic elucidation using small molecules – olaparib (PARPi), CTZ (Non-specific TRPM2 inhibitor), and EGTA (Calcium chelator) – was performed in order to assess their respective effects on determining their respective impact on acrolein-induced MTT metabolism and cell viability. Furthermore, the same small molecules were utilized in order to determine their effect on calcium transients and reduction in $\Delta\Psi_m$ due to acrolein exposure. In order to do so, the latter two phenomena were assessed quantitatively using intracellular calcium- (Fluo-4) and mitochondrial membrane potential-specific (JC-1) fluoroprobes.

3.2.1 Acrolein Treatment-Response on Cellular MTT Metabolism and Viability

3.2.1.1 TCA substrate- and glucose-supplemented media. The MTT reduction assay was performed on acrolein-exposed differentiated H9c2 cells maintained under 20.1 % and 5 % oxygen conditions for two differing time points: 2 and 24 hours post-treatment. The two time points respectively provide a proxy of short-term metabolic competency under a restricted acute response as well as a proxy of cellular viability. In order to ascertain the influence of TCA- and glycolytic substrates on acrolein-induced insult, acrolein was diluted in substrate media containing enriched, glucose, pyruvate, glutamine, or glutamate, except for one group which was, compared to the physiological rat medium, deficient in glucose (1.0 mM). A group exposed

to acrolein in low-serum DME medium was included to compare MTT reduction with respect to a typical treatment conditions found within the literature using growth medium as the vehicle, which contains enriched concentrations of glucose (25 mM), pyruvate (1.0 mM), and glutamine (2.0 mM) that are beyond physiological concentrations encountered. Early trials including the 5.0 mM α-ketoglutarate group were included, but subsequently excluded from further testing, due to the substrate interference with the MTT reduction assay; otherwise, all other substrate group-bathed cells retained the capacity to metabolize MTT tetrazolium salt. Three concentrations of acrolein selected for comparison across substrate media were: 1 μM, 25 μM, and 250 μM, the highest of which provides a comparison group against all subsequent mechanistic elucidation trials, e.g., assurance that the stock acrolein (90 %) utilized for testing repeatedly reduces MTT reduction in the H9c2 cells. Failure to do so would indicate degradation of acrolein or heterogeneity in acrolein dilution formulation. Expectedly, normalized MTT reduction measures among all groups at two hours demonstrated pseudo-concentration-response across acrolein concentrations, and similar patterns at 24 hours post-treatment were observed, albeit with lowered MTT signaling among treatment groups. Assessment of MTT reduction following a two-hour post-treatment washout period resulted in a consistent dose-dependent response in differentiated H9c2 cardiomyoblasts, irrespective of culture oxygen conditions. Two overarching caveats of were observed: 1) oxygen concentration consistently elevated MTT metabolism among low-concentration exposure cells (1 μM acrolein) but insignificantly affected acrolein IC_{50} among all substrate-medium supplemented groups, except in substrate media with enriched pyruvate concentrations and 2) glucose supplementation likely modulated MTT reduction estimates (*Table 6 and Figure 9*).

Under standard culturing conditions (20.1 % oxygen), MTT metabolism was concentration-dependently reduced among all substrate groups, even after exposure to 1 μM acrolein for the brief 30-minute exposure time, though the magnitude depended upon the substrate medium (*Table 6*). No statistical comparisons were to be made except those between modeled IC_{50} values. As such, only descriptive statistics are presented. Among substrate groups exposed to 1 μM compared to their respective controls, except for the RP medium group, MTT reduction capacity was changed only minimally (≥ 89 % Controls). Cells exposed to acrolein in RP medium metabolized MTT to 79 ± 5 % of respective controls. Pyruvate-enriched media groups (1 mM and 2.5 mM pyruvate and the 1 mM pyruvate-containing low-serum DMEM) as well as the 5.0 mM L-glutamine group consistently retained MTT metabolic reduction capacity compared to the other substrate media groups at this treatment concentration. The media containing 2.5 mM pyruvate resulted in a mean MTT reduction higher than its respective control (102 ± 8 %). A similar pattern was observed H9c2 cells exposed to 25 μM. However, the only groups for which substantial retention of MTT reduction after acrolein exposure was afforded were the 1 mM (88 ± 8 %) and 2.5 mM (87 ± 8 %) pyruvate-enriched groups; all other substrate media demonstrated MTT metabolism reductions to ≤ 78 % compared to their respective controls. Paradoxically, the 1 mM pyruvate-containing low-serum medium provided intermediate rescue (80 ± 6 %), and was more similar to the other non-pyruvate containing substrate media. Increasing the treatment concentration of acrolein to 250 μM significantly reduced the magnitude of MTT reduction among all substrate-supplemented groups. Since the treatment group in RP medium would most closely recapitulate rat whole blood, further comparisons of this group against the remaining substrate-containing treatment media groups exemplified a lack of comparative rescue among any of the glucose-, glutamine-, and glutamate-

supplemented media, especially the glucose-deficient (1.0 mM) medium group. Among such groups, normalized MTT reduction after acrolein exposure ranged from 32 ± 2 % (5.0 mM glutamine) to 36 ± 3 % (RP Medium), with all others residing therein. The notable exceptions to this trend were the pyruvate-containing media groups for which relative rescue by pyruvate supplementation persisted even after this high-concentration exposure (53-58 % of respective controls). 2.5 mM pyruvate (58 % of controls) did not provided additional benefit compared to the 1.0 mM pyruvate-containing medium group. As with H9c2 cells exposed to 25 μM, the low-serum DMEM group analogously lacked attenuation of acrolein treatment-related reductions in MTT metabolism; with an estimate (35 ± 2 %) similar to groups lacking enriched pyruvate concentrations. Two trials with 5.0 mM α-KG were performed with negligible MTT formazan reduction (No different than 0 c/well-containing blanks), possibly suggesting heightened cytotoxic insult followed by complete cellular degeneration. Upon brightfield microscopy, however, H9c2 cells did not overtly appear to exhibit a stressed morphology. Thereupon, later acrolein treatment groups included trypan blue exclusion as the measure of viability.

When H9c2 cardiomyoblasts were acclimated to 5 % oxygen, similar acrolein-dependent reductions in MTT metabolism was demonstrated (*Table 6*). However, stark differences in the relative magnitude of partial rescue by pyruvate were observed compared to standard condition cultures (20.1 % oxygen) and in normalized MTT metabolism when exposed to 1 μM acrolein. Unexpectedly, consistent elevations in normalized MTT reduction measures (> 100 % Controls) among the differentiated H9c2 cells when exposed to 1 μM acrolein were observed, even at 24 hours; analogous groups cultured under 20.1 % oxygen did not exhibit such an analogous re sponse except for minor elevations among the 2.5 mM pyruvate group (102 ± 8 %) exposed to 1 μM acrolein. Increasing the acrolein concentration to 25 μM resulted in MTT reduction to < 90

Table 6. MTT Reduction Two Hours Post-Acrolein Exposure

Substrate Group	Normalized MTT Reduction ± SEM (Percent Respective Control)					
	1 µM		25 µM		250 µM	
	5 % Oxygen	20.1 % Oxygen	5 % Oxygen	20.1 % Oxygen	5 % Oxygen	20.1 % Oxygen
Control	100 ± 0 %	100 ± 0 %	100 ± 0 %	100 ± 0 %	100 ± 0 %	100 ± 0 %
Low-Serum DMEM	111 ± 3 %	99 ± 1 %	83 ± 3 %	80 ± 6 %	48 ± 4 %	35 ± 2 %
Rat Physiological	125 ± 10 %	79 ± 5 %	99 ± 6 %	75 ± 8 %	46 ± 3 %	36 ± 3 %
1.0 mM d-Glucose	121 ± 7 %	91 ± 5 %	112 ± 8 %	78 ± 11 %	37 ± 2 %	35 ± 2 %
10 mM d-Glucose	113 ± 10 %	89 ± 9 %	84 ± 10 %	77 ± 6 %	39 ± 5 %	37 ± 4 %
1.0 mM Pyruvate	107 ± 8 %	96 ± 2 %	103 ± 10 %	88 ± 8 %	51 ± 2 %	53 ± 4 %
2.5 mM Pyruvate	116 ± 6 %	102 ± 8 %	97 ± 4 %	87 ± 8 %	51 ± 3 %	58 ± 5 %
5.0 mM L-Glutamine	126 ± 7 %	96 ± 2 %	103 ± 8 %	78 ± 4 %	47 ± 1 %	32 ± 2 %
1.0 mM L-Glutamate	105 ± 12 %	89 ± 5 %	97 ± 5 %	76 ± 6 %	48 ± 5 %	34 ± 3 %
*5.0 mM α-Ketoglutarate**	93 ± 2 %	95 ± 1 %	95 ± 2 %	94 ± 0 %	92 ± 2 %	89 ± 2 %

*One group was assessed via the trypan blue exclusion method, as cells exposed to α-ketoglutarate did not exhibit MTT reduction capability. Therefore, α-ketoglutarate at 5 mM was presumed to interfere with the MTT assay.

% respective controls among two groups: 10 mM glucose-supplemented (84 ± 10 %) and the low-serum DMEM substrate groups (83 ± 3 %); the remaining substrate groups metabolized MTT ≥ 90 % compared to their respective controls. Interestingly, a strong inverse relationship in MTT metabolism (Pearson's correlation coefficient = 0.9997) was observed with respect to medium glucose concentration. The 1 mM glucose group resulted in a MTT reduction capacity (112 ± 8 %) substantially higher than the 10 mM glucose group (84 ± 10 %) with the RP medium intermediary, though significance was not reached (Difference CI_{95}: -2 - 57 %; p = 0.063). The low-serum DMEM, containing 25 mM glucose, yielded a MTT reduction result (83 ± 3 %) quite similar to that of the 10 mM glucose-supplemented group. Otherwise, no substantial differences were observed among substrate groups, as well as compared to respective controls.

Acrolein-induced MTT metabolism reduction curves across substrate groups, and respective oxygen-concentration- and substrate-specific IC_{50} values, were derived in order to compare the effect (Curve displacement) of culturing oxygen conditions on between standard

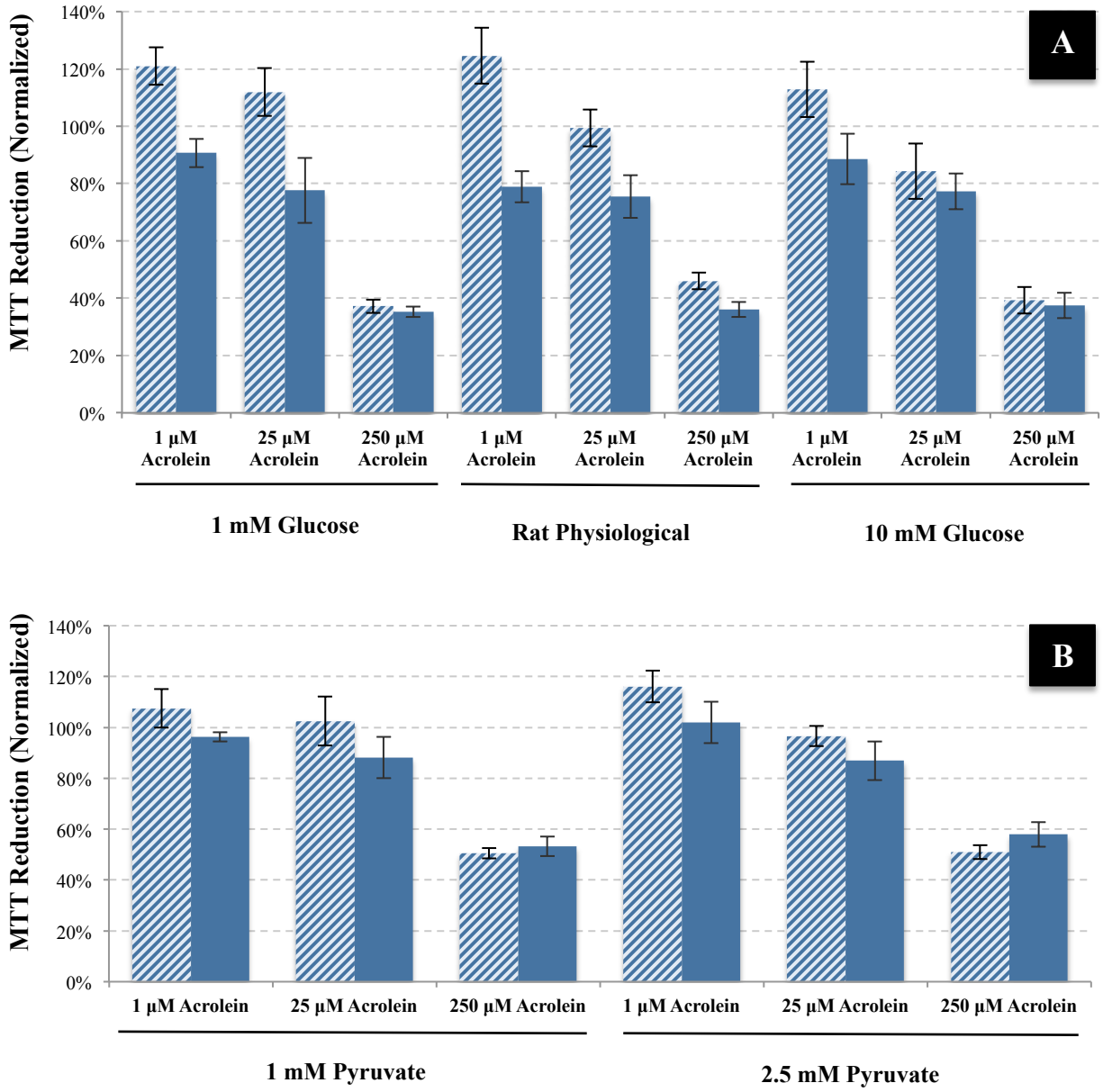

Figure 9. MTT Reduction Two Hours After Treatment by Substrate **(Continued to Next Page)**. Differentiated H9c2 cells were cultured and exposed under 5 (Striped Bars) or 20.1 % (Solid Bars) oxygen with three concentrations of acrolein for thirty minutes, followed by a 1.5 hour washout period and subsequent MTT assay initiation or trypan blue exclusion. Reductions in MTT metabolism were acrolein concentration-dependent across all substrate media, except for the 5 mM α-ketoglutarate group among which viability was assessed by trypan blue exclusion. All substrate groups were treated analogously, aside from the α-ketoglutarate group, and clustered within individual charts merely for clarity. A) H9c2 cells were exposed to acrolein in RP medium, glucose deficient (1.0 mM), or glucose enriched (10 mM) DMEM. B) H9c2 cells were exposed to acrolein in RP medium supplemented with 1.0 and 2.5 mM pyruvate. C) H9c2 cells were exposed to acrolein in RP medium supplemented with 5 mM glutamine, 1 mM glutamate, and 5 mM α-ketoglutarate. Bars denoting controls were not included as all values were normalized against the controls, and receive the designation 100 % without a measure of variance. As mentioned within the text, no statistical analyses were performed with regards to these data directly. Measures are the average of 3-6 individual experiments with associated SEM denoted by error bars.

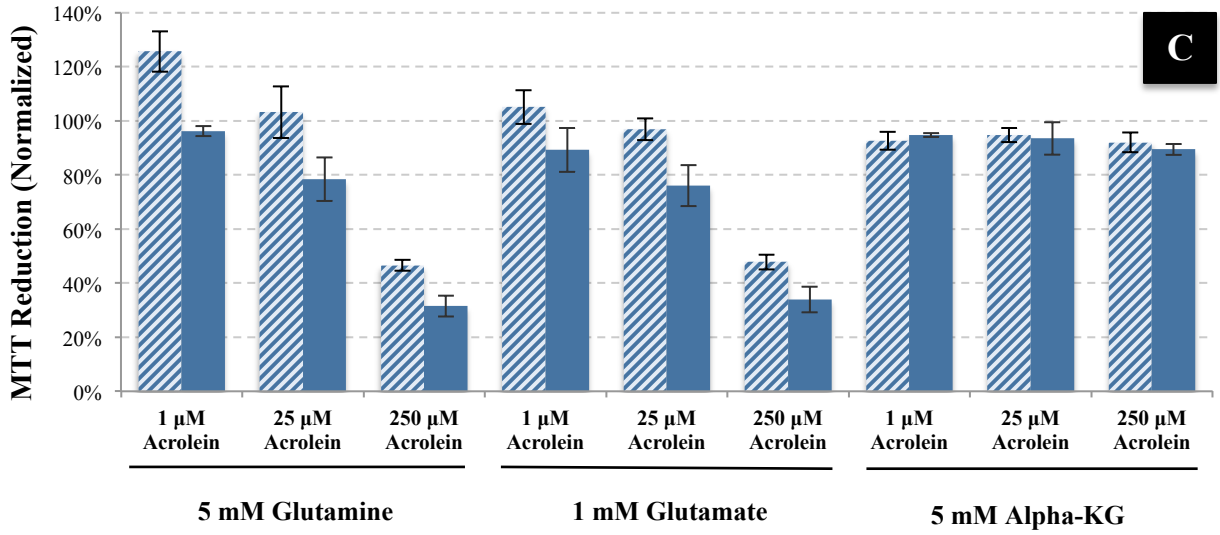

culturing (20.1 % oxygen) and physiologically relevant culturing conditions (5 % oxygen). For MTT metabolism values above 100 %, such values were presumed "100 %" for the purposes of IC_{50} modeling in order to accommodate precise modeling parameters. This assumption was valid since 24-hour viability on such respective groups with ≥ 100 % MTT reduction values retained MTT metabolic competence similar to respective control groups, indicating no functional viability decreases (See 24-hour viability data below). Aside from curve estimations, brief comparisons of acrolein concentration cross-sectional comparisons were made without statistical inferences drawn.

Comparisons of modeled acrolein-induced MTT reduction IC_{50} values resulted in consistent attenuation of MTT metabolism amongst H9c2 cells cultured under the lower oxygen tension, three of which substantial shifts were observed. Only one substrate group reached statistically significant difference between oxygen tensions (*Table 7*). Neither pyruvate-enriched substrate group resulted in significant differences between oxygen conditions, likely imparted by IC_{50} estimates above the highest tested acrolein concentration (250 µM); estimates were thereupon denoted simply as "> 250 µM". Lowered oxygen did substantially shift the toxicity

curve of the low-serum DMEM group, elevating the IC_{50} to 1.8-fold higher than the respective group at 20.1 % oxygen culture (217 ± 37 μM versus 120 ± 26 μM), but did not differ significantly. Similar curve shifts were observed with the 5.0 mM glutamine group (223 ± 27 μM versus 119 ± 25 μM; p = 0.011) and 1.0 mM glutamate group (> 250 ± 33 μM versus 147 ± 32 μM). An inverse relationship in MTT metabolism was observed with respect to medium glucose concentration, with the highest glucose concentration-containing substrate medium (10 mM) demonstrated the highest sensitivity to acrolein exposure among the 5 % oxygen cultured groups. This trend was not consistent among 20.1 % oxygen cultures (202 ± 42 μM; fourth highest estimate) where glucose deficiency was associated with the highest sensitivity of MTT metabolism reduction. Enriched pyruvate groups cultured across both oxygen tension cultures

Table 7. Modeled Acrolein-induced MTT Metabolism Reduction IC_{50} Concentrations Two Hours Post-Exposure

	IC_{50} ± SEM (μM Acrolein)	
Substrate Group	**5 % Oxygen†**	**20.1 % Oxygen†**
Low-Serum DMEM	217 ± 37 μM	120 ± 26 μM
Rat Physiological	218 ± 27 μM	220 ± 42 μM
1.0 mM d-Glucose	192 ± 59 μM	145 ± 35 μM
10 mM d-Glucose	165 ± 26 μM	202 ± 42 μM
1.0 mM Pyruvate	> 250 ± 34 μM[a]	> 250 ± 84 μM
2.5 mM Pyruvate	> 250 ± 31 μM	> 250 ± 159 μM
5.0 mM L-Glutamine	223 ± 27 μM*	119 ± 25 μM
1.0 mM L-Glutamate	> 250 ± 33 μM	147 ± 32 μM

†Each treatment dose-response curve was derived from 5+ (5 % Oxygen) or 4+ (20.1 % Oxygen) independent trials per substrate group over three acrolein concentrations and respective substrate control.
[a]Modeled IC_{50} estimates above 250 μM were designated as "> 250 μM", the respective modeled SEMs were reported here as conservative estimates of variance from extrapolation. Therefore, statistical designations for values > 250 μM were presumed 250 μM, and respective confidence intervals were established therefrom.
*p < 0.05 Compared to matched-substrate 20.1 % oxygen-cultured differentiated H9c2 cells.

conferred retention of MTT metabolism acutely after acrolein exposure. This becomes especially pronounced among the 5 % oxygen group simply arising from the intrinsically reduced variance among these modeled estimates compared to analogous estimates derived from 20.1 % oxygen

cultures; higher concentrations of acrolein would likely enable more confident estimation for such comparisons. The only substrate group, for which the 20.1 % oxygen modeled IC_{50} value was higher than the respective 5 % oxygen group, was derived from H9c2 cells exposed in the 10 mM glucose substrate medium; however, this difference was not significant.

When the washout period was extended to 24 hours post-treatment, a proxy of viability is presumed when subjecting the differentiated H9c2 cells to the MTT reduction assay. Acrolein exposure did result in concentration-dependent reductions in cell viability for all substrate groups, irrespective of oxygen culture conditions (*Table 8 and Figure 10*). For cells cultured under 5 % oxygen exposed to low-concentration acrolein (1 μM), viability estimates for all groups were equal or exceeded unexposed controls (≥ 100 % Respective Control) similarly to cells assessed for MTT metabolism two-hours post acrolein exposure. Most H9c2 cell substrate groups cultured under 20.1 % oxygen and exposed to the lowest acrolein concentration equaled or exceeded non-treatment controls, though notable exceptions were the 2.5 mM pyruvate (88 ± 3 %), 5.0 mM glutamine (80 ± 8 %), and the 1.0 mM glutamate (75 ± 11 %) groups – all of which were considerably lower than their respective controls. Only after 24-hours, this new pattern of consistent MTT metabolism elevation compared to respective control was demonstrated among 20.1 % oxygen cultures was in stark opposition to those assessed two hours post-exposure. Among the highest treatment concentration (250 μM), all substrate groups demonstrated substantial viability loss when cultured at 5 % oxygen (≥ 89 % viability loss) and 20.1 % oxygen (≥ 80 % viability loss). However, treatment of H9c2 cells with 25 μM acrolein under 5 % oxygen reduced cell viability to ≤ 37 % of controls among most substrate groups; groups with supra-physiological concentrations of pyruvate (≥ 1.0 mM) afforded substantial retention of MTT reduction potential. For example, supplementation of RP medium with 1.0 mM

and 2.5 mM pyruvate reduced viability loss to 88 ± 3 % and 87 ± 6 %, respectively, compared to RP medium viability estimates of 28 ± 8 %. Low-serum medium did produce a rescue phenotype analogously to simple pyruvate supplementation, though the viability estimate was intermediary (75 ± 6 %) between pyruvate-supplemented and the RP medium. The same substrate groups did not produce similar rescue among H9c2 cells cultured at 20.1 % oxygen, implicating the requirement of lowered oxygen tension for mediation of pyruvate rescue in this model.

Table 8. Viability Twenty-four Hours Post-Acrolein Exposure

Substrate Group	**Normalized Viability ± SEM (Percent Respective Control)***					
	1 µM		**25 µM**		**250 µM**	
	5 % Oxygen	**20.1 % Oxygen**	**5 % Oxygen**	**20.1 % Oxygen**	**5 % Oxygen**	**20.1 % Oxygen**
Control	100 ± 0 %	100 ± 0 %	100 ± 0 %	100 ± 0 %	100 ± 0 %	100 ± 0 %
Low-Serum DMEM	102 ± 8 %	100 ± 12 %	75 ± 6 %	20 ± 5 %	6 ± 2 %	16 ± 3 %
Rat Physiological	127 ± 13 %	111 ± 13 %	24 ± 8 %	16 ± 5 %	4 ± 2 %	18 ± 5 %
1.0 mM d-Glucose	112 ± 5 %	102 ± 11 %	28 ± 8 %	17 ± 4 %	11 ± 2 %	20 ± 6 %
10 mM d-Glucose	129 ± 11 %	107 ± 14 %	28 ± 8 %	15 ± 2 %	5 ± 2 %	16 ± 5 %
1.0 mM Pyruvate	107 ± 7 %	112 ± 9 %	88 ± 4 %	27 ± 4 %	2 ± 1 %	13 ± 3 %
2.5 mM Pyruvate	100 ± 6 %	88 ± 3 %	87 ± 6 %	18 ± 3 %	7 ± 2 %	18 ± 4 %
5.0 mM L-Glutamine	110 ± 6 %	80 ± 8 %	37 ± 10 %	19 ± 4 %	8 ± 2 %	15 ± 4 %
1.0 mM L-Glutamate	115 ± 10 %	75 ± 11 %	28 ± 9 %	13 ± 4 %	6 ± 2 %	13 ± 4 %

*No statistical comparisons were made, but rather made upon derivation of modeled IC_{50} values. All samples were normalized against their respective hydroquinone-only containing substrate medium.

Estimates of IC_{50} values across substrate groups affirmed a rescue phenotype bestowed upon pyruvate-supplemented media groups as well as the low-serum DMEM group among cells cultured under physiologically relevant oxygen tension compared to standard conditions (*Table 9*). While the modeled RP medium substrate group IC_{50} was 2 ± 12 µM using a three parameter log-normal model curve for cells cultured under 20.1 % oxygen, supplementation of any of the investigated TCA or glycolytic substrates did not protect H9c2 cell from acrolein-induced cytotoxicity. All parameter estimates resulted in IC_{50} values between 2 and 7 µM, though the 1.0 mM pyruvate tended to be higher than the remaining groups (7 ± 2 µM). Reduced oxygen

culturing shifted the estimated IC_{50} values for 1.0 mM and 2.5 mM pyruvate-supplemented groups significantly to 60 ± 18 μM (CI_{95} Difference: 11-95 μM, p = 0.0186) and 74 ± 16 μM (CI_{95} Difference: 23-121 μM; p < 0.0095), respectively. Similarly, acrolein exposure in low-serum DMEM resulted in a modeled IC_{50} of 51 ± 8 μM, which was significantly larger compared to the analogous culture at 20.1 % oxygen (CI_{95} Difference: 30-68 μM; p = 0.0035). Comparison of pyruvate-supplemented groups against the RP medium group confirmed that pyruvate alone conferred the observed metabolic rescue under 5 % oxygen (p < 0.05 for both 1.0 and 2.5 mM pyruvate groups compared to 5 % oxygen RP medium H9c2 cells exposed to acrolein); such conclusions cannot be definitively assigned to the low-serum DMEM, given the heterogeneous TCA/glycolytic substrate composition. Notwithstanding, low-serum medium and pyruvate-supplemented media provided substantial protection against acrolein treatment, attributable primarily to substantial viability differences observed between oxygen cultures exposed to 25 μM acrolein.

Table 9. Modeled Acrolein-induced Viability IC_{50} Estimates Twenty-four Hours Post-Exposure

	IC_{50} ± SEM (μM Acrolein)	
Substrate Group	**5 % Oxygen†**	**20.1 % Oxygen†**
Low-Serum DMEM	51 ± 8 μM**	2 ± 1 μM††
Rat Physiological	0.3 ± 1 μM	2 ± 12 μM
1.0 mM d-Glucose	2 ± 7 μM	2 ± 6 μM
10 mM d-Glucose	3 ± 8 μM	2 ± 5 μM
1.0 mM Pyruvate	60 ± 18 μM*	7 ± 2 μM
2.5 mM Pyruvate	74 ± 16 μM**	2 ± 14 μM
5.0 mM L-Glutamine	8 ± 9 μM	3 ± 1 μM
1.0 mM L-Glutamate	1 ± 2 μM	2 ± 2 μM

†Each treatment dose-response curve was derived from 5 (5 % Oxygen) or 6 (20.1 % Oxygen) independent trials per substrate group over three acrolein concentrations and respective substrate control. Fixing the upper asymptote of the regression curve for the 20.1 % oxygen provided an optimal reduction in model residua.

††SEM for low-serum DMEM derived from 4-parameter Weibull Type 2 model, as convergence of the three-parameter log-normal model reported "N/A" as SEM estimate.

*p < 0.05; **p < 0.01 Compared to 20.1 % Oxygen-cultured Differentiated H9c2 Cells.

Composition of a six-point dose-response curve for differentiated H9c2 cardiomyoblasts cultured under 5 % oxygen demonstrated an expected sigmoidal response across exposure concentrations of 1 to 250 μM (*Figure 11*). Judging from the dose-response curve produced, the modeled IC_{50} value for the RP medium group perceptively overestimates the IC_{50} value (0.3 ± 1 μM) compared to the apparent value suggested by the dose-response curve (≈16 μM). The certainty of this notion, however, remains tentative as the 5 and 10 μM values were derived from trials consisting of a batch of fetal bovine serum, which significantly altered baseline toxicity in H9c2 cells cultured under the same oxygen conditions (*See Discussion*). As such, the estimates for these two points may, indeed, be themselves overestimated, corresponding in a biased estimate of the IC_{50} value to a value higher than the three-parameter log-normal modeled value. Irrespective of the difference for the RP medium group, interpretation of estimated IC_{50} values attributed to other substrate-containing media is not expected, as the standard error for the remaining substrate media tended to be larger in magnitude, thus, controlling for discrepancies among the remaining estimates.

3.2.1.2 Pyruvate supplementation and medium acrolein. To ascertain whether rescue via pyruvate supplementation was attributable to an antioxidant effect through interference with free medium acrolein, acrolein concentration determination in pyruvate-supplemented medium was performed and compared against similar tests in RP medium over 24 hours. In order to maximize the likelihood of detecting interference of free acrolein with pyruvate, the highest pyruvate supplementation concentration, 2.5 mM, was chosen. At this concentration, pyruvate supplementation was determined to cause no alteration with free acrolein at 24 hours (*Table 10*). As the percentage of remaining free acrolein in medium was not altered by the initial acrolein

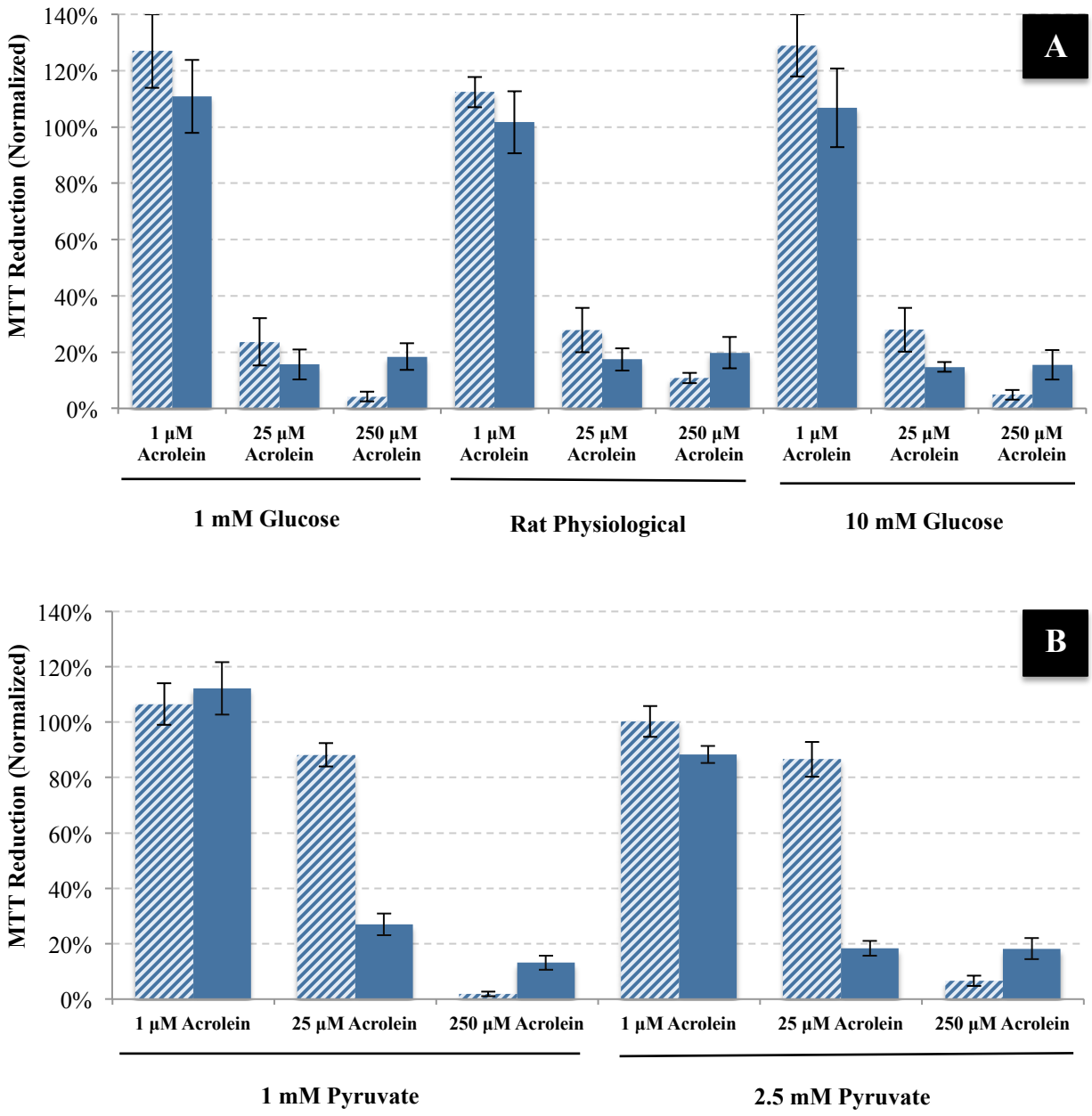

Figure 10. Viability Twenty-four Hours After Treatment by Substrate (Continued to Next Page). Differentiated H9c2 cells were cultured and exposed under 5 (Striped Bars) or 20.1 % (Solid Bars) with three concentrations of acrolein for thirty minutes, followed by a 23.5-hour washout period and subsequent MTT assay initiation. Reductions in viability were acrolein concentration-dependent across all substrate media groups. All substrate groups were treated analogously and clustered within individual charts merely for clarity. A) H9c2 cells were exposed to acrolein in RP medium, glucose deficient (1.0 mM), or glucose enriched (10 mM) DMEM. B) H9c2 cells were exposed to acrolein in RP medium supplemented with 1.0 and 2.5 mM pyruvate. C) H9c2 cells were exposed to acrolein in RP medium supplemented with 5 mM glutamine or 1 mM glutamate. Bars denoting controls were not included as all values were normalized against the controls, and receive the designation 100 % without a measure of variance. As mentioned within the text, no statistical analyses were performed with regards to these data directly. Measures are the average of 3-6 individual experiments with associated SEM denoted by error bars.

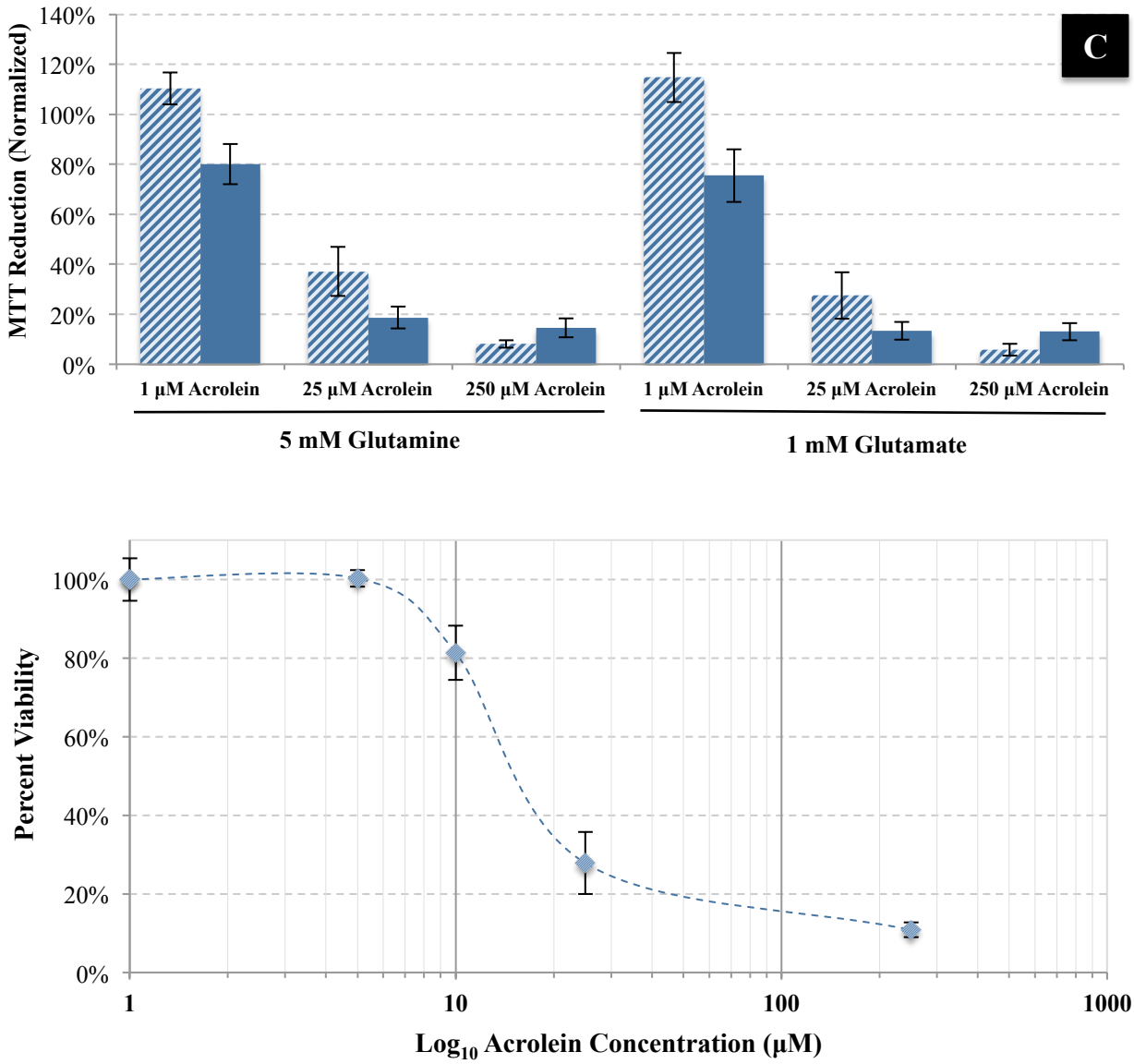

Figure 11. Log-transformed Dose-response Curve. H9c2 cells cultured, differentiated, and exposed under 5 % oxygen were exposed to a range of acrolein concentrations between 1 and 250 µM, and assessed for viability via MTT reduction after 24 hours; an accompanying control (Zero acrolein) has been incorporated, and falls on the y-axis. The resultant viability estimates were plotted against the log-transformed acrolein concentration, and a smoothed line fitted point-to-point. Each estimate is the average of four-five individual trials with associated SEM denoted by error bars.

concentration among the RP medium and pyruvate-supplemented medium measures over time when paring media spiked with 25, 50, and 250 µM acrolein, further tests were carried out utilizing the 250 µM initial concentration to avoid samples below the limit of quantification. In doing so, no differences were detected in free acrolein 30 minutes after addition to pyruvate-

supplemented medium compared to RP medium ($p > 0.05$); this time point remains most pertinent as experimentation for viability estimates were assessed after a 30-minute acrolein exposure period after which replacement with acrolein-deficient medium ensured the initial concentration within that 30-minute period attributed to the viability loss assessed after the washout period. Contrarily, free acrolein was consistently higher in pyruvate-enriched medium compared to RP medium at both time points, though this difference was not significant and may be simply attributable to the higher variance among pyruvate-supplemented medium acrolein measures. Therefore, the shift in IC_{50} in differentiated H9c2 cells observed by the pyruvate-supplemented substrate groups, 1.0 mM and 2.5 mM, cannot be attributed to simple acrolein quenching by medium pyruvate.

Table 10. Acrolein Degradation in Two Substrate Media

	Substrate Group			
Initial	***Rat Physiological***		**(+) *2.5 mM Pyruvate***	
Concentration	**30 Minutes**	**24 Hours**	**30 Minutes**	**24 Hours**
250 µM	234.6 ± 6.5 µM	154.8 ± 9.3 µM	230.5 ± 17.1 µM	160.5 ± 13.9 µM
50 µM	N.D.*	27.2 ± 0.7 µM	N.D.*	29.9 ± 2.1 µM
25 µM	N.D.*	13.1 ± 0.1 µM	N.D.*	15.4 ± 1.1 µM

*N.D. = Not Determined. Initial tests included 30-minute and 24-hour measures on the 250 µM concentration only, which were found to be show no statistical difference between media. Therefore, only 24-hour tests were performed at concentrations lower than 250 µM.

3.2.1.3 Low-serum DMEM viability assessment. Since treatment in *in vitro* testing is regularly conducted where the standard growth culture medium or low-serum medium becomes the toxicant vehicle, viability assessment of cells exposed to 25 µM acrolein in low-serum DMEM had been singled out for concentration-based statistical testing. By exposing differentiated H9c2 cardiomyoblasts in low-serum medium under standard culturing conditions, a significantly altered cytotoxic profile was clearly evident, whereby culturing under 5 % oxygen

conferred attenuation of cytotoxicity (75 ± 6 % versus 20 ± 5 %; CI_{95} Difference: 37-72 %; $p < 0.001$; *Figure 12*). While no differences were detected at 24 hours among the lowest (1 µM) or highest (250 µM) concentration groups between the two oxygen cultures, intermediary concentrations would likely yield implicit viability data requisite for fully characterizing acrolein sensitivity differences between the two oxygen conditions.

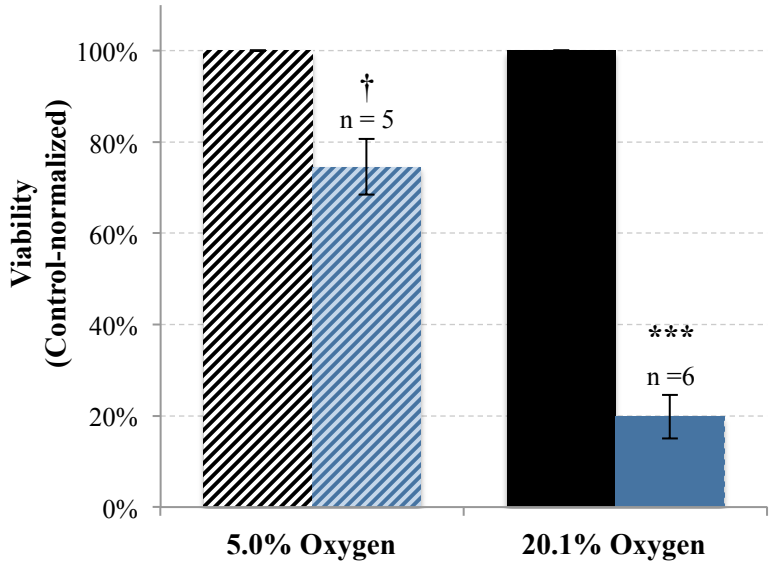

Figure 12. Viability in Low-serum DMEM After 25 µM Acrolein Exposure. H9c2 cells cultured and exposed under 5 (Striped Bars) or 20.1 % (Solid Bars) oxygen were exposed to 25 µM acrolein (Blue Bars) in standard low-serum (1 % v/v) DMEM for 30 minutes, followed by a 24 hour post-treatment washout period. H9c2 cells were then assessed for viability via MTT reduction and normalized against respective controls (Black Bars). After 24-hours, significant rescue was observed among exposed cells cultured and exposed under 5 % oxygen compared to 20.1 % oxygen cultures. Bars represent average of noted independent experiments with SEM denoted by error bars. ***$p < 0.001$ compared to 5 % oxygen cultures exposed to 25 µM acrolein. †$p < 0.05$ compared to unexposed controls.

3.2.2 Mechanistic Characterization of Acrolein-induced Cytotoxicity

Briefly, elucidation of the mechanistic contribution of calcium transients and involvement of poly(ADP-ribose) polymerase, the current investigation primarily focused of the mechanistic underpinnings of a single concentration of acrolein – 25 µM, with only few trials containing acrolein supplemented at lesser or greater concentrations. Initially, rescue with three

small molecules was pursued to implicate the contribution of extracellular calcium in determining cell fate; the impact of PARP activation in determining or exacerbating cell death; and the contribution of clotrimazole-sensitive calcium transients, i.e., through the TRPM2 channel. PARP activation shortly after acrolein exposure was confirmed by quantitative measurement of in whole-cell lysates. Subsequently, calcium influx within the cytosol was confirmed in acrolein-exposed H9c2 cells cultured under standard culture conditions by quantitative fluorescent measurements using Fluo-4AM; results were not conclusive for cells cultured at 5 % oxygen, but suggested a lack of cytosolic calcium influx. Lastly, insignificant $\Delta\Psi_m$ reductions were observed at four-hours post-exposure, affirming low-magnitude disruption of $\Delta\Psi_m$. During the course of experimentation a single batch of FBS was depleted, thus requiring acquisition of another to continue testing; results of baseline viability estimates at a fixed 25 μM acrolein concentration exemplified differential sensitivity to acrolein cytotoxicity between the two FBS batches, though only cells cultured under 5 % oxygen were affected.

3.2.2.1 Modulation of cytotoxicity with small molecules. In order to elucidate the comparative effect of extracellular calcium reduction in acrolein-induced cytotoxicity among differentiated H9c2 cardiomyoblasts, concomitant graded supplementation of the calcium chelator EGTA (1 and 5 mM) in the presence of 25 μM acrolein offered indirect evidence of extracellular calcium in modulating cytotoxicity. For reasons discussed below, results were obtained only for H9c2 cells cultured under 5 % oxygen.

For differentiated H9c2 cells exposed to 25 μM acrolein in RP medium for 30 minutes, cell viability was reduced to 26 ± 3 % of respective controls, which was consistent with the results from substrate-specific viability assessments above. Upon addition of 1 mM EGTA, non-significant elevations in viability were observed (41 ± 3 % of Respective Control, $p > 0.05$),

while further rescue was attained with supplementation of 5 mM EGTA (56 ± 6 %; $p < 0.01$; *Figure 13*). Graded concentrations of olaparib (10 and 100 μM) did not confer significant attenuation to acrolein-related viability loss, as neither concentration group elevated H9c2 viability (28 ± 4 % and 37 ± 4 %, respectively) compared to the vehicle-only containing acrolein exposure group. Nonetheless, attenuation was dose-dependent with respect to olaparib concentration despite insignificant differences compared to controls. Efficacy of the 100 μM olaparib group was still of lesser magnitude compared to 1 mM EGTA; however, further olaparib concentrations, e.g., 200 or 400 μM, were not assessed, as these values were not within the initial concentration ceiling determined at the onset (100 μM). Therefore, EGTA proved more efficacious in attenuating viability loss than did olaparib, despite extreme olaparib concentrations utilized in this investigation.

To examine whether CTZ-sensitive calcium stores associated with extracellular cation influx are implicated in determining cell fate, differentiated H9c2 cells were exposed to graded CTZ concentrations (5 and 10 μM) concomitant with exposure to 25 μM acrolein. After the 30-minute exposure to 25 μM acrolein in the presence of graded CTZ followed by a 24-hour washout, viability estimates for vehicle-containing acrolein-exposed cells demonstrated substantially differing baseline viability estimates (≈60 ± 4 %) compared to previous trials (≈26 ± 3 %); other exposure groups paired with other small molecule groups, 10 mM EGTA and 100 μM olaparib, demonstrated a similar shift in baseline viability ($n = 4$). Further replication of the experiment five more times on newly-revitalized H9c2 cardiomyoblasts confirmed the phenomenon of significantly alterations in baseline toxicity, denoting a consistent, significantly-altered viability baseline 2.2-fold higher than that of previous trials ($p < 0.001$). In total, nine replicates were included in the assessment of acrolein cytotoxicity among cultures under 5 %

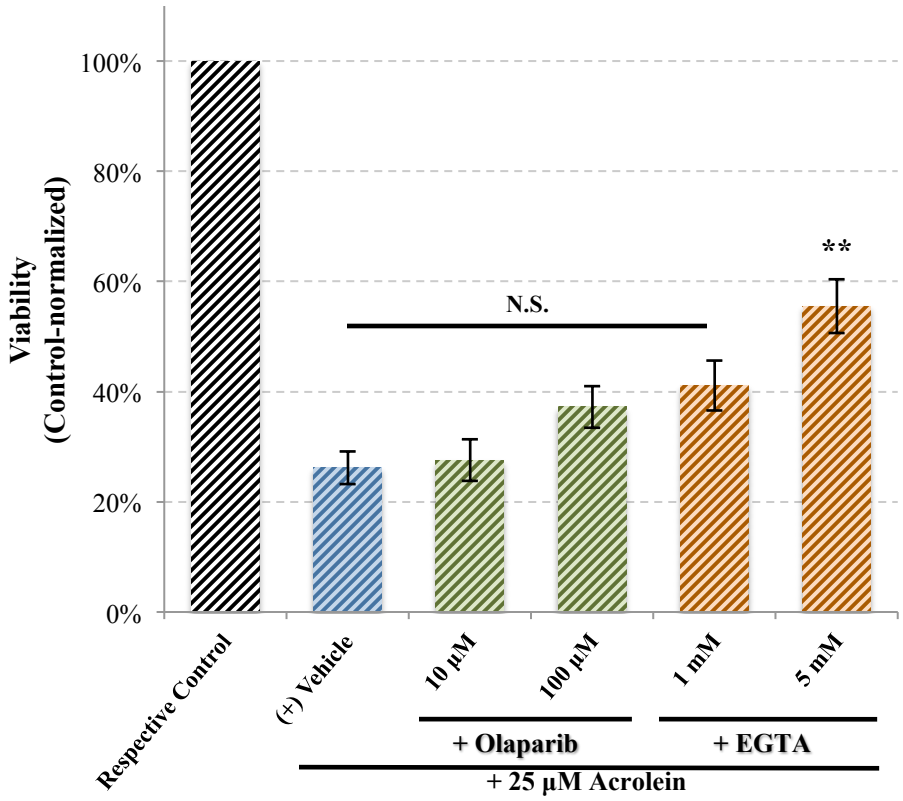

Figure 13. Small Molecule Rescue of Acrolein-induced Viability Reduction. Differentiated H9c2 cardiomyoblasts cultured under 5 % (Striped Bars) were exposed to 25 µM acrolein (Blue Bars) were supplemented with graded concentrations of EGTA or olaparib to examine their respective effects on viability reduction. Values derived are the respective vehicle-normalized average of three or four independent trials with associated SEMs denoted by error bars. Statistical comparisons were made only between small molecule-supplemented cells and their respective treatment-only cells. N.S. Not Significant compared to respective vehicle-controlled, treatment groups. **$p < 0.01$ compared to respective acrolein treatment-only cells.

oxygen. Cultures exposed to acrolein analogously, but cultured under 20.1 % did not exhibit a significantly altered viability baseline between media consisting of batch 1 (17 ± 4 %) and batch 2 (7 ± 1 %; CI_{95} Difference: 0-20 %; $p = 0.05$) FBS, denoting an inconsistency not in exposure metrics or culturing conditions, but rather a fundamental change likely within the composite medium. Of note, the two batches were also procured from another vendor (Batch 1: ATCC; Lot 62848232; Batch 2: Sigma-Aldrich; Lot 16A164). Therefore, the results of the latter viability assessments for mechanistic elucidation could not be aggregated with the previous results presented in *Figure 13*, and are, for the purposes of mechanistic elucidation, are considered

independent. Results are presented in *Figure 14*. Given the altered cytotoxic baseline, no results were derived for 20.1 % cultures analogous to those presented in *Figure 13*.

Exposure of differentiated H9c2 cardiomyoblasts resulted in an approximately 10-fold higher viability estimate among 5 % oxygen cultured cells (60 ± 4 %) versus 20.1 % oxygen cultured cells (6 ± 1 %; $p < 0.001$). Concomitant exposure of cells with CTZ (5 or 10 μM), 10 mM EGTA, or 100 μM olaparib in the presence of 25 μM acrolein did not translate to increases in viability among hyperoxic (20.1 % Oxygen) cultures, though the 100 μM olaparib group neared significance ($p = 0.072$). Conversely, rescue was afforded among some of the small molecule-supplemented groups cultures and exposed at 5 % oxygen ($F_{3,27} = 5.031$; $p = 0.007$). Though neither concentration of CTZ resulted in a significant reduction of viability loss, the 5 μM CTZ group tended to reduce cytotoxicity among the differentiated H9c2 cells compared to acrolein-only exposed cells; doubling the CTZ concentration to 10 μM, paradoxically, not only did not confer increased rescue, but actually completely negated the insignificant rescue afforded by the 5 μM CTZ co-exposure, reducing the viability estimates equivalent to those of exposed vehicle-containing H9c2 cells (60 ± 3 % versus 60 ± 4 % of acrolein-only vehicle-controlled cells). H9c2 cells supplemented were significantly rescued by either 10 mM EGTA (78 ± 4 %; $p < 0.01$) or 100 μM olaparib (86 ± 5 %; $p < 0.01$) when exposed to acrolein. Paradoxically, 100 μM olaparib rescued cells more efficaciously than EGTA, though the increased EGTA (10 mM versus previous trials with 5 mM) may have actually impeded rescue in a manner similar to that of the 10 μM CTZ. Nonetheless, it is prudent to note that EGTA conferred significant cell rescue, irrespective of baseline cytotoxicity. This was not the case for olaparib, which exhibited limited attenuation of large-magnitude cytotoxic acrolein-induced injury, but significant attenuation at lower-magnitude injury within the same system.

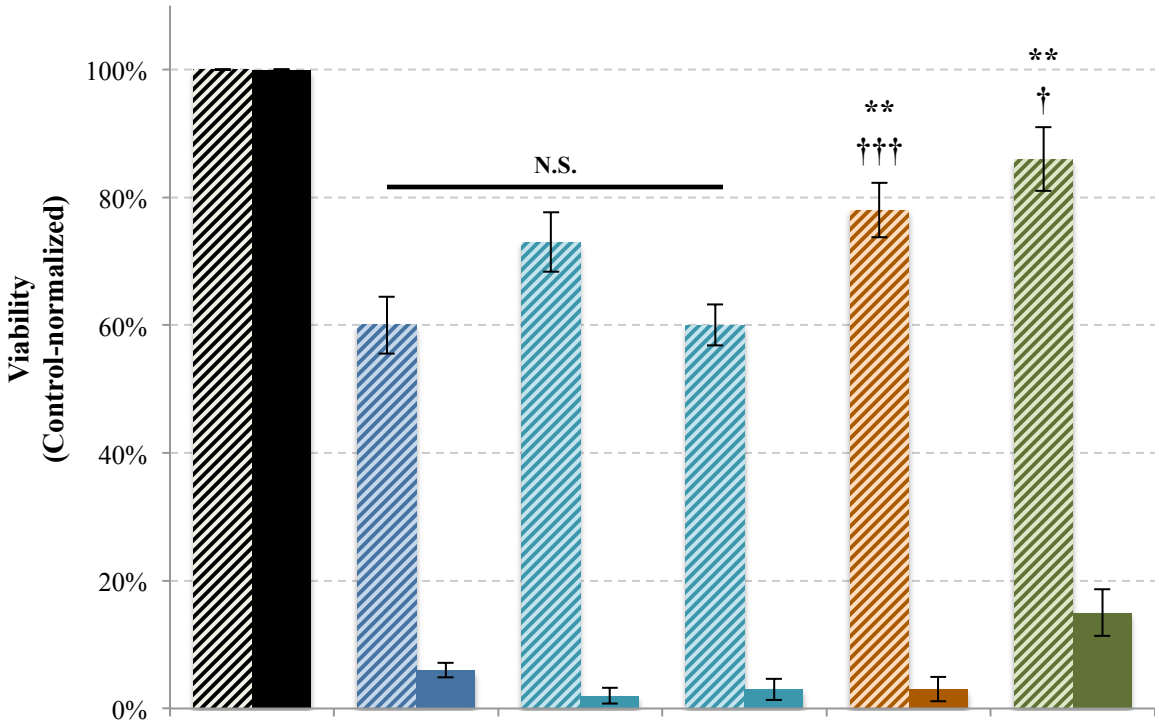

25 µM Acrolein	-	+	+	+	+	+
5 µM Clotrimazole	(+)	-	+	-	-	-
10 µM Clotrimazole	(+)	-	-	+	-	-
10 mM EGTA	(+)	-	-	-	+	-
100 µM Olaparib	(+)	-	-	-	-	+

Figure 14. Small Molecule Rescue of Acrolein-induced Viability Reduction – Shifted Baseline. Differentiated H9c2 cardiomyoblasts cultured under 5 % (Striped Bars) and 20.1 % oxygen (Solid Bars) exposed to 25 µM acrolein (Blue Bars) were supplemented with 10 mM EGTA, 5 or 10 µM CTZ, or 100 µM olaparib to examine their respective effects on viability reduction from acrolein exposure. Values derived are the respective vehicle-normalized average of five (20.1 % oxygen) or nine (5 % oxygen) independent trials with associated SEMs denoted by error bars. Statistical comparisons were made only between small molecule-supplemented cells and their respective treatment-only cells denoted formally as (+). N.S. Not Significant compared to respective vehicle-controlled, treatment groups. **$p < 0.01$ compared to respective acrolein-exposed cells. †$p < 0.05$; †††$p < 0.001$ compared to respective vehicle-only unexposed controls.

With respect to interference in viability explicitly due to either small molecule or respective vehicle, it is expected that neither EGTA nor olaparib deleteriously affected the viability of differentiated H9c2 cardiomyoblasts under the current culture and exposure conditions presented here. Neither small molecule produced significant reductions in viability, as viability estimates neither differed compared to their respective, vehicle-only controls (With

DMSO at respective dilutions carrying olaparib or CTZ or with water carrying EGTA) nor exacerbated viability reductions among cells exposed to acrolein concentrations below the threshold of toxicosis, e.g., 5 μM (Olaparib or EGTA, only – CTZ was not assessed during this battery of experimentation). Only with differentiated cells cultured under 5 % oxygen did either vehicle or inhibitor significantly confound the dose-response of acrolein at 10 μM – a concentration that was not extensively pursued in testing. The baseline viability estimate after treatment with 10 μM acrolein among EGTA-vehicle exposed cells resulted in viability loss to 78 ± 5 % respective controls, and was consistently different than DMSO-containing treatment groups exposed to the same concentration of acrolein: Olaparib-vehicle 93 ± 4 %; 5 μM CTZ-vehicle 95 ± 5 %; and 10 μM CTZ-vehicle 91 ± 3 %. DMSO itself only slightly interfered with the magnitude of acrolein cytotoxicity, either directly or indirectly – a phenomenon not observed among other acrolein treatment concentration groups (1, 5, or 25-250 μM), and biased viability to higher estimates compared to the water-only containing EGTA vehicle controls. With respect to EGTA supplementation, differentiated H9c2 cardiomyoblasts exposed to acrolein at 10 μM in the presence of 10 mM EGTA significantly attenuated viability (97 ± 4 %) compared to vehicle-containing acrolein-exposed H9c2 cells ($p < 0.01$).

3.2.2.2 Poly(ADP-ribose) polymerase activity. Since several compounds, including MNNG and hydrogen peroxide, have been shown to significantly activate PARP, little evidence exists with respect to acrolein-induced cytotoxic injury. Therefore, the current investigation aimed to confirm PARP activation in the differentiated H9c2 cell model under the current system to supply indirect evidence the rescue afforded by olaparib co-exposure with acrolein is associated with PARP activity stimulation by acrolein itself. Indeed, exposure of differentiated H9c2 cultured under 5 % oxygen to 25 μM acrolein for 5 and 15 minutes resulted in elevated,

time-dependent increases in PARP activity among acrolein-exposed H9c2 cells compared to time-matched controls (*Figure 15*). Even at 5 minutes post-treatment, PARP activity was increased by 20 ± 15 %, though not significantly different than controls (CI_{95} Of difference: 92-148 % of Respective Controls). At 15 minutes, PARP activity was further elevated in whole-cell lysate preparations to 45 ± 12 % (CI95: 21-69 %; $p < 0.05$) higher than time-matched controls.

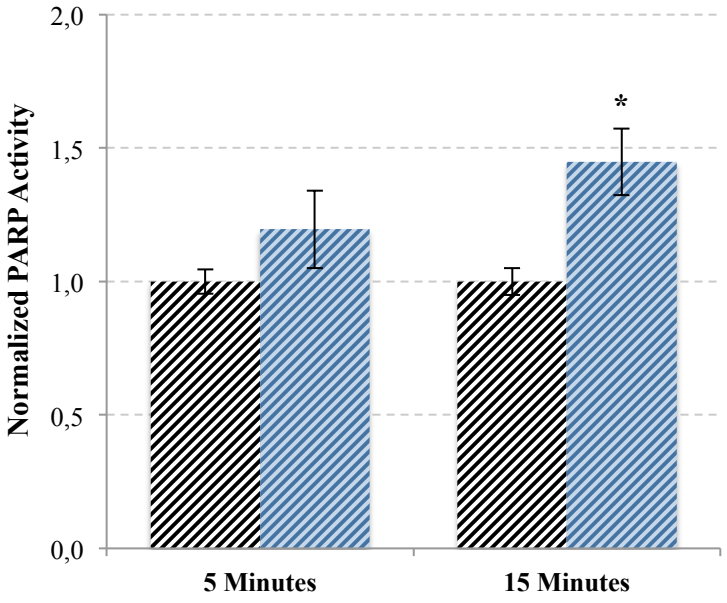

Figure 15. PARP Activity in Whole-cell Lysate Preparations. H9c2 cells cultured and differentiated under 5 % oxygen were exposed to 25 µM acrolein (Blue Bars) or hydroquinone (Black Bars; Controls) for the designated time period, after which the treatment-containing RP medium was cleared, cells washed, and then lysed in a PARP stabilizing lysis buffer. Whole-cell lysates were analyzed for PARP activity to which the activity (In International Units/well) was converted to Units/µg lysate based on protein concentration derived from the Bradford assay prior to normalization against control for comparisons. Bars represent average of 4-5 trials with SEM denoted by error bars. *$p < 0.05$ compared to time-matched control.

Therefore, acrolein acutely activates the catalytic activity of PARP in the differentiated H9c2 cardiomyoblast system under physiologically relevant oxygen tensions. Although PARP was indeed activated by acrolein, olaparib resulted in differential rescue potential under similar treatment conditions, but was confounded substantially by the magnitude of cytotoxic injury. At high-magnitude cytotoxic injury, viability was positively correlated with PARPi concentration

(R = 99.3 %) beginning with negligible viability increases at 10 μM (28 ± 4 %). Though the source of this discrepancy was not obliquely apparent, a change in FBS source did coincide with the alteration in baseline toxicity, revealing a coincidental shift in olaparib rescue potential. Since PARP activation was observed in this model, the modulatory effect of PARPi comparative to cytotoxic injury magnitude presents a complex interaction between small molecule inhibitor concentration and cell rescue potential.

3.2.2.3 Calcium conductance. As calcium is implicated in exacerbating toxicosis, especially under oxidative stress, the modulatory effect of calcium chelation on cellular viability was investigated. At high-concentration acrolein exposure, viability of differentiated H9c2 cells cultured under 5 % oxygen was significantly reduced to 27 % of respective controls. In the presence of EGTA, viability reduction was attenuated in a concentration-dependent manner at 5 mM EGTA (56 ± 5 %), with minimal rescue at 1 mM (45 ± 5 %). A higher concentration of EGTA, 10 mM, was investigated but interpretation of viability rescue along the three concentrations utilized remains convoluted due to the change in baseline toxicity among differentiated H9c2 cells exposed to acrolein in RP medium. Nonetheless, even 10 mM of EGTA significantly rescued cells. Therefore, extracellular calcium plausibly alters acrolein-induced viability response in H9c2 cells. To further characterize such an interaction, direct measure of intracellular calcium was performed using a cell-permeable Fluo-4 fluorescent indicator.

Differentiated H9c2 cells were exposed to acrolein immediately prior to fluorometric analysis for intracellular calcium using the cell-permeable version of the fluoroprobe Fluo-4AM. Among cells cultured under 20.1 % oxygen exposed to 25 μM acrolein, significant fluorescent signaling was observed beginning at approximately 300 seconds (≈5 minutes) after acrolein exposure, and returned to control levels at 500 seconds (8.3 minutes) (*Figure 16*). Consistent

calcium elevations became significant at 390 and 450 seconds compared to unexposed controls; significance was not reached at the 420-second peak, primarily due to the high observed point estimate variability. Following, fluorometric measurements among exposed cells decayed to control levels for subsequent time points until the final measurement at 540 seconds. These results coincide with the insignificant elevations in PARP activity at five minutes (300 seconds), though intracellular calcium transients decay prior to the sustained PARP activity observed at 15 minutes (900 seconds). As previously mentioned, the initial 150 seconds produce unstable readings; therefore, the perceptively reduced intracellular calcium levels among the acrolein-exposed cells cannot be interpreted as such. No discernable pattern of intracellular calcium influx was observed among 5 % oxygen cultured cells, though the variability was generally larger than those cells cultured at 20.1 % oxygen may have precluded definitive pattern recognition.

Simultaneous application of small molecule inhibitors (5 μM CTZ or 100 μM olaparib) or high concentrations (20 mM) of EGTA to differentiated H9c2 cells exposed to 25 μM acrolein resulted in substantially altered calcium transient patterns (*Figure 17*) among standard condition cultures. Ionomycin was normalized in an equivalent manner to treatment and small molecule-supplemented H9c2 cells, and depicted in *Figure 17* to demonstrate the method of normalization (Against vehicle-exposed controls) retains the overall calcium-influx trend reported in validation testing as reported in baseline adjusted relative fluorescent units (RFU) above, albeit with some reduction in curve smoothing. Therefore, the normalization of treatment and small molecule-supplemented differentiated H9c2 cells against vehicle-only hydroquinone containing controls appropriately retains the relative intensity of Fluo-4 reported calcium transients.

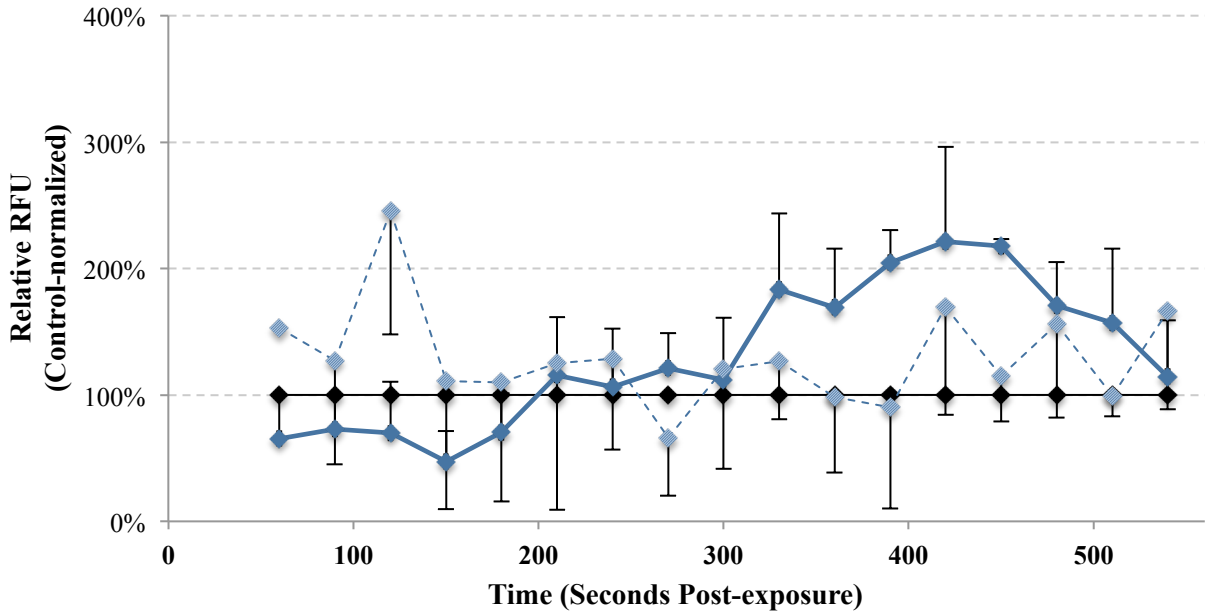

Figure 16. Acrolein-induced Fluo-4-reported Calcium Influx: 5 and 20.1 % Oxygen. H9c2 cells cultured and differentiated under 5 (Striped) and 20.1 % (Solid) oxygen prior to loading with Fluo-4AM and fluorophore de-esterification. After de-esterification, cells were exposed to 25 μM acrolein (Blue Diamonds) or hydroquinone (Controls; Black Diamonds) and immediately quantitated fluorometrically using the Synergy HT microplate reader with emission/excitation filters of 485/20 nm and 528/20 nm, respectively. The time between acrolein exposure and initial was consistently about 60 seconds, thus, the lead-time wherein no data are presented is presented without accompanying data points. After the fluorometric signal stabilized 210 seconds after acrolein exposure, Fluo-4 associated calcium signaling began elevating between 300 and 330 seconds, which was consistently elevated at 390 seconds, before returning to baseline after 500 seconds for standard condition cultures. Consistent transients were not observed for 5 % oxygen cultures. Individual points represent average of 3 trials with SEM denoted by error bars.

As reported previously, the calcium transient induced by acrolein was significant 390 and 450 seconds after exposure, as denoted by the superimposed horizontal solid black line, but not at the intermediary 420 second (7 minute) measurement. Despite not reaching significance, the peak of the calcium transient was observed at this measurement, and reached approximately 221 % of time-matched control measures. Application of 20 mM EGTA effectively ablated the calcium transient induced by acrolein, reducing the fluorometric measurement to 87-106 % of controls during the same time interval. As EGTA chelates extracellular calcium without altering intracellular calcium acutely, the method utilized retains specificity for measurement of

intracellular calcium within the conditions within this cell-based system presented in this investigation.

In assessing the mechanism leading to acrolein-induced calcium transients from the extracellular space, CTZ and olaparib were applied similarly to that of EGTA. In the presence of 5 μM CTZ, not only was the observed acrolein-induced calcium transient ablated, but a significant depression in measured intracellular calcium levels began at 300 seconds, and continued until the 450 second time-point. After 450 seconds, intracellular calcium levels remained depressed until the end of measurements. Similarly, olaparib also ablated the observed transient caused by acrolein. Between 390 and 450 seconds, the relative intracellular concentration decreased precipitously from 133 to 47 % of controls, after which the Fluo-4 signal remained below controls (< 50 %); no significant differences were observed compared to controls or EGTA-supplemented differentiated cardiomyoblasts. Since calcium transients were not detected among acrolein-exposed cells cultured at 5 %, no further comparisons between acrolein-only exposed cells and small molecule-supplemented cells were made.

3.2.2.4 Mitochondrial membrane potential. Exposure of differentiated H9c2 cells with 100 μM of CCCP resulted in a rapid reduction in $\Delta\Psi_m$ to 43-46 % of respective controls as reported by the ratio of J-aggregates to JC-1 monomers (*Figure 18*) at four hours; thus, the JC-1 labeling ratiometric analysis is specifically reporting $\Delta\Psi_m$ within the H9c2 cells under the test conditions. Differentiated H9c2 cells cultured under either 5 % or 20.1 % oxygen exposed to 25 μM acrolein resulted in insignificant decreases in $\Delta\Psi_m$ to 88 ± 7 % and 89 ± 7 %, respectively, compared to time-matched controls at four hours; intermediary $\Delta\Psi_m$ values were observed at one and two hours. While a slight time-dependent decrease in $\Delta\Psi_m$ among acrolein-exposed H9c2 cells, the magnitude was not altered by oxygen culturing conditions, at least within the initial

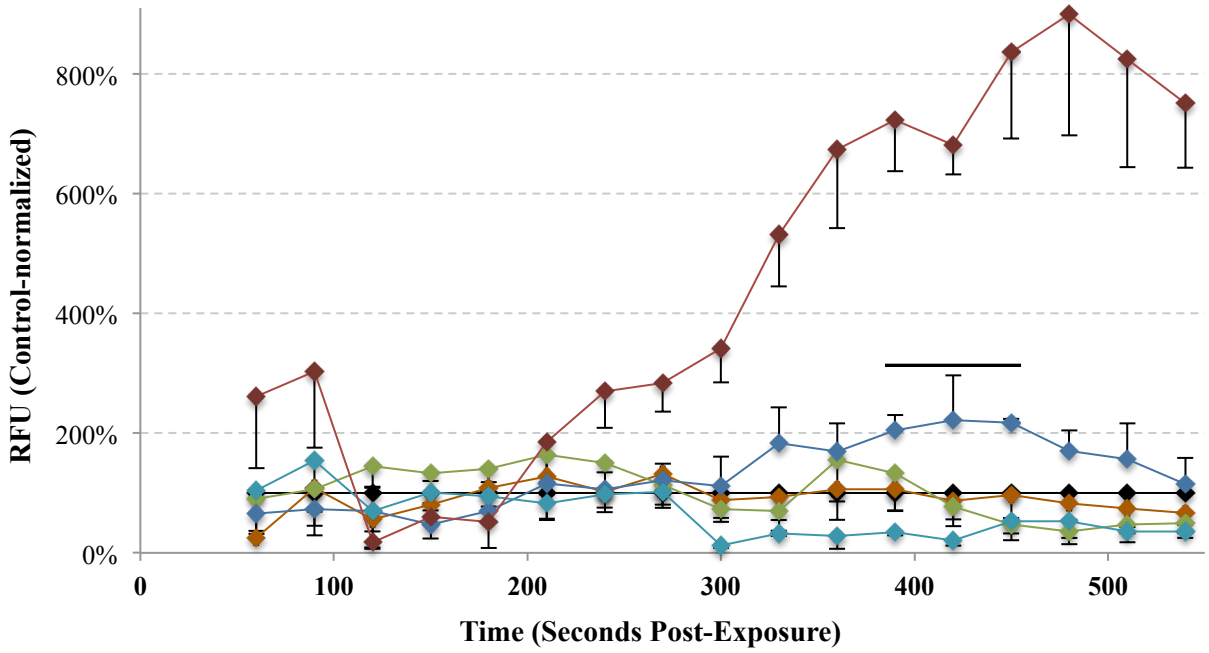

Figure 17. Fluo-4-reported Calcium Influx in H9c2 Cells Cultured Under Standard Conditions. H9c2 cells cultured under standard conditions were loaded Fluo-4AM, followed by de-esterification. After de-esterification, cells were exposed to 25 µM acrolein (Blue Diamonds; same as in *Figure 16* for comparison purposes) in the presence of 5 µM CTZ (Teal Diamonds), 100 µM olaparib (Green Diamonds), and 20 mM EGTA (Orange Diamonds), and immediately quantitated fluorometrically on the Synergy HT microplate reader with emission/excitation filters of 485/20 nm and 528/20 nm, respectively. Vehicle only-containing controls are designated by Black Diamonds. The calcium transient caused by ionomycin is presented here in order to establish maximal calcium influx. The calcium transient induced by acrolein (Denoted by a solid Black Line when significantly higher than Controls) was effectively disrupted by application of both CTZ and olaparib, both of which caused reductions in intracellular calcium over time. EGTA equally disrupted the calcium transient induced by acrolein, but retained the intracellular calcium levels equal to that of controls. The calcium transient becomes significantly higher than controls at 390 seconds and 450 seconds. Each point is the mean of 3-4 independent trials with associated SEM denoted by error bars.

four hours post-treatment. It is noteworthy to remark the J-aggregate/monomer ratio was significantly elevated by 39 % (8.71 ± 0.08 versus 6.28 ± 0.09; $p < 0.05$) among differentiated H9c2cells cultured under 5 % oxygen compared to equivalent 20.1 % oxygen cultures; the contribution of the net $\Delta\Psi_m$ reduction, rather than the relative reduction, was not pursued for further investigation.

Despite only modest reductions in $\Delta\Psi_m$ even at four hours, the influence of olaparib and extracellular calcium were investigated in modulating acrolein-induced $\Delta\Psi_m$ in RP medium. As

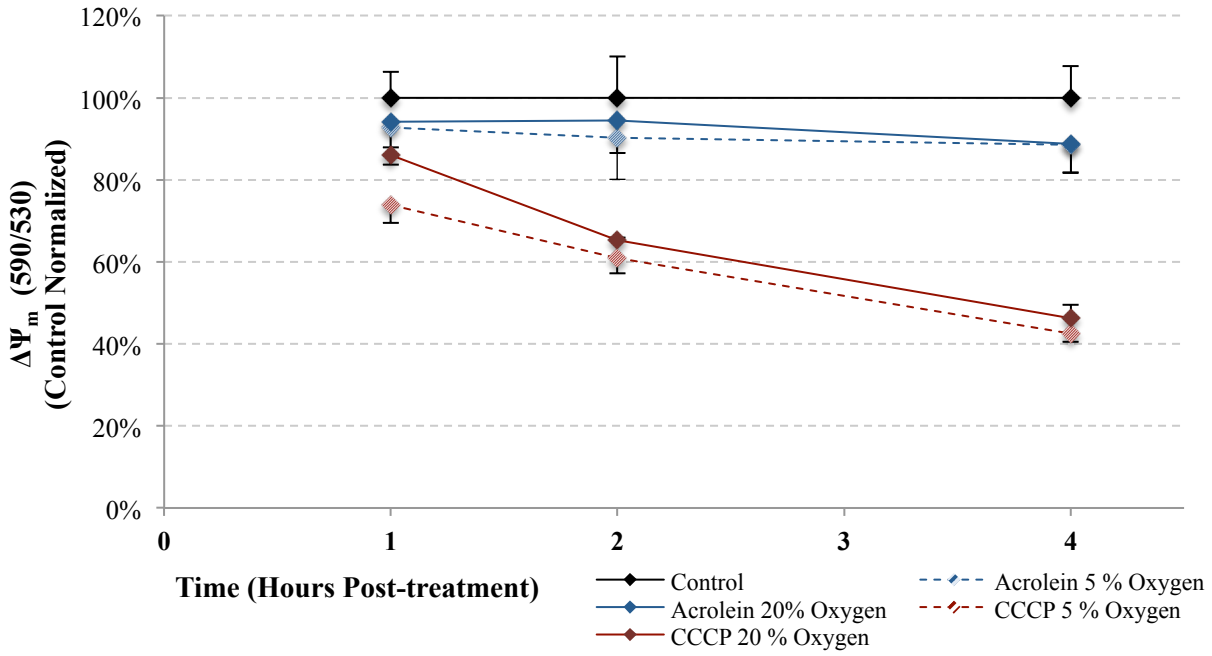

Figure 18. Mitochondrial Membrane Potential Measurements. Differentiated H9c2 cells cultured under either 5 or 20.1 % oxygen were exposed to 100 µM CCCP for four hours with repeated fluorometric measures during such time. The values expressed are normalized against the aggregate/monomer ratio of the control in order to exemplify the relative $\Delta\Psi_m$. CCCP significantly reduced $\Delta\Psi_m$ at four hours, though no difference in $\Delta\Psi_m$ reduction was observed dependent upon culturing oxygen tension. Individual points were the average of three (20.1 % oxygen) or four (5 % oxygen) independent experiments with SEM indicated by error bars.

previously mentioned, treatment with 25 µM acrolein resulted in insignificant decreases in $\Delta\Psi_m$ to 88 ± 7 % (5 % oxygen cultures) and 89 ± 7 % (20.1 % oxygen cultures) compared to respective oxygen tension controls. 5 µM CTZ-supplemented cells cultured under 20.1 % oxygen tended to attenuate the observed reduction in $\Delta\Psi_m$ compared to acrolein only-exposed cells; addition of 100 µM olaparib retained the $\Delta\Psi_m$ among acrolein-exposed cells to control levels (100 ± 2 %), while EGTA caused an unexpected increase in $\Delta\Psi_m$ (104 ± 3 %). Conversely, differentiated H9c2 cardiomyoblasts cultured under 5 % oxygen demonstrated a different response with respect to CTZ and olaparib supplementation at four hours (*Figure 19*). Addition of 10 mM EGTA elevated the basal $\Delta\Psi_m$ above respective controls (113 ± 5 %), and provided significant attenuation of $\Delta\Psi_m$ compared to acrolein-exposed cells (CI_{95} of Difference: 4-45 %, p

= 0.028). Similarly, addition of 5 µM CTZ elevated the basal $\Delta\Psi_m$ above respective CTZ controls (106 ± 3 %), but ultimately did not significantly attenuate $\Delta\Psi_m$ reduction among acrolein-exposed cells likely due to the wide variability of the acrolein-only treatment group. Co-exposure with 100 µM olaparib only modestly attenuated $\Delta\Psi_m$ upon exposure to acrolein to 93 ± 4 % control levels versus 88 ± 7 % of treatment only cells, and did not provide retention to control levels as did the standard culture H9c2 cells.

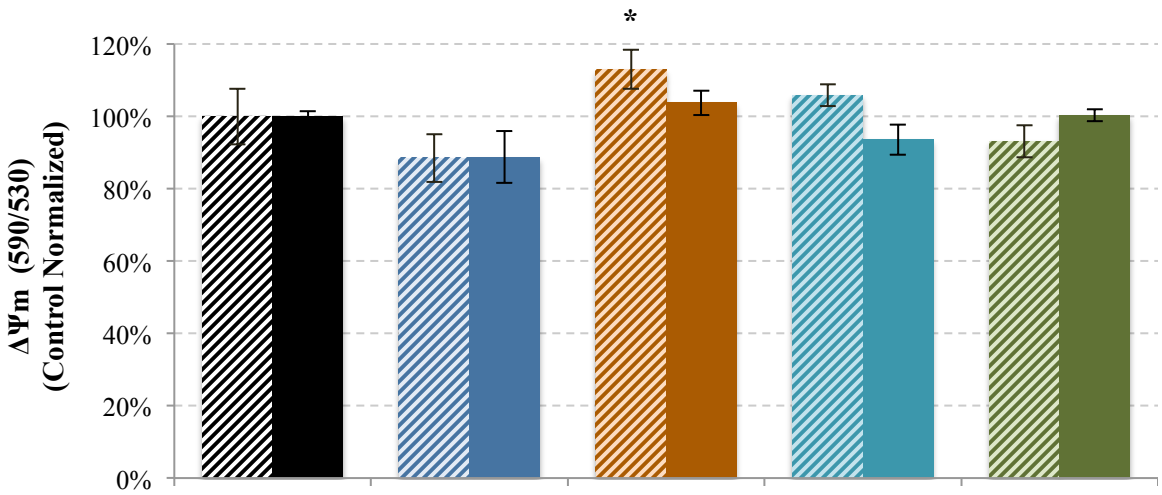

25 µM Acrolein	-	+	+	+	+
10 mM EGTA	(+)	-	+	-	-
5 µM Clotrimazole	(+)	-	-	+	-
100 µM Olaparib	(+)	-	-	-	+

Figure 19. Small Molecule Mitochondrial Membrane Potential Reduction Attenuation at Four Hours Post-exposure. Differentiated H9c2 cardiomyoblasts cultured under 5 % (Striped Bars) and 20.1 % oxygen (Solid Bars) exposed to 25 µM Acrolein (Blue Bars) were supplemented with small molecules in order to measure the effect of extracellular calcium chelation (10 mM EGTA; Orange), inhibition of TRPM2-associated calcium conductance (5 µM CTZ; Teal), or PARP inhibition (100 µM Olaparib; Green) on acrolein-induced $\Delta\Psi_m$ reductions. Values derived are the respective vehicle-normalized average of three (20.1 % oxygen) or four (5 % oxygen) independent trials with associated error bars denoting SEM. Statistical comparisons were made only between small molecule-supplemented cells exposed to acrolein and their respective small molecule controls cells denoted formally as (+). *$p < 0.05$ compared to respective acrolein-exposed cells.

CHAPTER FOUR:

DISCUSSION

4.1 Evaluation of Hypotheses

The current investigation aimed at examining the influence of oxygen tension in modulating acrolein-induced cytotoxicity in the differentiated H9c2 cardiomyoblast model. In order to elucidate the underlying factors causing significant alterations of the toxicogenic potential from acrolein, varying TCA and glycolytic substrates in vehicle media were utilized to measure their respective contribution to viability rescue. In doing so, the current investigation demonstrated significant changes in the cytotoxicity profile of the H9c2 cells after exposure to acrolein, particularly among media containing enriched pyruvate concentrations. For those standard condition culture cells, exposure to acrolein in the presence of enriched pyruvate did not offer cytoprotection. Therefore, the evidence from viability assessment suggests that reduction in oxygen tension would significantly attenuate cellular viability after exposure to acrolein only under certain circumstances. Rescue was not afforded for all TCA and glycolytic substrates, as glucose, glutamine, and glutamate did not significantly attenuate cell death at 24 hours after toxic insult. Pyruvate enrichment, especially among the standard low-serum DMEM, significantly attenuated viability loss after acrolein exposure. Therefore, hypothesis one was partially supported where only pyruvate attenuated cytotoxicity – all other substrate groups were similar to standard condition cultures with respect to viability.

Co-exposure of small molecule inhibitors, e.g., olaparib (PARPi), EGTA (Calcium chelator), and CTZ (Non-specific TRPM2 inhibitor) showed variable potential for viability attenuation. Under physiologically relevant oxygen culture, differentiated H9c2 cells were significantly protected by EGTA, while CTZ did not provide similar protection. Olaparib, however, demonstrated a particularly dubious pattern of rescue, which was associated with baseline toxicity. At high-magnitude acrolein cytotoxicity (Viability < 50 % controls), olaparib did not significantly provide protection from toxicosis. Conversely, at lower-magnitude cytotoxicity using the same concentration of acrolein, the same concentration of olaparib offered significant protection to H9c2 cells. Therefore, the evidence presented suggests that a complex interaction between cytotoxic injury and PARP inhibition exists, and PARP plays a partial role in acrolein toxicosis. As such, the second hypothesis regarding attenuation of viability loss under 5 % oxygen using a PARPi, was neither clearly rejected nor supported, though the potential exists for the latter scenario.

The effect of olaparib exposure during acrolein exposure on $\Delta\Psi_m$ alteration was assessed on cells maintained and exposed with acrolein cultured under 5 % and 20.1 % oxygen. Olaparib did not provide significant retention of $\Delta\Psi_m$ reductions observed after acrolein treatment, even at four hours post-acrolein exposure, though the $\Delta\Psi_m$ was not significantly different than controls either. Seemingly, olaparib exposure actually decreased the $\Delta\Psi_m$ among 5 % oxygen cultures compared to the 20.1 % cultures, though the difference was not significant. As previously mentioned, no obvious calcium transients were observed among cells cultured under 5 % oxygen and, thus, this parameter was not further explored. Therefore, the evidence of the current investigation does not clearly support the third hypothesis that PARP inhibition significantly altered $\Delta\Psi_m$ under acrolein toxicosis, though the $\Delta\Psi_m$ was significantly different than neither

controls nor acrolein-exposed cells; a latter tome-point may be prudent for elucidating this relationship further. Interestingly, both EGTA and CTZ did retain the $\Delta\Psi_m$ to control levels, indicating that extracellular calcium may generally contribute to baseline $\Delta\Psi_m$.

4.2 Methodology - MTT Reduction Assay

The MTT formazan reduction assay performed as a sensitive and stable proxy of individual well cell count, as denoted by the high coefficient of determination (R^2 = 99.7 %) when modeled as a polynomial-derived regression function. In some instances, however, estimated cell counts per well of proximal standards, especially those under 500 cells per well, were subject to reduced predictive power when utilizing a polynomial-derived regression model. Consequently, substantial underestimation of cell count quantification ensued. In such cases, exclusion of standard curve estimators, e.g., two of the highest calibration curve standards (7,500 and 5,000 cells per well), provided more accurate predictive power in quantifying low cell count samples, especially those standard curve wells seeded with 2,000 cells per well or less. Notwithstanding, when such a regression scheme was required, all samples under the 2,000 were similarly quantified using the linear regression equation to ensure homogeneity of quantitative methods; this practice was very reluctantly and infrequently required.

It is known that the MTT formazan reduction assay integrates both cellular number and metabolic profile of tested cells to derive "viability" estimates based on metabolically competent cells[207]. The metabolic profile described by Stepananko et al.[207] and Berridge et al.[217], to which MTT formazan reduction varies noticeably among endogenous anti-oxidant systems (e.g., SOD, HO-1), as well as endogenous respiratory machinery (Glycolysis and pyruvate metabolism), was likely demonstrated in the present investigation. In the present system, medium glucose proved a consistent modulator of overall formazan production (Blanked 570 nm optical density) when

comparing signaling among unexposed controls (*Figure 20*). In acrolein unexposed differentiated H9c2 cardiomyoblasts, a linear association consisting of basal MTT reduction among control cells was consistently observed up to 10 mM glucose; linearity was then lost up to the 25 mM glucose concentration found in the differentiation medium. A similar trend remained consistent among trial-matched cardiomyoblasts exposed to 250 μM acrolein for 30 minutes, albeit with a shallower slope compared to unexposed cells due to reduced MTT metabolism by H9c2 cells induced by acrolein exposure. The influence of medium glucose concentration on MTT metabolism was alluded by Vistica et al.[218], though that investigation provided predominantly circumstantial evidence. In the current investigation, we supply quantitative evidence to reinforce this notion. Therefore, utilization of respective medium controls was absolutely required. Since substrate medium controls were included, i.e., exposed cells were normalized against respective controls exposed with dilution-controlled hydroquinone in the respective substrate medium, the results would not have been construed; thus, the treatment effects observed would likely be closely representative of that attributable to acrolein. Furthermore, no substantial viability differences were observed at 24 hours among several substrate groups, thus the consequences of the apparent altered MTT metabolic kinetics does not reduce the integrity of toxicant-specific, viability analysis when controlling for medium glucose or other substrates utilized in this investigation.

4.3 Acrolein Treatment, Substrates, and Small Molecules

All glycolytic and TCA substrates chosen were based on available recognition of cardiac-specific membrane transporters which would allow potential influx of substrates within the H9c2 cells to modulate acrolein-induced alteration of metabolism and cell viability; data corresponding

to primary cardiac myocyte transporter identification and localization were considered applicable to the differentiated H9c2 model (*Table 11*). Results of MTT reduction among differing substrate- supplemented groups of differentiated H9c2 cells cultured under standard and 5 %

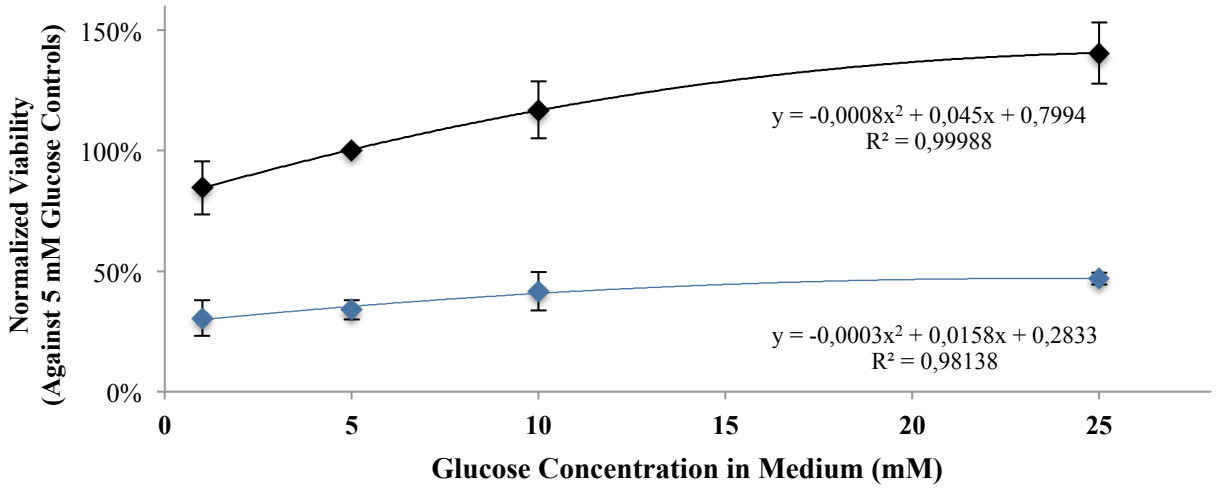

Figure 20. Dependency of MTT Reduction on Medium Glucose. The MTT reduction results from the two-hour washout controls (Black Diamonds) and acrolein-exposed (Blue Diamonds) differentiated H9c2 cells were aggregated and normalized against the RP medium (5 mM glucose-containing DMEM). The 25 mM glucose point was derived from the low-serum DMEM substrate group as pyruvate was not shown to significantly alter MTT reduction capacity, at least at the 1.0 mM found in the LS DME medium. Each point corresponds to the mean of 3-5 independent experiments with associated standard deviation denoted by error bars.

oxygen culturing conditions demonstrated two key patterns: 1) likely induction of acute-phase MTT-reducing xenobiotic machinery and 2) a glucose- and pyruvate-sensitive metabolic and respiratory rescue phenotype under 5 % oxygen. The former shall be discussed in detail, followed by substrate-specific effects.

Moghe and colleagues[219] published recently a poignant review highlighting not only the target organs affected by and mechanisms of acrolein as related to human disease, but also reported potential therapeutic agents specifically shown efficacious in attenuating mechanistic pathways, e.g., oxidative stress, mitochondrial dysfunction, endoplasmic reticulum stress, etc. The myriad of cell-based models and acrolein exposure conditions, i.e. concentration and

duration of exposure, however, can render interpretation of the current data difficult to decipher in perspective to other investigation. For example, our laboratory has shown a consistent concentration-dependent activation of poly(ADP-ribose) polymerase at concentrations between

Table 11. Relevant Cardiac Substrate Transporters

Substrate	**Transporter**	**Source(s)**
d-Glucose	*GLUT4* GLUT1	Liu et al., 2013a[220]
L-Pyruvate	MCT2	Lin et al., 1998[221]; Bonen, 2001[222]
L-Glutamine	*SN1* rATA2	Bode, 2001[223]; Sugawara et al., 2000[224]
L-Glutamate	GLT1v EAAT1	Kugler, 2004[225]
α-ketoglutarate*	2-OG Transporter mNaDC-3	Takeda et al., 2012[226]; Shank and Bennett, 1993[227]; Pajor, Gangula, and Yao, 2001[228]

*In the current investigation, 5.0 mM of α-ketoglutarate was shown to interfere with the MTT assay.

50 and 100 μM, but reduced activity at and above 250 μM acrolein when cells are exposed to acrolein for thirty minutes under standard culture conditions (Unpublished data Harand et al.); however, elevations were observed at 25 μM as early as 5 minutes post-exposure, reaching significant levels (45 % above controls) at 15 minutes (Current investigation). Though PARP activity may wane 30 minutes after exposure, it cannot be outright rejected that exposure metrics substantially alter mechanistic interpretation – the current example merely relates to acrolein toxicosis within the H9c2 model. Stevens and Maier[229], pre-dating the Moghe et al. review, pointed out some of the key experimental conditions, for example difference in cell lines, culture conditions, and medium compositions, which explain the multifaceted and, in some cases, conflicting *in vitro*-based mechanistic findings characterizing cell death modalities exacted by acrolein; the authors limited their review only necrosis and apoptosis as viable cell death

modalities. The current investigation has supplied evidence not to explain the differences in cell death modalities, but rather a complex interaction whereby specific medium constituents and physiologically relevant oxygen culture may alter the mechanism of cytotoxicity.

Acrolein exposure under standard culturing conditions did not induce supra-levels of MTT reduction compared to controls irrespective of initiation time of MTT analysis after treatment. Presuming MTT reduction as a proxy of viability, MTT analysis of acute exposure periods (2-hour washout) exemplified the rapid degeneration of H9c2 MTT reduction capacity, especially after high concentrations of acrolein (250 μM); however, lower concentrations consistently resulted in near-control MTT signals. In order to assess immediate MTT reduction capacity changes, similar exposure conditions were conducted across a broad range (0-250 μM) of concentrations of acrolein followed immediately by initiation of the MTT assay. All exposures were conducted in the low-serum DMEM. Even in this short period, large reductions in MTT metabolism capacity were noted at 100 μM (71 ± 6 %; $p < 0.01$) and 250 μM (64 ± 4 %; $p < 0.001$) compared to controls (*Figure 21*). However, no immediate increases in MTT were observed since transcriptional up-regulation of antioxidant response elements would likely not be manifested in such a short period after exposure to facilitate enhanced MTT conversion (*Discussed below*). Particularly of cells cultured under standard conditions, exposure to acrolein at even 1 μM consistently reduced MTT reduction capacity within 6 hours, which can reach levels above controls at 24-hours. These results demonstrate a potential delay in up-regulated or otherwise and enhanced metabolic pathways due to acrolein. However, transcription-based methods would undoubtedly confirm these preliminary findings.

Unfortunately, investigations in short-term metabolic competency of acrolein-exposed H9c2 cells are generally rare. Agarwal and colleagues[230] exposed isolated mouse Type II alveo-

lar ECs (pAT2 cells) with graded acrolein concentrations, and then assessed cytotoxicity via MTT reduction in deriving an IC_{50} value. At acrolein concentrations of 10 µM or less, MTT reduction exceeded respective controls: 5 µM (Approximately 115 %) and 10 µM (Approximat-

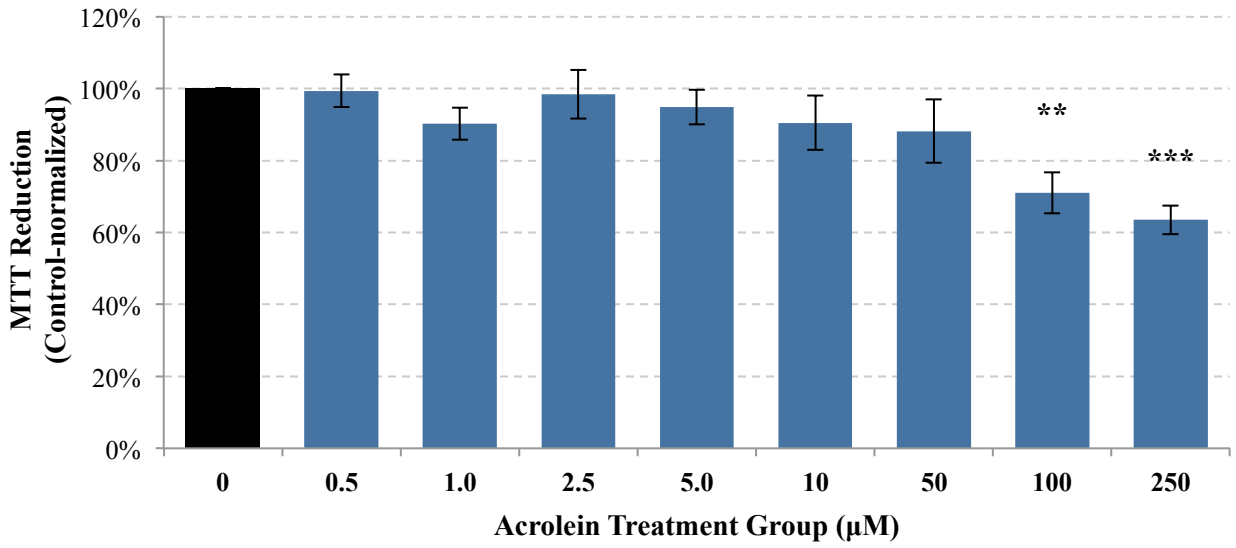

Figure 21. MTT Reduction Immediately After Acrolein Treatment. H9c2 cells were cultured and differentiated under standard conditions prior to 30-minute acrolein exposure. Immediately after acrolein exposure, H9c2 cells were assessed for MTT reduction capacity. A decreasing trend was observed beginning at 2.5 µM up to the highest concentration of 250 µM. Bars are the mean of 4-6 independent trials with associated SEM denoted by error bars. $^{**}p < 0.01$ and $^{***}p < 0.001$ compared to hydroquinone-only containing controls (Black Bar).

ely 108 %). Similar results were reported for neither primary rat lung epithelial (RLE-6TN) cells nor human lung adenocarcinoma (H441) cells within the same investigation; no explanation was given as to this inconsistent finding. It is known that oxidative insult in lung epithelial cells activates antioxidant response element transcription through nuclear factor erythroid 2–related factor 2 (Nrf-2) nuclear translocation, after which antioxidant systems, such as HO-1, TRx, GST, NQO-1, among others, become up-regulated or activated[231], and can confer significant cytoprotection[232] by re-establishing cellular redox balance (Succinctly reviewed in Nguyen and colleagues[233]). Nrf-2 activation occurs also in the presence of electrophiles, particularly the NAPQI-induced antioxidant response in rodent hepatocytes when treated with acetaminophen[234]

or acrolein[235]. What remains little known, contrarily, is the contribution of up-regulated antioxidant systems and microsomal xenobiotic metabolism in MTT reduction within 12 hours of oxidative injury. Ishii and colleagues[236] demonstrated that macrophages show significant Nrf-2-dependent up-regulation in HO-1 for select compounds, e.g., hydrogen peroxide, at 9 hours of treatment. Tirumalai and colleagues[235] showed increased NQO1 mRNA transcripts in as little as 30 minutes and heavy chain γ-glutamylcysteine synthetase at one hour, though functional metabolic competence was not characterized. In the CD-1 mouse, high-dose acetaminophen causes hepatic Nrf-2 nuclear translocation dose-dependently within 60 minutes[237], while total HO-1 protein was found insignificantly elevated to 150 % of controls at five hours, despite the significant elevations in mRNA transcripts[238]. Should a short-term Nrf-2-mediated response hold true in the current model, the potential for enhanced antioxidant up-regulation even within such a short exposure period may explain enhance MTT reduction at low treatment levels.

In the current investigation, low concentration acrolein-exposed differentiated H9c2 cells cultured under 5 % oxygen demonstrated consistent elevations in MTT reduction when assessed after a two hour exposure (In addition to a 3 hour MTT incubation period). Interestingly, the magnitude of MTT reduction did not depend upon substrate supplementation, for which all 1 μM-exposed groups were above controls. If pyruvate does act as an acrolein scavenger, it would be expected that such MTT reduction capacity increases would be minimally, if at all, observed among pyruvate groups, especially among the higher, 2.5 mM pyruvate concentration at the 1 μM acrolein exposure groups. In opposition, near-control MTT reduction values were, nonetheless, not observed for the pyruvate groups, and were actually inversely related to pyruvate concentration – statistical differences are not expected. At 25 μM of acrolein, MTT reduction was inversely related to medium glucose concentration, but not statistically significant.

Physiological concentrations and supra-physiological glucose levels (10 mM in glucose-enriched physiological medium as well as 25 mM in low-serum DME medium) seemingly sensitized H9c2 cells to acrolein toxicity, though this was not entirely unforeseen. Glucose has been shown to be cytotoxic (See below for extended discussion) in the H9c2 cells line[239], leading to reductions in viability. The results of the current investigation seemingly support this notion though the mechanism was not further explored.

After 24 hours, H9c2 cells exposed in pyruvate-supplemented medium (Including low-serum DMEM) did, indeed, provided significant rescue in cellular viability after 25 μM treatment. Pyruvate rescue has been reported extensively within the literature, particularly in conjunction with PARP activation[58]. Numerous mechanisms have been proposed including, but not limited to: increasing respiratory support[240], acting as an antioxidant[241], and promoting increases and retention in intracellular glutathione (Via GPx activity induction)[241]. Wang et al.[240], for example, showed rescue by pyruvate supplementation in the human neuroblastoma cell line, SK-N-SH, after treatment with modest concentrations of hydrogen peroxide. The authors attributed the rescue to pyruvate-dependent reduction in mitochondrial oxidative species secondary to H_2O_2 treatment, which was in concordance to significant retention of $\Delta\Psi_m$ among pyruvate-supplemented cells. Since pyruvate has also been implicated as an antioxidant in culture systems[241], indirect measurement of acrolein to characterize the interaction of acrolein with medium-supplemented pyruvate was undertaken. Consequently, pyruvate does not confer protection by mere scavenging since medium acrolein concentrations were not altered by 2.5 mM pyruvate supplementation compared to basal RP medium, 230.5 ± 17.1 μM versus 234.6 ± 6.5 μM, respectively, at 30 minutes post-addition to medium at room temperature. Some compounds, as do the arterial vasodilators hydralazine and dihydralazine and MAO inhibitor

phenelzine (Reviewed in Hamann and Shi[242]), have been shown to scavenge acrolein; the current investigation essentially ruled out this potential avenue of cytoprotection. Therefore, the mechanism of pyruvate rescue could not be attributed simply due to acrolein depletion from high pyruvate-supplemented medium, and likely suggests a compensatory mechanism in energy production or substrate utilization. This interpretation seems befitting as H9c2 cells cultured under standard culture conditions exposed to 25 and 250 μM resulted in significantly increased MTT reduction at 250 μM compared to RP medium exposed cells, but insignificant elevations at the intermediary 25 μM treatment group. Conclusively, a unified mechanism of pyruvate-based rescue most appropriately characterizes the results observed, but only for H9c2 cells under physiologically relevant oxygen tension. The pyruvate-dependent capacity for offering cytoprotection was limited under standard culturing conditions, i.e., the rescue by pyruvate after 25 μM acrolein treatment was no different than any other substrate group. As such, a metabolic reprogramming is most likely observed.

Notwithstanding, the actual medium composition has a contributory, but not absolute, effect on the magnitude of cytotoxicity. For example, freshly isolated mouse lung slices treated with acrolein displayed a profoundly heterogeneous ATP depletion pattern in L2 cells (Cultured cell line) compared to fresh lung slices[243]. Reduction of ATP to 80 % of control levels in lung slices required approximately one order of magnitude higher acrolein (50 μM versus 5 μM) compared to the more acrolein-sensitive L2 culture cells, though the heterogeneous cell matrix of precision lung slices undermine direct comparisons to L2 cells solely on a mechanistic basis. Some of the rescue found within precision lung slices may be attributed to the underlying microenvironment. Co-culture of cardiomyocytes with endothelial cells demonstrate a dynamic interaction between the two cells types to offer energy support via respiratory substrates,

including pyruvate[244]. Thereupon the microenvironment enshrouding any given cardiomyocyte *in situ* may provide more pyruvate equivalents than offered simply by the diffusive capacity from intra-cardiac blood supplies. Coupling the data with cell isolates[230] definitively demonstrates respiratory and metabolic differences between cell line- and tissue isolate-derived cytotoxicity investigations. With respect to the current investigation, the source of cytotoxic sensitivity likely relies in part upon oxygen-dependent increases in both energy production and xenobiotic detoxification induction reserve capacity under physiologically relevant oxygen culturing conditions (5 %) compared to the limited, to plausibly absent, potential within the 20.1 % cultures. If true, such a finding would have a substantial impact on *in vitro*-based cytotoxicity data interpretation when extrapolated to *in vivo* correlations.

Enrichment of medium with glucose did not offer cytoprotection under either oxygen culturing condition. As such, the results of the current investigation corroborates evidence demonstrating not only negligible rescue via glucose enrichment in either astrocytes or neurons[54], but short term metabolic MTT analysis suggest that high glucose, both in the 10 mM glucose and the low-serum DME medium (25 mM glucose), may actually be deleterious. An inverse relationship between acute MTT reduction and glucose supplementation after 25 μM acrolein exposure was observed, but was less pronounced among cells treated with 1 μM acrolein. These results are in corroboration with Li et al.[239] who reported increased TUNEL positivity and associated 72-hour viability reductions in H9c2 cells incubated with 35 mM glucose. The authors did not report values for an analogous 25 mM glucose concentration utilized in the current investigation. Conversely, 24-hour viability measurements among the 10 mM glucose group (129 ± 11 %) were similar to that of the 1 mM glucose group (127 ± 13 %), with the low-serum DME medium resulting in the lowest viability (102 ± 8 %). Since the MTT

assay is sensitive to incubation medium glucose[207](And this investigation), relative viability comparisons among unexposed H9c2 cells incubated in differing glucose-containing media in the current investigation are not permissible, but would provide additional evidence that enriched glucose does indeed result in viability/metabolic reductions in the present system.

Since pyruvate utilization for the TCA was likely enhanced in media containing 1.0 or 2.5 mM pyruvate, enrichment of glucose was hypothesized to contribute more pyruvate equivalent via the end-product of glycolysis. While glucose conversion can neither be ruled in nor out in the current investigation mechanistically, functional glycolytic production of energy equivalents for the TCA cycle resulting in metabolic rescue was not observed irrespective of culture oxygen conditions. There results are paradoxical as a shift in metabolic reprogramming was denoted by pyruvate rescue. It is to be presumed that a reduced oxygen tension would subsequently activate HIF-1α in the current culture system under 5 % oxygen, as previously demonstrated in other systems[245], though duration of oxygen tension reduction – chronically in the current investigation compared to typical acute hypoxic insults – may undermine such a simplistic extrapolation. Nonetheless, since virtually every enzyme involved in glucose metabolism has been shown to be up-regulated by HIF-1α induction (Reviewed in Semenza[246]), glucose supplementation would have the potential to provide metabolic rescue. A glucose-based rescue was not observed. Three plausible explanations exist: Firstly, while neither specific to cardiac tissue nor being the major cardiac glucose transporter for H9c2 cells[220], acrolein has been associated with inhibition of the GLUT3 isoform found primarily in primary cortical neurons *in vitro*[247]. Whether acrolein inhibits cardiac GLUT4 in H9c2 cells is unknown. Should GUT4 inhibition hold under acrolein exposure within the differentiated H9c2 model, enrichment or glucose deficiency would be expected to influence functional metabolism minimally – the

observed results corroborate this as a plausible notion. Secondly, glycolysis requires two oxidized NAD^+ equivalents as well as two ATP equivalents in the early phase of glycolysis – two adenine nucleotide substrates which become rapidly reduced or depleted under acrolein-associated oxidative stress[248]. Under this assumption, enriched glucose may provide rescue under metabolic stress, but whose efficacy may be restricted kinetically with respect to adenine nucleotide equivalents. Andrabi and colleagues[249] present stark evidence contesting NAD^+ as a major contributor to inhibition of glycolysis under DNA alkylation with MNNG, as NAD^+ and ATP levels were paradoxically retained after 15 minutes of exposure to MNNG. Furthermore, inhibition of glycolysis was shown significant within same investigation, and was reversed by pyruvate supplementation, suggesting specific sensitivity of the glycolytic pathway to acrolein exposure. Thirdly, enzyme-specific inhibition of glycolytic machinery may account for the observed negligent rescue. Martyniuk and colleagues[250] showed potent inhibition of purified glyceraldehyde-3-phosphate dehydrogenase (GAPDH) by acrolein via direct enzyme adduction with an acrolein-specific K_i of 38.1 ± 0.83 μM (Mean ± SD) – approximately 1.5-fold higher than the concentration utilized in the current investigation; other α,β-unsaturated carbonyl aldehydes also inhibited GAPDH in the same investigation, and likely demonstrates a class effect. Agarwal and colleagues[230] showed such inhibition effectively translates to consequential glycolytic inhibition within an *in vitro* system. All together, the negligible rescue afforded by glucose supplementation in the current investigation likely reflects a mechanism whereby glycolytic metabolism remains sensitive to acrolein adduction of GAPDH. Evidence suggesting a metabolic shift by low oxygen tension may alter glycolytic capacity, but direct acrolein inhibition may not permit rescue by acrolein due simply to GAPDH inhibition. The exact

mechanism in the H9c2 model after exposure to acrolein requires further attention in order to confirm these presumptions.

Finally, medium supplementation with glutamine (5.0 mM) and glutamate (1.0 mM) provided short-term MTT reduction capacity among 5 % oxygen cultures compared to those cultured at 20.1 % oxygen exposed to 25 μM, but did not offer significant long-term protection at 24 hours. Non-significant elevations in viability were observed among similarly-exposed H9c2 cells supplemented with 5.0 mM glutamine (37 ± 10 %) compared to the glucose- and glutamate-supplemented cells (24-28 % viability). Li and colleagues[239] rescued H9c2 cells from reperfusion in the presence of high concentrations of glucose concentration-dependently with glutamine supplementation. Isolated embryonic ventricular cardiomyocyte reduction in viability was attenuated significantly by glutamine after *in vitro* simulations of reperfusion injury[251]. On an organ level, isolated rat hearts tend to have increased intracellular ATP concentrations compared to tissue extracts[252], denoting, at least partially, rescue may be afforded by glutamine through respiratory support. Given the tendency of glutamine to rescue differentiated H9c2 cells in the current investigation, a lower acrolein (< 25 μM) may exemplify such a plausible end-point, though further testing is required to confirm. Since catalytic production of α-ketoglutarate requires glutamate and oxaloacetate via aspartate transaminase, restriction of pyruvate equivalents by GAPDH inhibition may shunt the efficacy of glutamine, which is converted via glutaminases to glutamate, or glutamate rescue observed in the ischemic models described. In summary, the results of the current investigation affirm the metabolic reprogramming when adapting cells to 5 % oxygen, as described by Pereira and colleagues[65] though the inhibitory effect of acrolein itself may restrict metabolic rescue via metabolic pathway shunting.

In the current investigation, acrolein exposure to 25 μM was shown to acutely activate poly(ADP-ribose) polymerase significantly at 15 minutes post-exposure, while insignificant activation was demonstrated in as little as 5 minutes. Earlier or latter time-points were not investigated. Hyper-activation of PARP is known to induce parthanatos, a relatively novel cellular death subroutine[253], consequently leading to cell death. Early activators of PARP included gamma radiation[254-257], hydrogen peroxide[160,255,258], and the DNA alkylator MNNG[58,160,172,259], among others. While the aforementioned three activators exemplify three canonical mechanisms of exacting DNA structure-altering lesions (Radiation, oxidative injury, and direct alkylation) leading to PARP activation[260], such a broad promotion of activation, e.g., non-B conformation DNA[261], suggests that a plethora of cytotoxicants could plausibly activate, and possibly over-activate, PARP. Indeed, interest in characterizing the activity of PARP with respect to acrolein toxicosis has been investigated. Abraham and Rabi[248] attributed, at least in part, PARP overactivation as a collateral mechanism of cyclophosphamide-associated hemorrhagic cystitis, as significant elevations in histochemical staining of poly(ADP-ribose) polymers with associated NAD^+ reductions was found in rat bladder tissue. Another investigation, however, suggested that PARP was cleaved early in CP-associated bladder tissue injury[262], but may demonstrate a dose-dependent phenomenon where low-dose CP (80 mg CP/kg BW[262]) induces early caspase activation, whilst higher doses (150 mg CP/kg BW[248]) causes PARP overactivation, thereby shunting reduction equivalent, e.g., NAD^+, input into apoptotic machinery with such a severity as to abrogate caspase induction and subsequent PARP cleavage. Tanel and Averill-Bates[263] demonstrated executioner caspase activity intensification at a remarkably low acrolein exposure window of 1-30 fmol acrolein per CHO cell, particularly that of caspase-7. Interestingly, at 50 fmol per cell, pan-caspase activation, with the exception of

caspase-9, was not significantly different than that observed at 30 fmol acrolein per cell in their CHO model. This result is in accordance with the current investigation as 80,000 seeded H9c2 cells exposed with 800 μL of medium supplemented to a concentration of 25 μM acrolein corresponds to approximately 250 pmol (250,000 fmol) per H9c2 cell - PARP inactivation, at least to the level whereby PARP activity was lower than controls, was not observed. It cannot be ruled out that some cells do exhibit caspase activation, while others do not – such a modality would undoubtedly be the product of microenvironment heterogeneities even within microplate wells. Should an acrolein concentration-dependent threshold of differential, or at least shifting contribution of, mechanistic initiation exist, the data point to a predominance of low-concentration caspase activation with high-concentration mediated PARP activation; the discussed *in vivo* data seemingly corroborate this ill-defined *in vitro* phenomenon.

A hyper-acute, modest exposure of acrolein significantly activated PARP in the H9c2 cell line under physiologically relevant oxygen tension. Since PARP activity was enhanced 20 % and 45 % at 5 minutes and 15 minutes, respectively, and the latter time-point was significantly higher than time-matched controls, PARP inhibition would be presumed efficacious in attenuating viability reductions if PARP contributes to the toxicogenic mechanism of acrolein-induced toxicosis at the investigated exposure concentration. Initial tests of high concentration olaparib (100 μM) provided limited rescue at 24-hours as viability loss was reduced by 14 % with concomitant olaparib exposure in RP medium derived from FBS batch 1; the analogous reduction of viability loss among cells exposed in RP medium supplemented with batch 2 FBS was approximately 5-fold higher at 65 % (*Figure 22*).

The results may overtly suggest an issue with toxic insult irreproducibility; however, modulation of viability to acrolein exposure was not observed among H9c2 cells cultured under

standard oxygen culturing condition, restricting the heterologous response to a single group. Since the current investigation had shown demonstrative increases in cellular viability during pyruvate supplementation, the observed effect may represent a change in exogenous pyruvate

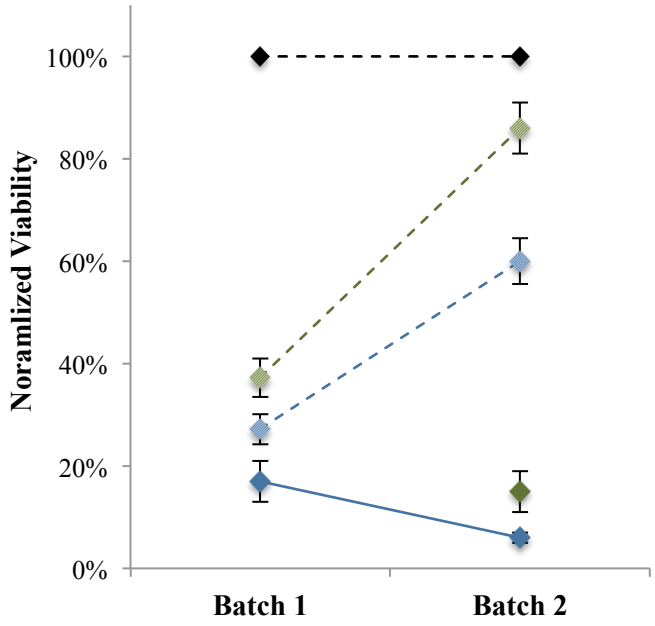

Figure 22. Rescue Enhancement by Olaparib in the Presence of Two Differing FBS Batches. H9c2 cells were cultured in either 20.1 % oxygen (Solid Diamonds) or 5 % oxygen (Striped Diamonds) prior to differentiation and treatment with 25 µM acrolein (Blue Diamonds) or respective controls (Black Diamonds; both 5 and 20.1 % oxygen cultures included in single point estimate). Concomitant exposure with 100 µM olaparib (Orange Diamonds) in the presence of acrolein resulted in differential rescue, and depended on FBS batch. Furthermore, increases in baseline viability were also observed. PARPi efficacy was only observed among cells cultured at 5 % oxygen with medium containing batch 2 FBS. Each point represents the mean of 4-9 individual treatments with associated SEM denoted by error bars.

concentration contributed by FBS; the effects of other FBS-containing constituents cannot be dissected for contribution under the limited scope of this investigation, but warrants further characterization. Heterogeneous composition of FBS, especially between production sources, has been long identified and implicated in undermining the certainty of cell-based research reproducibility[264,265]. The current investigation likely reports another manifestation of this insidious notion with a major caveat: the division of impact across cell cultures maintained and

exposed in differing oxygen tensions undermines an overly simplistic batch-to-batch effect, since cells under 20.1 % oxygen were unaffected. Furthermore, a substantially different proportional rescue of acrolein-exposed differentiated H9c2 cells was observed, and deserves considerable discussion. The implication of these seemingly unfortunate results may have inadvertently unveiled differential weights of mechanistic cellular fate, which could act independently of toxicant concentration. Thereupon, the rescue potential of PARP inhibition went from insignificant under demonstrative toxicant insult, i.e., batch one baseline toxicity versus olaparib administration, to largely efficacious when baseline toxicity was reduced (FBS batch 2 containing medium). Of note, olaparib did not ablate viability reductions, as olaparib-supplemented acrolein-exposed cells still demonstrated significantly lower viability than respective controls (86 ± 5 % versus 100 %; $p < 0.05$). Conclusively, two separate key findings are to be observed from this phenomenon: 1) batch-to-batch variation may affect viability estimates within the same cell system differentially, especially when physiologically relevant oxygen tensions are introduced; and 2) the influence of PARP activation in determining cell fate may impinge upon the magnitude of cytotoxicity, rather than simply upon toxicant concentration.

Acrolein exposure did not significantly reduce $\Delta\Psi_m$ at either oxygen culture four hours post-treatment, though a decreasing trend was noted. Furthermore, no difference in normalized $\Delta\Psi_m$ after treatment between the two oxygen concentrations was found. Given a decreasing trend up to four hours, it is expected that further $\Delta\Psi_m$ reductions would occur when the post-treatment period is extended, especially since viability estimates denote substantial cytotoxic injury after a 24-hour exposure. Jia and colleagues[266] did not observe significant reductions in human retinal epithelial ARPE-19 cells exposed to 25 μM one day post-exposure. Cells analyzed 8 days post-exposure to as little 5 μM acrolein showed significant $\Delta\Psi_m$ reductions via JC-1 labeling

compared to controls, denoting a latent disruption of mitochondrial integrity in the ARPE-19 model. Nonetheless, even small reductions in ΔΨm were substantially reversed among exposed cells cultured under 20.1 % oxygen in the presence of the extracellular calcium chelator, EGTA, but only minimally attenuated in the presence of CTZ (94 % Controls); the PARPi olaparib retained the $\Delta\Psi_m$ to 100 % of controls. Territo and colleagues[94] demonstrated relative changes in oxygen consumption with respect to free calcium using an isolated mitochondrial system. Though they did not isolate the $\Delta\Psi_m$ as a dependent factor, they showed that: 1) oxidative uncoupling does not occur at extra-mitochondrial free calcium concentrations even up to 500 nM; and 2) increases in extra-mitochondrial calcium did result in reductions in $\Delta\Psi_m$, despite increases in oxygen consumption. These results denote an inverse relationship between calcium and $\Delta\Psi_m$. With H9c2 cells cultured at 20.1 % in the current investigation, consistent, low-grade calcium transients were observed when cells were exposed to 25 μM. Ablation of this transient by extracellular EGTA provided complete $\Delta\Psi_m$ retention after acrolein exposure, affirming the likely role of extracellular stores in determining mitochondrial integrity. This observation was mimicked in cultures under 5 % oxygen, though calcium transients were not consistently found among cells cultured at the lower oxygen tension. It is known that $\Delta\Psi_m$ can undergo a transient voltage potential reduction and recover, especially when calcium influx from extracellular stores is prevented[267]. The current investigation likely affirmed this notion among EGTA-exposed H9c2 cultured under both oxygen conditions; however, the insignificant reductions in $\Delta\Psi_m$ may indeed signify a persistent, progressive reduction in $\Delta\Psi_m$, from which cells may not be able to recover in the long-term, i.e., 24 hours. Since viability assessment definitively shows drastic viability losses at the same acrolein concentration, particularly among standard cultures, it would be expected that $\Delta\Psi_m$ measurements beyond four hours would definitively provide evidence of

eventual mitochondrial dysfunction and collapse. Extension of the $\Delta\Psi_m$ assessment period would also provide additional evidence regarding the mechanistic underpinnings of PARP activation and possibly related clotrimazole-sensitive calcium transient, i.e., TRPM2 channels in determining cell sensitivity or fate under acrolein toxicosis. Otherwise, increases in $\Delta\Psi_m$ among samples exposed to 20 mM EGTA suggest a definitive role of calcium in determining mitochondrial membrane potential, irrespective of oxygen tension.

While the current investigation was not able to demonstrate a calcium conductance among cells cultured in 5 % oxygen after acrolein exposure, a Fluo-4 reported peak 221 % of controls was observed among standard condition cultures and decayed after a lapse in time. Therefore, at least among standard condition cultures, rapid calcium transients were confirmed which was explicably due to an intracellular flux through extracellular conductance channels, suggestive by ablation by high concentrations of extracellular EGTA. To characterize if conductance via PAR-gated TRPM2 channels was involved in this transient, H9c2 were exposed in the presence of 5 μM CTZ, which, similarly to EGTA, retained intracellular calcium to control levels up to 270 second post-exposure. Thereafter, intracellular calcium reduced significantly at 300 seconds until the end of measurements. The current results are consistent with patch-clamp studies investigating the effect of clotrimazole-sensitive calcium conductance in the presence of high intracellular PAR levels[268]. Since time-dependent activation of PARP in this model was confirmed in as little as five minutes, whereby significant PARP activation occurred at 15 minutes, the potential for excluding extracellular calcium from CTZ-sensitive transients initiated by free PAR with CTZ would implicate TRPM2 channels in contributing in calcium transients. Indeed, ablation of the calcium transient observed affirmed this potential mechanism. Since CTZ has been associated with PARP activation-associated calcium transients through the TRPM2

channel in the presence of oxidative species, i.e., H_2O_2 and other oxidants, it may be presumed that CTZ was successful in inhibiting TRPM2 channels and subsequent calcium influx. However, since this only provides circumstantial activation of PARP involvement, co-exposure with high-concentrations of PARPi olaparib (100 μM) similarly blunted the calcium transient. At 360 seconds insignificant calcium transients were observed and corresponded to an increase of 55 ± 100 % above controls in the presence of olaparib. Nonetheless, these results demonstrate that an acute exposure to 25 μM acrolein induces an extracellularly-derived calcium transient through a PARP activation-initiated conductance mechanism which was sensitive to CTZ. This describes the consistent pattern of TRPM2-associated calcium transients. Since the current investigation did not confirm that acrolein induces a rise in intracellular calcium in 5 % oxygen cultures, likely credited to inexplicably high variation among those cells cultured under low oxygen, concordance between extracellular calcium depletion and the rescue phenotype observed remain tentative for this culture condition. It is important to note that cells cultured under 20.1 % were not protected by the same concentration of EGTA, despite confirmation of a calcium transient, and remains an important caveat to the proposed mechanism. The demonstrative viability loss observed among these cultures (> 90 % loss) suggests that standard cultured cells are intrinsically primed for cellular death by acrolein, and that calcium influx may play a minimal role in the summation of toxicogenic insult. However, concordance to calcium transient data and PARP activation may still be applicable to 20.1 % oxygen cultures at lower acrolein exposure concentrations.

4.4 Why the Transient, and What is With the Delay in Transient?

It is prudent at this time to state that acrolein, at the concentration investigated under the tested conditions, likely did not cause a disintegration and permeation of the plasma membrane. This was concluded since acrolein-only exposed cells exhibited a self-limiting calcium transient of approximately 240 seconds in duration. Should membrane permeability be enhanced, a persistent spike in intracellular calcium would have been noted. Additionally, small molecule-supplemented cells also did not exhibit consistent rises in intracellular calcium, denoting the membrane remained effectively intact during calcium transient measurements.

As for the rapid transient observed, the time to peak may offer support in a PARP-activation-mediated induction of intracellular calcium rise. In patch clamp experiments, various toxicants are delivered through the patch pipette, allowing direct access to the site of action, e.g., hydrogen peroxide[143]. ADP-ribose polymers are delivered in this manner, as they cannot traverse the hydrophobic plasma membrane readily[115]. In doing so, however, a significant reduction in the time between the rise intracellular PAR levels and calcium conductance reporting would be observed. Where PAR is injected intracellularly, the direct ligation of the cell membrane in whole-cell patch clamping can, however, reduce the time to adequately facilitate PAR-induced gating of TRPM2 channels, thus reducing the requisite time to activate TRPM2 channels. Under physiological conditions, the cytosolic PAR concentration would depend on diffusive capacity from the point of origination within the nucleus. For example, in whole-cell models, cytosolic PARP increases requires not only PARP activation, but preceding DNA damage causes PARG liberation of auto-ribosylated PARP-associated PAR to activate PARP in the repair signaling cascade; subsequent PARG-, and possibly ARH3-, dependent hydrolysis of histone-associated PAR upon completion of DNA repair is the most prominent contributor to free PAR[269,270]. In the

current investigation, the duration of time from acrolein exposure to initiation of fluorometric measurements was monitored, and resultant reported time post-exposure adjusted accordingly. Such an adjustment was made in order to coordinate cytosolic calcium data with PARP activation characterization and to offer insight in the absolute time-to-calcium rise characteristics in differentiated whole-cell H9c2 cardiomyoblasts. In doing so, the initial activation of PARP coincides with initial influx of calcium recordings. Which event, e.g., PARP associated auto-ribosylated PAR or histone-associated PAR hydrolysis, contributed to the observed calcium transient activation remains unknown. Data implicating the initial liberation source of PAR in TRPM2 activation simply does not exist. The rapid phase of DNA damage and PARP activation does not lend itself readily to discerning the exact time between DNA damage and following PARP overactivation, from which post-repair PAR may be distinguished from pre-liberated PAR associated with initial PARP activation.

Fluorometric measurements of calcium transients were performed until 960 seconds post-exposure, and even acrolein-only exposed cells even under standard culture conditions returned to the baseline levels (≈100-130 %) of unexposed controls (Data not shown) without further transients. Considering significant PARP activation at 15 minutes (900 seconds), the lack of latent or recurring calcium transients up to 16 minutes remains unknown. One source could have arisen from depletion of intracellular Fluo-4 fluoroprobe via extracellular extrusion. Investigations measuring intracellular calcium concentrations with Fluo-4 typically include probenecid or sulfinpyrazone, inhibitors of the organic anion transport system, to prevent Fluo-4 extrusion[271]. Therefore, it is expected that the fluorophore would be extruded from H9c2 cells, biasing calcium transients towards lower magnitudes, and resulting in a decreasing signal. The current investigation did not include the use of inhibitors for the following reason: Transport

inhibitors, such as probenecid for example, were excluded, as this drug actually inhibits TRPV1[272] and activates TRPV2[273] calcium channels simultaneously. Though these TRPV isoforms do not have confirmed expression profiles in differentiated H9c2 cells, TRPV2 channels have been found in rodent (Both mouse and rat) cardiac tissue[274,275], while TRPV1 channels have been confirmed undifferentiated H9c2 cell line[276] and in murine cardiomyocytes[277]. Inclusion of OAT inhibitors could have confounded the source and specificity of calcium transients observed, thus requiring caution towards mechanistic interpretation. As for the interpretation of the current investigation, a calcium transient among standard cultures exposed to acrolein was indeed observed, and the magnitude of calcium influx may have been underestimated within the present system. An investigation using hydrogen peroxide as the treatment did result in an intracellular calcium rise equivalent[143] to that observed here, though the authors attributed calcium transients independent of ADP-ribose concentrations. Since the delay roughly coincides with a period of increasing PARP activity, the results suggest that a cytosolic ADP-ribose concentration builds rapidly after acrolein treatment and subsequently activates clotrimazole-sensitive calcium conductance channels, i.e., TRPM2. The instantaneous activity level of PARP likely does not determine cytosolic PAR levels, but rather an integration of cumulative PARP activity integrated with time. As for the calcium reduction shortly after transient induction, a rise in cytosolic calcium to an indeterminate threshold likely triggered sequestration of calcium into store-operated calcium channels, e.g., extracellularly, mitochondria, and the ER (most important calcium uptake store in conjunction with mitochondria)[278]. Specifically, the H9c2 cell line has been shown to preferentially load excess cytosolic calcium into reticular stores[279]. Measurement of this compartment as well as the mitochondria would be beneficial in confirming this phenomenon under the model utilized here.

The calcium transient observed in the current investigation likely reflects such a mechanism, whereby intracellular calcium elevations were rapidly reversed after reaching a specific threshold, but a transient was observed nonetheless.

4.5 Limitations

No investigation is complete without discussion of the study limitations. Firstly, the presentation of possible inter-batch variation in acrolein cytotoxicity modulation undermined the comparative mechanistic comparisons between viability data and the later mechanistic elucidation studies, e.g., $\Delta\Psi_m$ and calcium conductance. Since the baseline viability estimates were unchanged among standard culture H9c2 cells, this was viewed as both an advantage, especially regarding baseline-specific modulation of olaparib efficacy, but also as a disadvantage as the viability IC_{50} for the 5 % oxygen culture estimates will quite likely be severely altered, depending on the underlying FBS composite of the medium. With respect to serum supplementation in medium, the use of a serum-free composition for comparative purposes could have contributed a more stable baseline viability estimate of IC_{50} derivation, but the applicability of such exposure metrics to the physiologically relevant *in situ* circumstance would be limited, especially given the complex composition of FBS. For example, the current investigation has shown significant changes in cytotoxicity depending on the medium TCA/glycolytic substrate composition, but the influence of hormones and growth factors in serum could have also contributed to the modulatory effects observed. It is imperative to note this, as serum-free physiological buffers generally lack the specificity of presence and/or concentration of hormones, free amino acids, and growth factors present in serum-containing medium[280]. While facilitation of stabilizing viability estimates when minor concentration changes of pyruvate, for

example, could increase observed variance, the lack of TCA and glycolytic substrates in such buffers would likely overestimate cytotoxicity when physiologically relevant oxygen tension studies are conducted. Since even modest additions of pyruvate (1.0 mM) to the basal pyruvate supplied in the RP medium (160 μM) demonstratively increased viability estimates, actual biochemical derivations of batch pyruvate would have supplied evidence in explaining the observed inter-batch variation in viability due to serum contents.

Utilization of the statistical program R, and the associated "drc" Package synthesized the viability and short-term metabolic IC_{50} curves well. However, the standard error estimates were comparatively large, and may have reduced the likelihood of uncovering significant rescue potential for particular TCA substrates, e.g., glutamine and glutamate. On the one hand, the limited number of points, the totality of which composed the individual substrate-specific curves, may have inadvertently inflated the uncertainty in curve parameter estimation. Further acrolein concentrations could have been included, but the amount of data generation required would have limited the resources required to enable the characterization of cytotoxic mechanisms pursued in this investigation. Additionally, the influence of medium FBS on viability may have rendered interpretation difficult or inconclusive; at least viability and metabolic estimates were derived from the same batch and are, therefore, comparable. On the other hand, this method substantially reduced the probability of a Type I error by reducing the number of statistical comparisons required for complete data summarization.

For short-term (2 hour) MTT analyses, an accompaniment of Nrf-2 activation, and associated downstream target genes responsible for antioxidant response, would have greatly contributed to the affirmation that MTT reduction values above respective controls were certainly caused by an increase in metabolic potential. Since cultures at 20.1 % demonstrated a

limited capacity to evoke such a response, at least within two hours, it is assumed that Nrf-2 response time or capacity were enhanced under 5 % oxygen culture conditions; the latter was presumed as the likely explanation. Further characterization would shed light on this matter. As previously stated, other mechanistic phenomena were pursued in the current investigation, and a possible Nrf-2-mediated metabolic activation was not expected at the onset. As such, this plausible mechanism was not pursued in the initial research plan.

With respect to mechanistic elucidation, continued measurements of $\Delta\Psi_m$ up to 24 hours would have supplied evidence that, indeed, reductions of $\Delta\Psi_m$ or complete potential ablation occur under the experimental conditions. The method proposed for measuring $\Delta\Psi_m$ included pre-loading cells with JC-1 prior to acrolein exposure; reversal of acrolein exposure and later JC-1 loading, followed by measurements, would have allowed for further characterization of mitochondrial fate at later time-points. Evidence in other cells lines, particularly ARPE-19 cells, have demonstrated dose-dependent reductions in $\Delta\Psi_m$ with acrolein, especially at 25 μM. Since AIF is typically characterized as both a marker of parthanatos and key player in $\Delta\Psi_m$ dissipation, characterization of AIF nuclear mobilization would have enhanced the mechanistic characterization of the phenomenon observed. Furthermore, the specificity of PARP-1 involvement in calcium transients and cell death could have been investigated using siRNA knock-down or transfection knock-out studies to attain conclusive evidence of parthanatos induction. Currently, the technology and infrastructure do not accommodate such technical capabilities, and may be later pursued for confirmatory purposes. Nonetheless, the primary focus of the investigation remained characterization of oxygen tension on acrolein cytotoxicity using TCA and glycolytic substrates.

Finally, the current investigation only attempted to characterize a single modulatory oxygen tension, 5 % mol/mol. While many would denote this as “hypoxic”, 5 % was interpreted as physiologically normal based on *in vivo* measurements (*See Introduction*), especially in balancing the venous and arterial oxygen tension of cardiac tissue. The literature base has proposed a range of “normal” oxygen tensions, ranging from 3 % up to greater than blood oxygen tension (100-120 mm Hg), depending on the investigation team and method of oxygen concentration determination utilized, e.g., Clark electrode. Based on the evidence, 5 % was chosen as a compromise of the variability present in the literature as well as for venous and arterial tension differences; others have also included 10 % oxygen. Nonetheless, undifferentiated H9c2 cells were acclimatized for a minimum of one week in 5 % oxygen prior to subdivision and plating in preparation for the week-long differentiation regimen (2 days attachment and five days differentiation). With respect to acclimatization to low oxygen, Hif-1α activation was not affirmed via biochemical assessment after shifting the H9c2 cells to 5 % oxygen. Therefore, it is not expected that the results could be due to hypoxic precondition, though this phenomenon cannot be ruled out definitively. Such long acclimatization was presumed to minimize such confounding, especially given the duration of culture prior to experimentation and adherence to medium changes, cell plating, acrolein treatment, and MTT reduction assay execution within an oxygen-controlled acrylic exposure chamber.

The translation of this investigation to an *in vivo* setting would provide a logical progression towards the potential of PARP inhibition in cyclophosphamide-induced cardiac failure. While this investigation cannot implicitly provide sufficient evidence to support the notion that acrolein alone imparts the progression to heart failure among chemotherapy patients treated with cyclophosphamide, the results offer promising evidence that PARP activation

contributes to the cytotoxic events of the potent α,β-unsaturated aldehyde, acrolein. Further still, evidence *in vivo* with ischemia/reperfusion, for which PARPi have proven partially efficacious, consistently show TRPM2 involvement in the significant reduction of necrotic tissue damage after an ischemic event; this effect has been coincidently observed in murine cerebral ischemia models[281] which were genetically deficient in Trpm2 expression. The authors noted significant reductions in neutrophilic invasion – an event associated with exacerbation of infarct volume and intensity, though the exact role of TRPM2 in cardiac ischemia remains the subject of debate[282]. As for the model presented in the current investigation, the utilization of a whole-organism model may provide further evidence of potential efficacy as the indirect effect of inflammatory-mediated tissue damage cannot be captured in monoculture *in vitro* models, such as the one presented here.

CHAPTER FIVE:

CONCLUSION

Conclusively, the results of the current investigation demonstrate that H9c2 cells maintained, differentiated, and exposed to acrolein under physiologically relevant oxygen tension likely results in metabolic reprogramming which likely involves the TCA cycle; an observation exemplified by pyruvate rescue only among cells cultured under 5 % oxygen. Pyruvate did not spare differentiated H9c2 cells cultured under standard conditions; thus, concluding that reduction of oxygen tension promotes metabolic reprogramming among 5 % cultures. Further, extracellular calcium was demonstrated as a partial contributor in determining cell fate during acrolein exposure, as 5-10 mM of EGTA significantly attenuated cell death from exposure to acrolein. However, the contribution of TRPM2 channels may only be partial, since extracellular influx was shown to be completely blocked via CTZ, but did not reduced cell viability loss significantly as did EGTA. Olaparib demonstrated a complex interaction with respect to cell rescue. Similar to CTZ, olaparib reduced calcium conductance to EGTA levels among cells cultured under standard conditions, though a similar reduction in calcium transients under 5 % oxygen was not conclusive. Therefore, the evidence suggests that modest-high acrolein exposure activates PARP and induces extracellular influx partially through clotrimazole-sensitive stores, all of which operate in concert and ultimately contribute to reductions in $\Delta\Psi_m$ and resultant cell death. The influence of PARP-associated reductions in viability remains closely influenced by the magnitude of cytotoxic insult. Consideration of physiologically

relevant culture conditions may enhance *in vitro* representation of *in vivo* responses with respect to toxicogenic insult in preclinical phases of drug discovery or in toxicological analyses.

REFERENCES

1. Chabner BA, Bertino J, Cleary J, et al. Cytotoxic Agents. In: Brunton LL, Chabner B, Knollmann BC, eds. *Goodman & Gilman's the Pharmacological Basis of Therapeutics*. 12th ed. New York, N.Y.: McGraw-Hill Medical; 2011.
2. Storb R, Thomas ED, Weiden PL, et al. Aplastic anemia treated by allogeneic bone marrow transplantation: a report on 49 new cases from Seattle. *Blood.* 1976;48(6):817-841.
3. Cox PJ. Cyclophosphamide cystitis--identification of acrolein as the causative agent. *Biochemical Pharmacology.* 1979;28(13):2045-2049.
4. Luce JK, Simons JA. Efficacy of mesna in preventing further cyclophosphamide-induced hemorrhagic cystitis. *Medical and Pediatric Oncology.* 1988;16(6):372-374.
5. Hows JM, Mehta A, Ward L, et al. Comparison of mesna with forced diuresis to prevent cyclophosphamide induced haemorrhagic cystitis in marrow transplantation: a prospective randomised study. *British Journal of Cancer.* 1984;50(6):753-756.
6. Goldberg MA, Antin JH, Guinan EC, Rappeport JM. Cyclophosphamide cardiotoxicity: an analysis of dosing as a risk factor. *Blood.* 1986;68(5):1114-1118.
7. Gottdiener JS, Appelbaum FR, Ferrans VJ, Deisseroth A, Ziegler J. Cardiotoxicity associated with high-dose cyclophosphamide therapy. *Archives of Internal Medicine.* 1981;141(6):758-763.

8. Braverman AC, Antin JH, Plappert MT, Cook EF, Lee RT. Cyclophosphamide cardiotoxicity in bone marrow transplantation: a prospective evaluation of new dosing regimens. *Journal of Clinical Oncology.* 1991;9(7):1215-1223.

9. Steinherz LJ, Steinherz PG, Mangiacasale D, et al. Cardiac changes with cyclophosphamide. *Medical and Pediatric Oncology.* 1981;9(5):417-422.

10. Gharib MI, Burnett AK. Chemotherapy-induced cardiotoxicity: current practice and prospects of prophylaxis. *European Journal of Heart Failure.* 2002;4(3):235-242.

11. Dow E, Schulman H, Agura E. Cyclophosphamide cardiac injury mimicking acute myocardial infarction. *Bone Marrow Transplantation.* 1993;12(2):169-172.

12. Gardner SF, Lazarus HM, Bednarczyk EM, et al. High-dose cyclophosphamide-induced myocardial damage during BMT: assessment by positron emission tomography. *Bone Marrow Transplantation.* 1993;12(2):139-144.

13. Meserve EE, Lehmann LE, Perez-Atayde AR, Labelle JL. Cyclophosphamide-associated cardiotoxicity in a child after stem cell transplantation for beta-thalassemia major: case report and review of the literature. *Pediatric and Developmental Pathology.* 2014;17(1):50-54.

14. Katayama M, Imai Y, Hashimoto H, et al. Fulminant fatal cardiotoxicity following cyclophosphamide therapy. *Journal of Cardiology.* 2009;54(2):330-334.

15. Dadfarmay S, Berkowitz R, Kim B. Irreversible end-stage cardiomyopathy following a single dose of cyclophosphamide. *Congestive Heart Failure.* 2012;18(4):234-237.

16. Wagner T, Heydrich D, Jork T, Voelcker G, Hohorst HJ. Comparative study on human pharmacokinetics of activated ifosfamide and cyclophosphamide by a modified fluorometric test. *Journal of Cancer Research and Clinical Oncology.* 1981;100(1):95-104.

17. Draminski W, Eder E, Henschler D. A new pathway of acrolein metabolism in rats. *Archives of Toxicology.* 1983;52(3):243-247.

18. Kehrer JP, Biswal SS. The molecular effects of acrolein. *Toxicological Sciences.* 2000;57(1):6-15.

19. Ren S, Kalhorn TF, Slattery JT. Inhibition of human aldehyde dehydrogenase 1 by the 4-hydroxycyclophosphamide degradation product acrolein. *Drug Metabolism and Disposition: The Biological Fate of Chemicals.* 1999;27(1):133-137.

20. Alarcon RA. Fluorometric determination of acrolein and related compounds with m-aminophenol. *Analytical Chemistry.* 1968;40(11):1704-1708.

21. Baumann F, Schmidt R, Teichert J, Preiss R. Influence of protein binding on acrolein turnover in vitro by oxazaphosphorines and liver microsomes. *Journal of Clinical Laboratory Analysis.* 2005;19(3):103-109.

22. Günther M, Wagner E, Ogris M. Acrolein: unwanted side product or contribution to antiangiogenic properties of metronomic cyclophosphamide therapy? *Journal of Cellular and Molecular Medicine.* 2008;12(6b):2704-2716.

23. Chaudhary KR, Batchu SN, Seubert JM. Cytochrome P450 enzymes and the heart. *International Union of Biochemistry and Molecular Biology: Life.* 2009;61(10):954-960.

24. Michaud V, Frappier M, Dumas MC, Turgeon J. Metabolic activity and mRNA levels of human cardiac CYP450s involved in drug metabolism. *PloS One.* 2010;5(12):e15666.

25. Dorr RT, Lagel K. Effect of sulfhydryl compounds and glutathione depletion on rat heart myocyte toxicity induced by 4-hydroperoxycyclophosphamide and acrolein in vitro. *Chemico-Biological Interactions.* 1994;93(2):117-128.

26. Bjelogrlic SK, Lukic ST, Djuricic SM. Activity of dexrazoxane and amifostine against late cardiotoxicity induced by the combination of doxorubicin and cyclophosphamide in vivo. *Basic & Clinical Pharmacology & Toxicology.* 2013;113(4):228-238.

27. Conklin DJ, Haberzettl P, Jagatheesan G, et al. Glutathione S-transferase P protects against cyclophosphamide-induced cardiotoxicity in mice. *Toxicology and Applied Pharmacology.* 2015;285(2):136-148.

28. Adams JD, Jr., Klaidman LK. Acrolein-induced oxygen radical formation. *Free Radical Biology and Medicine.* 1993;15(2):187-193.

29. Yoshida M, Tomitori H, Machi Y, et al. Acrolein toxicity: Comparison with reactive oxygen species. *Biochemical and Biophysical Research Communications.* 2009;378(2):313-318.

30. Fischer B, Bavister BD. Oxygen tension in the oviduct and uterus of rhesus monkeys, hamsters and rabbits. *Journal of Reproduction and Fertility.* 1993;99(2):673-679.

31. Dole WP, Nuno DW. Myocardial oxygen tension determines the degree and pressure range of coronary autoregulation. *Circulation Research.* 1986;59(2):202-215.

32. Grunewald WA, Sowa W. Distribution of the myocardial tissue PO2 in the rat and the inhomogeneity of the coronary bed. *Pflügers Archiv. European Journal of Physiology.* 1978;374(1):57-66.

33. Kondrikov D, Elms S, Fulton D, Su Y. eNOS-beta-actin interaction contributes to increased peroxynitrite formation during hyperoxia in pulmonary artery endothelial cells and mouse lungs. *Journal of Biological Chemistry.* 2010;285(46):35479-35487.

34. Meuter A, Rogmann LM, Winterhoff BJ, Tchkonia T, Kirkland JL, Morbeck DE. Markers of cellular senescence are elevated in murine blastocysts cultured in vitro: molecular consequences of culture in atmospheric oxygen. *Journal of Assisted Reproduction and Genetics.* 2014;31(10):1259-1267.

35. Csete M. Oxygen in the cultivation of stem cells. *Annals of the New York Academy of Sciences.* 2005;1049:1-8.

36. Peura TT, Bosman A, Stojanov T. Derivation of human embryonic stem cell lines. *Theriogenology.* 2007;67(1):32-42.

37. Li TS, Marban E. Physiological levels of reactive oxygen species are required to maintain genomic stability in stem cells. *Stem Cells.* 2010;28(7):1178-1185.

38. Hoffman DL, Salter JD, Brookes PS. Response of mitochondrial reactive oxygen species generation to steady-state oxygen tension: implications for hypoxic cell signaling. *American Journal of Physiology: Heart and Circulatory Physiology.* 2007;292(1):H101-108.

39. Chen Q, Fischer A, Reagan JD, Yan LJ, Ames BN. Oxidative DNA damage and senescence of human diploid fibroblast cells. *Proceedings of the National Academy of Sciences.* 1995;92(10):4337-4341.

40. Fehrer C, Brunauer R, Laschober G, et al. Reduced oxygen tension attenuates differentiation capacity of human mesenchymal stem cells and prolongs their lifespan. *Aging Cell.* 2007;6(6):745-757.

41. Kilburn DG, Lilly MD, Self DA, Webb FC. The effect of dissolved oxygen partial pressure on the growth and carbohydrate metabolism of mouse LS cells. *Journal of Cell Science.* 1969;4(1):25-37.

42. Sher PK. The effects of acidosis on chronically hypoxic neurons in culture. *Experimental Neurology.* 1990;107(3):256-262.

43. Estrada JC, Albo C, Benguria A, et al. Culture of human mesenchymal stem cells at low oxygen tension improves growth and genetic stability by activating glycolysis. *Cell Death and Differentiation.* 2012;19(5):743-755.

44. Bambrick LL, Kostov Y, Rao G. In vitro cell culture pO2 is significantly different from incubator pO2. *Biotechnology Progress.* 2011;27(4):1185-1189.

45. Kim J-w, Tchernyshyov I, Semenza GL, Dang CV. HIF-1-mediated expression of pyruvate dehydrogenase kinase: a metabolic switch required for cellular adaptation to hypoxia. *Cell Metabolism.* 2006;3(3):177-185.

46. Papandreou I, Cairns RA, Fontana L, Lim AL, Denko NC. HIF-1 mediates adaptation to hypoxia by actively downregulating mitochondrial oxygen consumption. *Cell Metabolism.* 2006;3(3):187-197.

47. Konigsberg M, Perez VI, Rios C, et al. Effect of oxygen tension on bioenergetics and proteostasis in young and old myoblast precursor cells. *Redox Biology.* 2013;1:475-482.

48. Wilson DF, Erecinska M, Drown C, Silver IA. Effect of oxygen tension on cellular energetics. *American Journal of Physiology.* 1977;233(5):C135-140.

49. Galluzzi L, Vitale I, Abrams JM, et al. Molecular definitions of cell death subroutines: recommendations of the Nomenclature Committee on Cell Death 2012. *Cell Death and Differentiation.* 2012;19(1):107-120.

50. Cregan SP, Dawson VL, Slack RS. Role of AIF in caspase-dependent and caspase-independent cell death. *Oncogene.* 2004;23(16):2785-2796.

51. Wielckens K, Schmidt A, George E, Bredehorst R, Hilz H. DNA fragmentation and NAD depletion. Their relation to the turnover of endogenous mono(ADP-ribosyl) and poly(ADP-ribosyl) proteins. *Journal of Biological Chemistry.* 1982;257(21):12872-12877.

52. Kovacs K, Hanto K, Bognar Z, et al. Prevalent role of Akt and ERK activation in cardioprotective effect of Ca(2+) channel- and beta-adrenergic receptor blockers. *Molecular and Cellular Biochemistry.* 2009;321(1-2):155-164.

53. Ying W, Alano CC, Garnier P, Swanson RA. NAD+ as a metabolic link between DNA damage and cell death. *Journal of Neuroscience Research.* 2005;79(1-2):216-223.

54. Ying W, Chen Y, Alano CC, Swanson RA. Tricarboxylic acid cycle substrates prevent PARP-mediated death of neurons and astrocytes. *Journal of Cerebral Blood Flow and Metabolism.* 2002;22(7):774-779.

55. Zeng J, Yang GY, Ying W, et al. Pyruvate improves recovery after PARP-1-associated energy failure induced by oxidative stress in neonatal rat cerebrocortical slices. *Journal of Cerebral Blood Flow and Metabolism.* 2007;27(2):304-315.

56. Zong WX, Ditsworth D, Bauer DE, Wang ZQ, Thompson CB. Alkylating DNA damage stimulates a regulated form of necrotic cell death. *Genes and Development.* 2004;18(11):1272-1282.

57. Cheung EC, Joza N, Steenaart NA, et al. Dissociating the dual roles of apoptosis-inducing factor in maintaining mitochondrial structure and apoptosis. *EMBO Journal.* 2006;25(17):4061-4073.

58. Alano CC, Garnier P, Ying W, Higashi Y, Kauppinen TM, Swanson RA. NAD+ depletion is necessary and sufficient for poly(ADP-ribose) polymerase-1-mediated neuronal death. *Journal of Neuroscience.* 2010;30(8):2967-2978.

59. Alano CC, Tran A, Tao R, Ying W, Karliner JS, Swanson RA. Differences among cell types in NAD(+) compartmentalization: a comparison of neurons, astrocytes, and cardiac myocytes. *Journal of Neuroscience Research.* 2007;85(15):3378-3385.

60. Liu J, Segal M, Yoo S, et al. Antioxidant effect of ethyl pyruvate in respiring neonatal cerebrocortical slices after H(2)O(2) stress. *Neurochemistry International.* 2009;54(2):106-110.

61. Chiu SC, Huang SY, Tsai YC, et al. Poly (ADP-ribose) polymerase plays an important role in intermittent hypoxia-induced cell death in rat cerebellar granule cells. *Journal of Biomedical Science.* 2012;19:29.

62. Cregan SP, Fortin A, MacLaurin JG, et al. Apoptosis-inducing factor is involved in the regulation of caspase-independent neuronal cell death. *Journal of Cell Biology.* 2002;158(3):507-517.

63. Yu SW, Wang H, Poitras MF, et al. Mediation of poly(ADP-ribose) polymerase-1-dependent cell death by apoptosis-inducing factor. *Science.* 2002;297(5579):259-263.

64. Yarana C, Sripetchwandee J, Sanit J, Chattipakorn S, Chattipakorn N. Calcium-induced cardiac mitochondrial dysfunction is predominantly mediated by cyclosporine A-dependent mitochondrial permeability transition pore. *Archives of Medical Research.* 2012;43(5):333-338.

65. Pereira SL, Ramalho-Santos J, Branco AF, Sardao VA, Oliveira PJ, Carvalho RA. Metabolic remodeling during H9c2 myoblast differentiation: relevance for in vitro toxicity studies. *Cardiovascular Toxicology.* 2011;11(2):180-190.

66. Ménard C, Pupier S, Mornet D, Kitzmann M, Nargëot J, Lory P. Modulation of L-type calcium channel expression during retinoic acid-induced differentiation of H9C2 cardiac cells. *Journal of Biological Chemistry.* 1999;274(41):29063-29070.

67. Pagano M, Naviglio S, Spina A, et al. Differentiation of H9c2 cardiomyoblasts: The role of adenylate cyclase system. *Journal of Cellular Physiology.* 2004;198(3):408-416.

68. Brostrom MA, Reilly BA, Wilson FJ, Brostrom CO. Vasopressin-induced hypertrophy in H9c2 heart-derived myocytes. *International Journal of Biochemistry and Cell Biology.* 2000;32(9):993-1006.

69. Fukuzawa J, Haneda T, Kikuchi K. Arginine vasopressin increases the rate of protein synthesis in isolated perfused adult rat heart via the V1 receptor. *Molecular and Cellular Biochemistry.* 1999;195(1-2):93-98.

70. Mejia-Alvarez R, Tomaselli GF, Marban E. Simultaneous expression of cardiac and skeletal muscle isoforms of the L-type Ca2+ channel in a rat heart muscle cell line. *Journal of Physiology.* 1994;478 (Pt 2):315-329.

71. Bregant E, Renzone G, Lonigro R, et al. Down-regulation of SM22/transgelin gene expression during H9c2 cells differentiation. *Molecular and Cellular Biochemistry.* 2009;327(1-2):145-152.

72. Branco AF, Pereira SP, Gonzalez S, Gusev O, Rizvanov AA, Oliveira PJ. Gene Expression Profiling of H9c2 Myoblast Differentiation towards a Cardiac-Like Phenotype. *PloS One.* 2015;10(6):e0129303.

73. Branco AF, Sampaio SF, Moreira AC, et al. Differentiation-dependent doxorubicin toxicity on H9c2 cardiomyoblasts. *Cardiovascular Toxicology.* 2012;12(4):326-340.

74. Yi M, Weaver D, Eisner V, et al. Switch from ER-mitochondrial to SR-mitochondrial calcium coupling during muscle differentiation. *Cell Calcium.* 2012;52(5):355-365.

75. Comelli M, Domenis R, Bisetto E, et al. Cardiac differentiation promotes mitochondria development and ameliorates oxidative capacity in H9c2 cardiomyoblasts. *Mitochondrion.* 2011;11(2):315-326.

76. Olah G, Szczesny B, Brunyanszki A, et al. Differentiation-Associated Downregulation of Poly(ADP-Ribose) Polymerase-1 Expression in Myoblasts Serves to Increase Their Resistance to Oxidative Stress. *PloS One.* 2015;10(7):e0134227.

77. Crawford RM, Jovanovic S, Budas GR, et al. Chronic mild hypoxia protects heart-derived H9c2 cells against acute hypoxia/reoxygenation by regulating expression of the SUR2A subunit of the ATP-sensitive K+ channel. *Journal of Biological Chemistry.* 2003;278(33):31444-31455.

78. Garnier P, Ying W, Swanson RA. Ischemic preconditioning by caspase cleavage of poly(ADP-ribose) polymerase-1. *Journal of Neuroscience.* 2003;23(22):7967-7973.

79. Sarkar K, Cai Z, Gupta R, et al. Hypoxia-inducible factor 1 transcriptional activity in endothelial cells is required for acute phase cardioprotection induced by ischemic preconditioning. *Proceedings of the National Academy of Sciences.* 2012;109(26):10504-10509.

80. Cai Z, Luo W, Zhan H, Semenza GL. Hypoxia-inducible factor 1 is required for remote ischemic preconditioning of the heart. *Proceedings of the National Academy of Sciences.* 2013;110(43):17462-17467.

81. Martin-Puig S, Tello D, Aragones J. Novel perspectives on the PHD-HIF oxygen sensing pathway in cardioprotection mediated by IPC and RIPC. *Frontiers in Physiology.* 2015;6:137.

82. Huang C, Andres AM, Ratliff EP, Hernandez G, Lee P, Gottlieb RA. Preconditioning involves selective mitophagy mediated by Parkin and p62/SQSTM1. *PloS One.* 2011;6(6):e20975.

83. Narendra DP, Jin SM, Tanaka A, et al. PINK1 is selectively stabilized on impaired mitochondria to activate Parkin. *PLoS Biology.* 2010;8(1):e1000298.

84. Diers AR, Broniowska KA, Chang CF, Hogg N. Pyruvate fuels mitochondrial respiration and proliferation of breast cancer cells: effect of monocarboxylate transporter inhibition. *Biochemical Journal.* 2012;444(3):561-571.

85. Juhaszova M, Zorov DB, Kim SH, et al. Glycogen synthase kinase-3beta mediates convergence of protection signaling to inhibit the mitochondrial permeability transition pore. *Journal of Clinical Investigation.* 2004;113(11):1535-1549.

86. Branco AF, Pereira SL, Moreira AC, Holy J, Sardao VA, Oliveira PJ. Isoproterenol cytotoxicity is dependent on the differentiation state of the cardiomyoblast H9c2 cell line. *Cardiovascular Toxicology.* 2011;11(3):191-203.

87. di Giacomo V, Rapino M, Sancilio S, et al. PKC-delta signalling pathway is involved in H9c2 cells differentiation. *Differentiation.* 2010;80(4-5):204-212.

88. de Jesus García-Rivas G, Carvajal K, Correa F, Zazueta C. Ru(360), a specific mitochondrial calcium uptake inhibitor, improves cardiac post-ischaemic functional recovery in rats in vivo. *British Journal of Pharmacology.* 2006;149(7):829-837.

89. Zorov DB, Juhaszova M, Sollott SJ. Mitochondrial reactive oxygen species (ROS) and ROS-induced ROS release. *Physiological Reviews.* 2014;94(3):909-950.

90. Schonekess BO, Brindley PG, Lopaschuk GD. Calcium regulation of glycolysis, glucose oxidation, and fatty acid oxidation in the aerobic and ischemic heart. *Canadian Journal of Physiology and Pharmacology.* 1995;73(11):1632-1640.

91. Glancy B, Balaban RS. Role of mitochondrial Ca2+ in the regulation of cellular energetics. *Biochemistry.* 2012;51(14):2959-2973.

92. Balaban RS, Bose S, French SA, Territo PR. Role of calcium in metabolic signaling between cardiac sarcoplasmic reticulum and mitochondria in vitro. *American Journal of Physiology: Cell Physiology.* 2003;284(2):C285-293.

93. Das AM, Harris DA. Control of mitochondrial ATP synthase in heart cells: inactive to active transitions caused by beating or positive inotropic agents. *Cardiovascular Research.* 1990;24(5):411-417.

94. Territo PR, Mootha VK, French SA, Balaban RS. Ca(2+) activation of heart mitochondrial oxidative phosphorylation: role of the F(0)/F(1)-ATPase. *American Journal of Physiology: Cell Physiology.* 2000;278(2):C423-435.

95. Territo PR, French SA, Dunleavy MC, Evans FJ, Balaban RS. Calcium activation of heart mitochondrial oxidative phosphorylation: rapid kinetics of mVO2, NADH, AND light scattering. *Journal of Biological Chemistry.* 2001;276(4):2586-2599.

96. de Jesus García-Rivas G, Guerrero-Hernandez A, Guerrero-Serna G, Rodriguez-Zavala JS, Zazueta C. Inhibition of the mitochondrial calcium uniporter by the oxo-bridged dinuclear ruthenium amine complex (Ru360) prevents from irreversible injury in postischemic rat heart. *FEBS Journal.* 2005;272(13):3477-3488.

97. Kirichok Y, Krapivinsky G, Clapham DE. The mitochondrial calcium uniporter is a highly selective ion channel. *Nature.* 2004;427(6972):360-364.

98. Kwong JQ, Lu X, Correll RN, et al. The Mitochondrial Calcium Uniporter Selectively Matches Metabolic Output to Acute Contractile Stress in the Heart. *Cell Reports.* 2015;12(1):15-22.

99. Holmuhamedov EL, Ozcan C, Jahangir A, Terzic A. Restoration of Ca2+-inhibited oxidative phosphorylation in cardiac mitochondria by mitochondrial Ca2+ unloading. *Molecular and Cellular Biochemistry.* 2001;220(1-2):135-140.

100. Duan Y, Gross RA, Sheu SS. Ca2+-dependent generation of mitochondrial reactive oxygen species serves as a signal for poly(ADP-ribose) polymerase-1 activation during glutamate excitotoxicity. *Journal of Physiology.* 2007;585(Pt 3):741-758.

101. Kushnareva YE, Wiley SE, Ward MW, Andreyev AY, Murphy AN. Excitotoxic injury to mitochondria isolated from cultured neurons. *Journal of Biological Chemistry.* 2005;280(32):28894-28902.

102. Luongo TS, Lambert JP, Yuan A, et al. The Mitochondrial Calcium Uniporter Matches Energetic Supply with Cardiac Workload during Stress and Modulates Permeability Transition. *Cell Reports.* 2015;12(1):23-34.

103. Litsky ML, Pfeiffer DR. Regulation of the mitochondrial Ca2+ uniporter by external adenine nucleotides: the uniporter behaves like a gated channel which is regulated by nucleotides and divalent cations. *Biochemistry.* 1997;36(23):7071-7080.

104. Holmström KM, Pan X, Liu JC, et al. Assessment of cardiac function in mice lacking the mitochondrial calcium uniporter. *Journal of Molecular and Cellular Cardiology.* 2015;85:178-182.

105. Liu T, O'Rourke B. Enhancing mitochondrial Ca2+ uptake in myocytes from failing hearts restores energy supply and demand matching. *Circulation Research.* 2008;103(3):279-288.

106. Matlib MA, Zhou Z, Knight S, et al. Oxygen-bridged dinuclear ruthenium amine complex specifically inhibits Ca2+ uptake into mitochondria in vitro and in situ in single cardiac myocytes. *Journal of Biological Chemistry.* 1998;273(17):10223-10231.

107. Kimchi-Sarfaty C, Kasir J, Ambudkar SV, Rahamimoff H. Transport activity and surface expression of the Na+-Ca2+ exchanger NCX1 are inhibited by the immunosuppressive agent cyclosporin A and by the nonimmunosuppressive agent PSC833. *Journal of Biological Chemistry.* 2002;277(4):2505-2510.

108. Griffiths EJ. Reversal of mitochondrial Na/Ca exchange during metabolic inhibition in rat cardiomyocytes. *FEBS Letters.* 1999;453(3):400-404.

109. Elbaz B, Valitsky M, Davidov G, Rahamimoff H. Cyclophilin A is involved in functional expression of the Na(+)-Ca(2+) exchanger NCX1. *Biochemistry.* 2010;49(35):7634-7642.

110. Rahamimoff H, Elbaz B, Alperovich A, et al. Cyclosporin A-dependent downregulation of the Na+/Ca2+ exchanger expression. *Annals of the New York Academy of Sciences.* 2007;1099:204-214.

111. Braun FJ, Broad LM, Armstrong DL, Putney JW, Jr. Stable activation of single Ca2+ release-activated Ca2+ channels in divalent cation-free solutions. *Journal of Biological Chemistry.* 2001;276(2):1063-1070.

112. Togashi K, Inada H, Tominaga M. Inhibition of the transient receptor potential cation channel TRPM2 by 2-aminoethoxydiphenyl borate (2-APB). *British Journal of Pharmacology.* 2008;153(6):1324-1330.

113. Dobrydneva Y, Blackmore P. 2-Aminoethoxydiphenyl borate directly inhibits store-operated calcium entry channels in human platelets. *Molecular Pharmacology.* 2001;60(3):541-552.

114. Sano Y, Inamura K, Miyake A, et al. Immunocyte Ca2+ influx system mediated by LTRPC2. *Science.* 2001;293(5533):1327-1330.

115. Yu P, Wang Q, Zhang LH, Lee HC, Zhang L, Yue J. A cell permeable NPE caged ADP-ribose for studying TRPM2. *PloS One.* 2012;7(12):e51028.

116. Montell C. The TRP superfamily of cation channels. *Science: Signal Transduction Knowledge Environment.* 2005;2005(272):re3.

117. Bari MR, Akbar S, Eweida M, et al. H2O2-induced Ca2+ influx and its inhibition by N-(p-amylcinnamoyl) anthranilic acid in the beta-cells: involvement of TRPM2 channels. *Journal of Cellular and Molecular Medicine.* 2009;13(9b):3260-3267.

118. Chokshi R, Fruasaha P, Kozak JA. 2-aminoethyl diphenyl borinate (2-APB) inhibits TRPM7 channels through an intracellular acidification mechanism. *Channels.* 2012;6(5):362-369.

119. Liu X, Cotrim A, Teos L, et al. Loss of TRPM2 function protects against irradiation-induced salivary gland dysfunction. *Nature Communications.* 2013b;4:1515.

120. Jia J, Verma S, Nakayama S, et al. Sex differences in neuroprotection provided by inhibition of TRPM2 channels following experimental stroke. *Journal of Cerebral Blood Flow and Metabolism.* 2011;31(11):2160-2168.

121. Verma S, Quillinan N, Yang YF, et al. TRPM2 channel activation following in vitro ischemia contributes to male hippocampal cell death. *Neuroscience Letters.* 2012;530(1):41-46.

122. Harteneck C, Frenzel H, Kraft R. N-(p-amylcinnamoyl)anthranilic acid (ACA): a phospholipase A(2) inhibitor and TRP channel blocker. *Cardiovascular Drug Reviews.* 2007;25(1):61-75.

123. Kraft R, Grimm C, Frenzel H, Harteneck C. Inhibition of TRPM2 cation channels by N-(p-amylcinnamoyl)anthranilic acid. *British Journal of Pharmacology.* 2006;148(3):264-273.

124. Hill K, Benham CD, McNulty S, Randall AD. Flufenamic acid is a pH-dependent antagonist of TRPM2 channels. *Neuropharmacology.* 2004a;47(3):450-460.

125. Hill K, McNulty S, Randall AD. Inhibition of TRPM2 channels by the antifungal agents clotrimazole and econazole. *Naunyn-Schmiedebergs Archives of Pharmacology.* 2004b;370(4):227-237.

126. Chen SJ, Zhang W, Tong Q, et al. Role of TRPM2 in cell proliferation and susceptibility to oxidative stress. *American Journal of Physiology: Cell Physiology.* 2013;304(6):C548-560.

127. Takahashi K, Sakamoto K, Kimura J. Hypoxic stress induces transient receptor potential melastatin 2 (TRPM2) channel expression in adult rat cardiac fibroblasts. *Journal of Pharmacological Sciences.* 2012;118(2):186-197.

128. Gasser A, Glassmeier G, Fliegert R, et al. Activation of T cell calcium influx by the second messenger ADP-ribose. *Journal of Biological Chemistry.* 2006;281(5):2489-2496.

129. Starkus J, Beck A, Fleig A, Penner R. Regulation of TRPM2 by extra- and intracellular calcium. *Journal of General Physiology.* 2007;130(4):427-440.

130. Shimizu S, Yonezawa R, Hagiwara T, et al. Inhibitory effects of AG490 on H2O2-induced TRPM2-mediated Ca(2+) entry. *European Journal of Pharmacology.* 2014;742:22-30.

131. Hu HZ, Gu Q, Wang C, et al. 2-aminoethoxydiphenyl borate is a common activator of TRPV1, TRPV2, and TRPV3. *Journal of Biological Chemistry.* 2004;279(34):35741-35748.

132. Xu SZ, Zeng F, Boulay G, Grimm C, Harteneck C, Beech DJ. Block of TRPC5 channels by 2-aminoethoxydiphenyl borate: a differential, extracellular and voltage-dependent effect. *British Journal of Pharmacology.* 2005;145(4):405-414.

133. Peppiatt CM, Collins TJ, Mackenzie L, et al. 2-Aminoethoxydiphenyl borate (2-APB) antagonises inositol 1,4,5-trisphosphate-induced calcium release, inhibits calcium pumps and has a use-dependent and slowly reversible action on store-operated calcium entry channels. *Cell Calcium.* 2003;34(1):97-108.

134. Bilmen JG, Michelangeli F. Inhibition of the type 1 inositol 1,4,5-trisphosphate receptor by 2-aminoethoxydiphenylborate. *Cellular Signalling.* 2002;14(11):955-960.

135. Iwasaki H, Mori Y, Hara Y, Uchida K, Zhou H, Mikoshiba K. 2-Aminoethoxydiphenyl borate (2-APB) inhibits capacitative calcium entry independently of the function of inositol 1,4,5-trisphosphate receptors. *Receptors and Channels.* 2001;7(6):429-439.

136. Takahashi K, Yokota M, Ohta T. Molecular mechanism of 2-APB-induced Ca(2)(+) influx in external acidification in PC12. *Experimental Cell Research.* 2014;323(2):337-345.

137. Kukkonen JP, Lund PE, Akerman KE. 2-aminoethoxydiphenyl borate reveals heterogeneity in receptor-activated Ca(2+) discharge and store-operated Ca(2+) influx. *Cell Calcium.* 2001;30(2):117-129.

138. Hwang SM, Koo NY, Jin M, et al. Intracellular acidification is associated with changes in free cytosolic calcium and inhibition of action potentials in rat trigeminal ganglion. *Journal of Biological Chemistry.* 2011;286(3):1719-1729.

139. Li S, Hao B, Lu Y, Yu P, Lee HC, Yue J. Intracellular alkalinization induces cytosolic Ca2+ increases by inhibiting sarco/endoplasmic reticulum Ca2+-ATPase (SERCA). *PloS One.* 2012;7(2):e31905.

140. Kwak YG, Park SK, Kim UH, et al. Intracellular ADP-ribose inhibits ATP-sensitive K+ channels in rat ventricular myocytes. *American Journal of Physiology.* 1996;271(2 Pt 1):C464-468.

141. Noma A. ATP-regulated K+ channels in cardiac muscle. *Nature.* 1983;305(5930):147-148.

142. Hecquet CM, Ahmmed GU, Vogel SM, Malik AB. Role of TRPM2 channel in mediating H2O2-induced Ca2+ entry and endothelial hyperpermeability. *Circulation Research.* 2008;102(3):347-355.

143. Wehage E, Eisfeld J, Heiner I, Jungling E, Zitt C, Luckhoff A. Activation of the cation channel long transient receptor potential channel 2 (LTRPC2) by hydrogen peroxide. A splice variant reveals a mode of activation independent of ADP-ribose. *Journal of Biological Chemistry.* 2002;277(26):23150-23156.

144. Heiner I, Eisfeld J, Halaszovich CR, et al. Expression profile of the transient receptor potential (TRP) family in neutrophil granulocytes: evidence for currents through long TRP channel 2 induced by ADP-ribose and NAD. *Biochemical Journal.* 2003;371(Pt 3):1045-1053.

145. Zhang Z, Zhang W, Jung DY, et al. TRPM2 Ca2+ channel regulates energy balance and glucose metabolism. *American Journal of Physiology: Endocrinology and Metabolism.* 2012;302(7):E807-816.

146. Akaishi T, Nakazawa K, Sato K, Saito H, Ohno Y, Ito Y. Hydrogen peroxide modulates whole cell Ca2+ currents through L-type channels in cultured rat dentate granule cells. *Neuroscience Letters.* 2004;356(1):25-28.

147. Hudasek K, Brown ST, Fearon IM. H2O2 regulates recombinant Ca2+ channel alpha1C subunits but does not mediate their sensitivity to acute hypoxia. *Biochemical and Biophysical Research Communications.* 2004;318(1):135-141.

148. Csanády L, Törocsik B. Four Ca2+ ions activate TRPM2 channels by binding in deep crevices near the pore but intracellularly of the gate. *Journal of General Physiology.* 2009;133(2):189-203.

149. Ishii M, Hagiwara T, Mori Y, Shimizu S. Involvement of TRPM2 and L-type Ca(2)(+) channels in Ca(2)(+) entry and cell death induced by hydrogen peroxide in rat beta-cell line RIN-5F. *Journal of Toxicological Sciences.* 2014;39(2):199-209.

150. Kühn FJ, Lückhoff A. Sites of the NUDT9-H domain critical for ADP-ribose activation of the cation channel TRPM2. *Journal of Biological Chemistry.* 2004;279(45):46431-46437.

151. Perraud AL, Fleig A, Dunn CA, et al. ADP-ribose gating of the calcium-permeable LTRPC2 channel revealed by Nudix motif homology. *Nature.* 2001;411(6837):595-599.

152. Heiner I, Eisfeld J, Warnstedt M, Radukina N, Jungling E, Luckhoff A. Endogenous ADP-ribose enables calcium-regulated cation currents through TRPM2 channels in neutrophil granulocytes. *Biochemical Journal.* 2006;398(2):225-232.

153. Toth B, Iordanov I, Csanady L. Ruling out pyridine dinucleotides as true TRPM2 channel activators reveals novel direct agonist ADP-ribose-2'-phosphate. *Journal of General Physiology.* 2015;145(5):419-430.

154. Lange I, Penner R, Fleig A, Beck A. Synergistic regulation of endogenous TRPM2 channels by adenine dinucleotides in primary human neutrophils. *Cell Calcium.* 2008;44(6):604-615.

155. Beck A, Kolisek M, Bagley LA, Fleig A, Penner R. Nicotinic acid adenine dinucleotide phosphate and cyclic ADP-ribose regulate TRPM2 channels in T lymphocytes. *FASEB Journal.* 2006;20(7):962-964.

156. Hara Y, Wakamori M, Ishii M, et al. LTRPC2 Ca2+-permeable channel activated by changes in redox status confers susceptibility to cell death. *Molecular Cell.* 2002;9(1):163-173.

157. Magnone M, Bauer I, Poggi A, et al. NAD+ levels control Ca2+ store replenishment and mitogen-induced increase of cytosolic Ca2+ by Cyclic ADP-ribose-dependent TRPM2 channel gating in human T lymphocytes. *Journal of Biological Chemistry.* 2012;287(25):21067-21081.

158. Kolisek M, Beck A, Fleig A, Penner R. Cyclic ADP-ribose and hydrogen peroxide synergize with ADP-ribose in the activation of TRPM2 channels. *Molecular Cell.* 2005;18(1):61-69.

159. Perraud AL, Takanishi CL, Shen B, et al. Accumulation of free ADP-ribose from mitochondria mediates oxidative stress-induced gating of TRPM2 cation channels. *Journal of Biological Chemistry.* 2005;280(7):6138-6148.

160. Buelow B, Song Y, Scharenberg AM. The Poly(ADP-ribose) polymerase PARP-1 is required for oxidative stress-induced TRPM2 activation in lymphocytes. *Journal of Biological Chemistry.* 2008;283(36):24571-24583.

161. Gerace E, Masi A, Resta F, et al. PARP-1 activation causes neuronal death in the hippocampal CA1 region by increasing the expression of Ca(2+)-permeable AMPA receptors. *Neurobiology of Disease.* 2014;70:43-52.

162. Herson PS, Ashford ML. Activation of a novel non-selective cation channel by alloxan and H2O2 in the rat insulin-secreting cell line CRI-G1. *Journal of Physiology.* 1997;501 (Pt 1):59-66.

163. Tong Q, Zhang W, Conrad K, et al. Regulation of the transient receptor potential channel TRPM2 by the Ca2+ sensor calmodulin. *Journal of Biological Chemistry.* 2006;281(14):9076-9085.

164. McHugh D, Flemming R, Xu SZ, Perraud AL, Beech DJ. Critical intracellular Ca2+ dependence of transient receptor potential melastatin 2 (TRPM2) cation channel activation. *Journal of Biological Chemistry.* 2003;278(13):11002-11006.

165. Roberge S, Roussel J, Andersson DC, et al. TNF-alpha-mediated caspase-8 activation induces ROS production and TRPM2 activation in adult ventricular myocytes. *Cardiovascular Research.* 2014;103(1):90-99.

166. Ishii M, Oyama A, Hagiwara T, et al. Facilitation of H2O2-induced A172 human glioblastoma cell death by insertion of oxidative stress-sensitive TRPM2 channels. *Anticancer Research.* 2007;27(6b):3987-3992.

167. Fonfria E, Marshall IC, Benham CD, et al. TRPM2 channel opening in response to oxidative stress is dependent on activation of poly(ADP-ribose) polymerase. *British Journal of Pharmacology.* 2004;143(1):186-192.

168. Yang KT, Chang WL, Yang PC, et al. Activation of the transient receptor potential M2 channel and poly(ADP-ribose) polymerase is involved in oxidative stress-induced cardiomyocyte death. *Cell Death and Differentiation.* 2006;13(10):1815-1826.

169. Blenn C, Wyrsch P, Bader J, Bollhalder M, Althaus FR. Poly(ADP-ribose)glycohydrolase is an upstream regulator of Ca2+ fluxes in oxidative cell death. *Cellular and Molecular Life Sciences.* 2011;68(8):1455-1466.

170. Buelow B, Uzunparmak B, Paddock M, Scharenberg AM. Structure/function analysis of PARP-1 in oxidative and nitrosative stress-induced monomeric ADPR formation. *PloS One.* 2009;4(7):e6339.

171. Bentle MS, Reinicke KE, Bey EA, Spitz DR, Boothman DA. Calcium-dependent modulation of poly(ADP-ribose) polymerase-1 alters cellular metabolism and DNA repair. *Journal of Biological Chemistry.* 2006;281(44):33684-33696.

172. Malanga M, Althaus FR. Poly(ADP-ribose) molecules formed during DNA repair in vivo. *Journal of Biological Chemistry.* 1994;269(26):17691-17696.

173. Yu SW, Andrabi SA, Wang H, et al. Apoptosis-inducing factor mediates poly(ADP-ribose) (PAR) polymer-induced cell death. *Proceedings of the National Academy of Sciences.* 2006;103(48):18314-18319.

174. Fujihara H, Ogino H, Maeda D, et al. Poly(ADP-ribose) Glycohydrolase deficiency sensitizes mouse ES cells to DNA damaging agents. *Current Cancer Drug Targets.* 2009;9(8):953-962.

175. Illuzzi G, Fouquerel E, Ame JC, et al. PARG is dispensable for recovery from transient replicative stress but required to prevent detrimental accumulation of poly(ADP-ribose) upon prolonged replicative stress. *Nucleic Acids Research.* 2014;42(12):7776-7792.

176. Hatakeyama K, Nemoto Y, Ueda K, Hayaishi O. Purification and characterization of poly(ADP-ribose) glycohydrolase. Different modes of action on large and small poly(ADP-ribose). *Journal of Biological Chemistry.* 1986;261(32):14902-14911.

177. Geistrikh I, Visochek L, Klein R, et al. Ca2+-induced PARP-1 activation and ANF expression are coupled events in cardiomyocytes. *Biochemical Journal.* 2011;438(2):337-347.

178. Niere M, Kernstock S, Koch-Nolte F, Ziegler M. Functional localization of two poly(ADP-ribose)-degrading enzymes to the mitochondrial matrix. *Molecular and Cellular Biology.* 2008;28(2):814-824.

179. Abramov AY, Duchen MR. Mechanisms underlying the loss of mitochondrial membrane potential in glutamate excitotoxicity. *Biochimica et Biophysica Acta.* 2008;1777(7-8):953-964.

180. Baines CP, Kaiser RA, Purcell NH, et al. Loss of cyclophilin D reveals a critical role for mitochondrial permeability transition in cell death. *Nature.* 2005;434(7033):658-662.

181. Yang JC, Cortopassi GA. Induction of the mitochondrial permeability transition causes release of the apoptogenic factor cytochrome c. *Free Radical Biology and Medicine.* 1998;24(4):624-631.

182. Susin SA, Lorenzo HK, Zamzami N, et al. Molecular characterization of mitochondrial apoptosis-inducing factor. *Nature.* 1999;397(6718):441-446.

183. Cao G, Clark RS, Pei W, et al. Translocation of apoptosis-inducing factor in vulnerable neurons after transient cerebral ischemia and in neuronal cultures after oxygen-glucose deprivation. *Journal of Cerebral Blood Flow and Metabolism.* 2003;23(10):1137-1150.

184. Zhang X, Chen J, Graham SH, et al. Intranuclear localization of apoptosis-inducing factor (AIF) and large scale DNA fragmentation after traumatic brain injury in rats and in neuronal cultures exposed to peroxynitrite. *Journal of Neurochemistry.* 2002;82(1):181-191.

185. Klein JA, Longo-Guess CM, Rossmann MP, et al. The harlequin mouse mutation downregulates apoptosis-inducing factor. *Nature.* 2002;419(6905):367-374.

186. Gagne JP, Isabelle M, Lo KS, et al. Proteome-wide identification of poly(ADP-ribose) binding proteins and poly(ADP-ribose)-associated protein complexes. *Nucleic Acids Research.* 2008;36(22):6959-6976.

187. Andrabi SA, Kim NS, Yu SW, et al. Poly(ADP-ribose) (PAR) polymer is a death signal. *Proceedings of the National Academy of Sciences.* 2006;103(48):18308-18313.

188. Cipriani G, Rapizzi E, Vannacci A, Rizzuto R, Moroni F, Chiarugi A. Nuclear poly(ADP-ribose) polymerase-1 rapidly triggers mitochondrial dysfunction. *Journal of Biological Chemistry.* 2005;280(17):17227-17234.

189. Artus C, Boujrad H, Bouharrour A, et al. AIF promotes chromatinolysis and caspase-independent programmed necrosis by interacting with histone H2AX. *EMBO Journal.* 2010;29(9):1585-1599.

190. Elrod JW, Wong R, Mishra S, et al. Cyclophilin D controls mitochondrial pore-dependent Ca(2+) exchange, metabolic flexibility, and propensity for heart failure in mice. *Journal of Clinical Investigation.* 2010;120(10):3680-3687.

191. Zhu C, Wang X, Deinum J, et al. Cyclophilin A participates in the nuclear translocation of apoptosis-inducing factor in neurons after cerebral hypoxia-ischemia. *Journal of Experimental Medicine.* 2007;204(8):1741-1748.

192. Griffiths EJ, Halestrap AP. Mitochondrial non-specific pores remain closed during cardiac ischaemia, but open upon reperfusion. *Biochemical Journal.* 1995;307 (Pt 1):93-98.

193. Yu SW, Wang Y, Frydenlund DS, Ottersen OP, Dawson VL, Dawson TM. Outer mitochondrial membrane localization of apoptosis-inducing factor: mechanistic implications for release. *American Society for Neurochemistry: Neuro.* 2009;1(5).

194. Bollman JL, Flock EV. Pyruvate in working muscles of normal and vitamin B1-deficient rats. *Journal of Biological Chemistry.* 1939;130(2):565-571.

195. Frohman CE, Day HG. Effect of oxythiamine on blood pyruvate-lactate relationships and the excretion of thiamine in rats. *Journal of Biological Chemistry.* 1949;180(1):93-98.

196. Lu G. Studies on the metabolism of pyruvic acid in normal and vitamin B1-deficient states: Blood pyruvate levels in the rat, pigeon, rabbit and man. III. The relation of blood pyruvate to cardiac changes. *Biochemical Journal.* 1939;33(5):774.

197. Babich H, Liebling EJ, Burger RF, Zuckerbraun HL, Schuck AG. Choice of DMEM, formulated with or without pyruvate, plays an important role in assessing the in vitro cytotoxicity of oxidants and prooxidant nutraceuticals. *In Vitro Cellular and Developmental Biology: Animal.* 2009;45(5-6):226-233.

198. Vahsen N, Cande C, Briere JJ, et al. AIF deficiency compromises oxidative phosphorylation. *EMBO Journal.* 2004;23(23):4679-4689.

199. Villeneuve L, Tiede LM, Morsey B, Fox HS. Quantitative proteomics reveals oxygen-dependent changes in neuronal mitochondria affecting function and sensitivity to rotenone. *Journal of Proteome Research.* 2013;12(10):4599-4606.

200. Ali SS, Hsiao M, Zhao HW, Dugan LL, Haddad GG, Zhou D. Hypoxia-adaptation involves mitochondrial metabolic depression and decreased ROS leakage. *PloS One.* 2012;7(5):e36801.

201. Moubarak RS, Yuste VJ, Artus C, et al. Sequential activation of poly(ADP-ribose) polymerase 1, calpains, and Bax is essential in apoptosis-inducing factor-mediated programmed necrosis. *Molecular and Cellular Biology.* 2007;27(13):4844-4862.

202. Daugas E, Susin SA, Zamzami N, et al. Mitochondrio-nuclear translocation of AIF in apoptosis and necrosis. *FASEB Journal.* 2000;14(5):729-739.

203. Kimes BW, Brandt BL. Properties of a clonal muscle cell line from rat heart. *Experimental Cell Research.* 1976;98(2):367-381.

204. Cselenyak A, Pankotai E, Horvath EM, Kiss L, Lacza Z. Mesenchymal stem cells rescue cardiomyoblasts from cell death in an in vitro ischemia model via direct cell-to-cell connections. *BMC Cell Biology.* 2010;11:29.

205. Chen PA, Xu ZH, Huang YL, et al. Increased serum 2-oxoglutarate associated with high myocardial energy expenditure and poor prognosis in chronic heart failure patients. *Biochimica et Biophysica Acta.* 2014;1842(11):2120-2125.

206. Mosmann T. Rapid colorimetric assay for cellular growth and survival: application to proliferation and cytotoxicity assays. *Journal of Immunological Methods.* 1983;65(1-2):55-63.

207. Stepanenko AA, Dmitrenko VV. Pitfalls of the MTT assay: Direct and off-target effects of inhibitors can result in over/underestimation of cell viability. *Gene.* 2015;574(2):193-203.

208. Bradford MM. A rapid and sensitive method for the quantitation of microgram quantities of protein utilizing the principle of protein-dye binding. *Analytical Biochemistry.* 1976;72:248-254.

209. Smiley ST, Reers M, Mottola-Hartshorn C, et al. Intracellular heterogeneity in mitochondrial membrane potentials revealed by a J-aggregate-forming lipophilic cation JC-1. *Proceedings of the National Academy of Sciences.* 1991;88(9):3671-3675.

210. Salvioli S, Ardizzoni A, Franceschi C, Cossarizza A. JC-1, but not DiOC6(3) or rhodamine 123, is a reliable fluorescent probe to assess delta psi changes in intact cells: implications for studies on mitochondrial functionality during apoptosis. *FEBS Letters.* 1997;411(1):77-82.

211. Owen CS. Phorbol ester (12-O-tetradecanoylphorbol 13-acetate) partially inhibits rapid intracellular free calcium transients triggered by anti-immunoglobulin in murine lymphocytes. *Journal of Biological Chemistry.* 1988;263(6):2732-2737.

212. Roychowdhury S, Noack J, Engelmann M, Wolf G, Horn TF. AMPA receptor-induced intracellular calcium response in the paraventricular nucleus is modulated by nitric oxide: calcium imaging in a hypothalamic organotypic cell culture model. *Nitric Oxide.* 2006;14(4):290-299.

213. Justel A, Peña D, Zamar R. A multivariate Kolmogorov-Smirnov test of goodness of fit. *Statistics & Probability Letters.* 1997;35(3):251-259.

214. Peat JKa, Barton Ba. *Medical statistics : A guide to SPSS, data analysis, and critical appraisal.* Second edition. ed. Chichester, West Sussex ; Hoboken, NJ: John Wiley & Sons Inc; 2014.

215. Ritz C, Baty F, Streibig JC, Gerhard D. Dose-Response Analysis Using R. *PloS One.* 2015;10(12):e0146021.

216. International Conference on Harmonisation Expert Working Group. Guidance for Industry: Q2B Validation of Analytical Procedures: Methodology. In: Harmonisation ICo, ed. Brussels, Belgium: International Conference on Harmonisation; 1996.

217. Berridge MV, Herst PM, Tan AS. Tetrazolium dyes as tools in cell biology: new insights into their cellular reduction. *Biotechnology Annual Review.* 2005;11:127-152.

218. Vistica DT, Skehan P, Scudiero D, Monks A, Pittman A, Boyd MR. Tetrazolium-based assays for cellular viability: a critical examination of selected parameters affecting formazan production. *Cancer Research.* 1991;51(10):2515-2520.

219. Moghe A, Ghare S, Lamoreau B, et al. Molecular mechanisms of acrolein toxicity: relevance to human disease. *Toxicological Sciences.* 2015;143(2):242-255.

220. Liu Q, Huang QX, Lou FC, et al. Effects of glucose and insulin on the H9c2 (2-1) cell proliferation may be mediated through regulating glucose transporter 4 expression. *Chinese Medical Journal.* 2013a;126(21):4037-4042.

221. Lin RY, Vera JC, Chaganti RS, Golde DW. Human monocarboxylate transporter 2 (MCT2) is a high affinity pyruvate transporter. *Journal of Biological Chemistry.* 1998;273(44):28959-28965.

222. Bonen A. The expression of lactate transporters (MCT1 and MCT4) in heart and muscle. *European Journal of Applied Physiology.* 2001;86(1):6-11.

223. Bode BP. Recent molecular advances in mammalian glutamine transport. *Journal of Nutrition.* 2001;131(9 Suppl):2475S-2485S; discussion 2486S-2477S.

224. Sugawara M, Nakanishi T, Fei YJ, et al. Cloning of an amino acid transporter with functional characteristics and tissue expression pattern identical to that of system A. *Journal of Biological Chemistry.* 2000;275(22):16473-16477.

225. Kugler P. Expression of glutamate transporters in rat cardiomyocytes and their localization in the T-tubular system. *Journal of Histochemistry and Cytochemistry.* 2004;52(10):1385-1392.

226. Takeda K, Ishida A, Takahashi K, Ueda T. Synaptic vesicles are capable of synthesizing the VGLUT substrate glutamate from α-ketoglutarate for vesicular loading. *Journal of Neurochemistry.* 2012;121(2):184-196.

227. Shank RP, Bennett DJ. 2-Oxoglutarate transport: a potential mechanism for regulating glutamate and tricarboxylic acid cycle intermediates in neurons. *Neurochemical Research.* 1993;18(4):401-410.

228. Pajor AM, Gangula R, Yao X. Cloning and functional characterization of a high-affinity Na(+)/dicarboxylate cotransporter from mouse brain. *American Journal of Physiology: Cell Physiology*. 2001;280(5):C1215-1223.

229. Stevens JF, Maier CS. Acrolein: sources, metabolism, and biomolecular interactions relevant to human health and disease. *Molecular Nutrition & Food Research*. 2008;52(1):7-25.

230. Agarwal AR, Yin F, Cadenas E. Metabolic shift in lung alveolar cell mitochondria following acrolein exposure. *American Journal of Physiology: Lung Cellular and Molecular Physiology*. 2013;305(10):L764-773.

231. Reddy NM, Kleeberger SR, Yamamoto M, et al. Genetic dissection of the Nrf2-dependent redox signaling-regulated transcriptional programs of cell proliferation and cytoprotection. *Physiological Genomics*. 2007;32(1):74-81.

232. Osburn WO, Wakabayashi N, Misra V, et al. Nrf2 regulates an adaptive response protecting against oxidative damage following diquat-mediated formation of superoxide anion. *Archives of Biochemistry and Biophysics*. 2006;454(1):7-15.

233. Nguyen T, Nioi P, Pickett CB. The Nrf2-antioxidant response element signaling pathway and its activation by oxidative stress. *Journal of Biological Chemistry*. 2009;284(20):13291-13295.

234. Enomoto A, Itoh K, Nagayoshi E, et al. High sensitivity of Nrf2 knockout mice to acetaminophen hepatotoxicity associated with decreased expression of ARE-regulated drug metabolizing enzymes and antioxidant genes. *Toxicological Sciences*. 2001;59(1):169-177.

235. Tirumalai R, Rajesh Kumar T, Mai KH, Biswal S. Acrolein causes transcriptional induction of phase II genes by activation of Nrf2 in human lung type II epithelial (A549) cells. *Toxicology Letters*. 2002;132(1):27-36.

236. Ishii T, Itoh K, Takahashi S, et al. Transcription factor Nrf2 coordinately regulates a group of oxidative stress-inducible genes in macrophages. *Journal of Biological Chemistry*. 2000;275(21):16023-16029.

237. Goldring CE, Kitteringham NR, Elsby R, et al. Activation of hepatic Nrf2 in vivo by acetaminophen in CD-1 mice. *Hepatology*. 2004;39(5):1267-1276.

238. Randle LE, Goldring CE, Benson CA, et al. Investigation of the effect of a panel of model hepatotoxins on the Nrf2-Keap1 defence response pathway in CD-1 mice. *Toxicology*. 2008;243(3):249-260.

239. Li K, Cui YC, Zhang H, et al. Glutamine Reduces the Apoptosis of H9C2 Cells Treated with High-Glucose and Reperfusion through an Oxidation-Related Mechanism. *PloS One*. 2015;10(7):e0132402.

240. Wang X, Perez E, Liu R, Yan LJ, Mallet RT, Yang SH. Pyruvate protects mitochondria from oxidative stress in human neuroblastoma SK-N-SH cells. *Brain Research*. 2007;1132(1):1-9.

241. Fernandez-Gomez FJ, Pastor MD, Garcia-Martinez EM, et al. Pyruvate protects cerebellar granular cells from 6-hydroxydopamine-induced cytotoxicity by activating the Akt signaling pathway and increasing glutathione peroxidase expression. *Neurobiology of Disease*. 2006;24(2):296-307.

242. Hamann K, Shi R. Acrolein scavenging: a potential novel mechanism of attenuating oxidative stress following spinal cord injury. *Journal of Neurochemistry.* 2009;111(6):1348-1356.

243. Monteil C, Le Prieur E, Buisson S, Morin JP, Guerbet M, Jouany JM. Acrolein toxicity: comparative in vitro study with lung slices and pneumocytes type II cell line from rats. *Toxicology.* 1999;133(2-3):129-138.

244. Garcia NA, Moncayo-Arlandi J, Sepulveda P, Diez-Juan A. Cardiomyocyte exosomes regulate glycolytic flux in endothelium by direct transfer of GLUT transporters and glycolytic enzymes. *Cardiovascular Research.* 2016;109(3):397-408.

245. Malhotra R, Tyson DW, Rosevear HM, Brosius FC, 3rd. Hypoxia-inducible factor-1alpha is a critical mediator of hypoxia induced apoptosis in cardiac H9c2 and kidney epithelial HK-2 cells. *BMC Cardiovascular Disorders.* 2008;8:9.

246. Semenza GL. Hypoxia-inducible factor 1 and cardiovascular disease. *Annual Review of Physiology.* 2014;76:39-56.

247. Lovell MA, Xie C, Markesbery WR. Acrolein, a product of lipid peroxidation, inhibits glucose and glutamate uptake in primary neuronal cultures. *Free Radical Biology & Medicine.* 2000;29(8):714-720.

248. Abraham P, Rabi S. Protein nitration, PARP activation and NAD+ depletion may play a critical role in the pathogenesis of cyclophosphamide-induced hemorrhagic cystitis in the rat. *Cancer Chemotherapy and Pharmacology.* 2009;64(2):279-285.

249. Andrabi SA, Umanah GK, Chang C, et al. Poly(ADP-ribose) polymerase-dependent energy depletion occurs through inhibition of glycolysis. *Proceedings of the National Academy of Sciences.* 2014;111(28):10209-10214.

250. Martyniuk CJ, Fang B, Koomen JM, et al. Molecular mechanism of glyceraldehyde-3-phosphate dehydrogenase inactivation by alpha,beta-unsaturated carbonyl derivatives. *Chemical Research in Toxicology.* 2011;24(12):2302-2311.

251. Wischmeyer PE, Vanden Hoek TL, Li C, et al. Glutamine preserves cardiomyocyte viability and enhances recovery of contractile function after ischemia-reperfusion injury. *Journal of Parenteral & Enteral Nutrition.* 2003;27(2):116-122.

252. Liu J, Marchase RB, Chatham JC. Glutamine-induced protection of isolated rat heart from ischemia/reperfusion injury is mediated via the hexosamine biosynthesis pathway and increased protein O-GlcNAc levels. *Journal of Molecular and Cellular Cardiology.* 2007;42(1):177-185.

253. David KK, Andrabi SA, Dawson TM, Dawson VL. Parthanatos, a messenger of death. *Front Biosci (Landmark Ed).* 2009;14:1116-1128.

254. Fernet M, Ponette V, Deniaud-Alexandre E, et al. Poly(ADP-ribose) polymerase, a major determinant of early cell response to ionizing radiation. *International Journal of Radiation Biology.* 2000;76(12):1621-1629.

255. Cristovao L, Rueff J. Effect of a poly(ADP-ribose) polymerase inhibitor on DNA breakage and cytotoxicity induced by hydrogen peroxide and gamma-radiation. *Teratogenesis, Carcinogenesis, and Mutagenesis.* 1996;16(4):219-227.

256. Wang X, Ohnishi K, Takahashi A, Ohnishi T. Poly(ADP-ribosyl)ation is required for p53-dependent signal transduction induced by radiation. *Oncogene.* 1998;17(22):2819-2825.

257. Weinfeld M, Chaudhry MA, D'Amours D, et al. Interaction of DNA-dependent protein kinase and poly(ADP-ribose) polymerase with radiation-induced DNA strand breaks. *Radiation Research.* 1997;148(1):22-28.

258. Zhang S, Lin Y, Kim YS, Hande MP, Liu ZG, Shen HM. c-Jun N-terminal kinase mediates hydrogen peroxide-induced cell death via sustained poly(ADP-ribose) polymerase-1 activation. *Cell Death and Differentiation.* 2007;14(5):1001-1010.

259. Chiu LY, Ho FM, Shiah SG, Chang Y, Lin WW. Oxidative stress initiates DNA damager MNNG-induced poly(ADP-ribose)polymerase-1-dependent parthanatos cell death. *Biochemical Pharmacology.* 2011;81(3):459-470.

260. Lonskaya I, Potaman VN, Shlyakhtenko LS, Oussatcheva EA, Lyubchenko YL, Soldatenkov VA. Regulation of poly(ADP-ribose) polymerase-1 by DNA structure-specific binding. *Journal of Biological Chemistry.* 2005;280(17):17076-17083.

261. Langelier MF, Planck JL, Roy S, Pascal JM. Structural basis for DNA damage-dependent poly(ADP-ribosyl)ation by human PARP-1. *Science.* 2012;336(6082):728-732.

262. Hughes FM, Jr., Corn AG, Nimmich AR, Pratt-Thomas JD, Purves JT. Cyclophosphamide Induces an Early Wave of Acrolein-Independent Apoptosis in the Urothelium. *Advances in Bioscience and Biotechnology.* 2013;4(88).

263. Tanel A, Averill-Bates DA. Activation of the death receptor pathway of apoptosis by the aldehyde acrolein. *Free Radical Biology and Medicine.* 2007;42(6):798-810.

264. Boone CW, Mantel N, Caruso TD, Jr., Kazam E, Stevenson RE. Quality control studies on fetal bovine serum used in tissue culture. *In Vitro.* 1971;7(3):174-189.

265. Price PJ, Gregory EA. Relationship between in vitro growth promotion and biophysical and biochemical properties of the serum supplement. *In Vitro.* 1982;18(6):576-584.

266. Jia L, Liu Z, Sun L, et al. Acrolein, a toxicant in cigarette smoke, causes oxidative damage and mitochondrial dysfunction in RPE cells: protection by (R)-alpha-lipoic acid. *Investigative Ophthalmology and Visual Science.* 2007;48(1):339-348.

267. Petit PX, Goubern M, Diolez P, Susin SA, Zamzami N, Kroemer G. Disruption of the outer mitochondrial membrane as a result of large amplitude swelling: the impact of irreversible permeability transition. *FEBS Letters.* 1998;426(1):111-116.

268. Olah ME, Jackson MF, Li H, et al. Ca2+-dependent induction of TRPM2 currents in hippocampal neurons. *Journal of Physiology.* 2009;587(Pt 5):965-979.

269. Cozzi A, Cipriani G, Fossati S, et al. Poly(ADP-ribose) accumulation and enhancement of postischemic brain damage in 110-kDa poly(ADP-ribose) glycohydrolase null mice. *Journal of Cerebral Blood Flow and Metabolism.* 2006;26(5):684-695.

270. Bonicalzi ME, Vodenicharov M, Coulombe M, Gagne JP, Poirier GG. Alteration of poly(ADP-ribose) glycohydrolase nucleocytoplasmic shuttling characteristics upon cleavage by apoptotic proteases. *Biologie Cellulaire.* 2003;95(9):635-644.

271. Di Virgilio F, Steinberg TH, Silverstein SC. Inhibition of Fura-2 sequestration and secretion with organic anion transport blockers. *Cell Calcium.* 1990;11(2-3):57-62.

272. McClenaghan C, Zeng F, Verkuyl JM. TRPA1 agonist activity of probenecid desensitizes channel responses: consequences for screening. *Assay Drug Development Technologies.* 2012;10(6):533-541.

273. Bang S, Kim KY, Yoo S, Lee SH, Hwang SW. Transient receptor potential V2 expressed in sensory neurons is activated by probenecid. *Neuroscience Letters.* 2007;425(2):120-125.

274. Koch SE, Gao X, Haar L, et al. Probenecid: novel use as a non-injurious positive inotrope acting via cardiac TRPV2 stimulation. *Journal of Molecular and Cellular Cardiology.* 2012;53(1):134-144.

275. Entin-Meer M, Levy R, Goryainov P, et al. The transient receptor potential vanilloid 2 cation channel is abundant in macrophages accumulating at the peri-infarct zone and may enhance their migration capacity towards injured cardiomyocytes following myocardial infarction. *PloS One.* 2014;9(8):e105055.

276. Sun Z, Han J, Zhao W, et al. TRPV1 activation exacerbates hypoxia/reoxygenation-induced apoptosis in H9C2 cells via calcium overload and mitochondrial dysfunction. *International Journal of Molecular Sciences.* 2014;15(10):18362-18380.

277. Wu Z, He EY, Scott GI, Ren J. alpha,beta-Unsaturated aldehyde pollutant acrolein suppresses cardiomyocyte contractile function: Role of TRPV1 and oxidative stress. *Environmental Toxicology.* 2015;30(6):638-647.

278. Wieckowski MR, Szabadkai G, Wasilewski M, Pinton P, Duszynski J, Rizzuto R. Overexpression of adenine nucleotide translocase reduces Ca2+ signal transmission between the ER and mitochondria. *Biochemical and Biophysical Research Communications.* 2006;348(2):393-399.

279. Lax A, Soler F, Fernandez-Belda F. Intracellular ca(2+) pools and fluxes in cardiac muscle-derived h9c2 cells. *Journal of Bioenergetics and Biomembranes.* 2005;37(4):249-259.

280. Freshney IR. Serum-Free Medium. *Culture of Animal Cells: A Manual of Basic Technique and Specialized Applications*. 6th ed. Hoboken, NJ: John Wiley & Sons, Inc.; 2010.

281. Gelderblom M, Melzer N, Schattling B, et al. Transient receptor potential melastatin subfamily member 2 cation channel regulates detrimental immune cell invasion in ischemic stroke. *Stroke.* 2014;45(11):3395-3402.

282. Zhan KY, Yu PL, Liu CH, Luo JH, Yang W. Detrimental or beneficial: the role of TRPM2 in ischemia/reperfusion injury. *Acta Pharmacologica Sinica.* 2016;37(1):4-12.

283. Purnell MR, Whish WJ. Novel inhibitors of poly(ADP-ribose) synthetase. *Biochemical Journal.* 1980;185(3):775-777.

284. Motulsky HJ, Christopoulos A. *Fitting models to biological data using linear and nonlinear regression. A practical guide to curve fitting.* San Diego, CA: GraphPad Software Inc.; 2003.

APPENDICES

Appendix 1: Theory

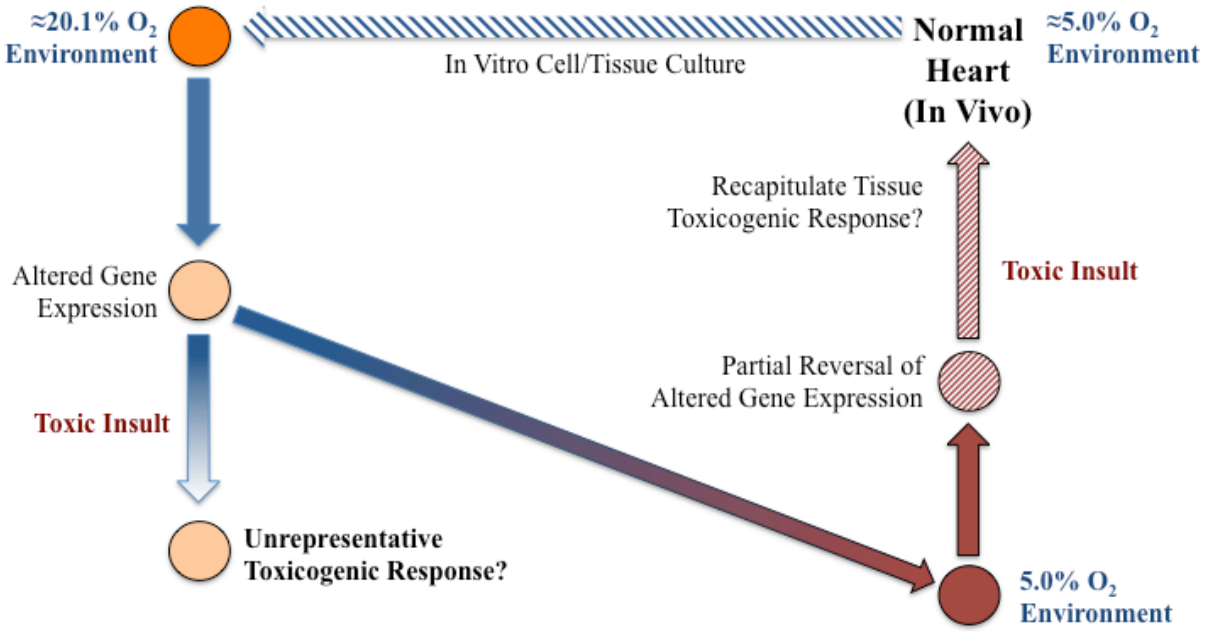

Figure A1. Diagram of Problem Statement and Theoretical Framework. Removal of cardiac cells from an *in vivo* system into an *in vitro* system with altered oxygen tension likely alters gene expression and underlying metabolic and respiratory machinery. When *in vitro* cytotoxicity studies are conducted, the distance of gene expression alteration remains unknown, and has an ill-defined modulation on *in vitro* toxicogenic response. Plausibly, returning cells back to physiologically relevant oxygen tension culture system may reprogram the cells to a phenotype similar to niche protein expression within the *in vivo* system, and, therefore, recapitulate nearer a toxicogenic response observed in *in vivo* cardiac cells.

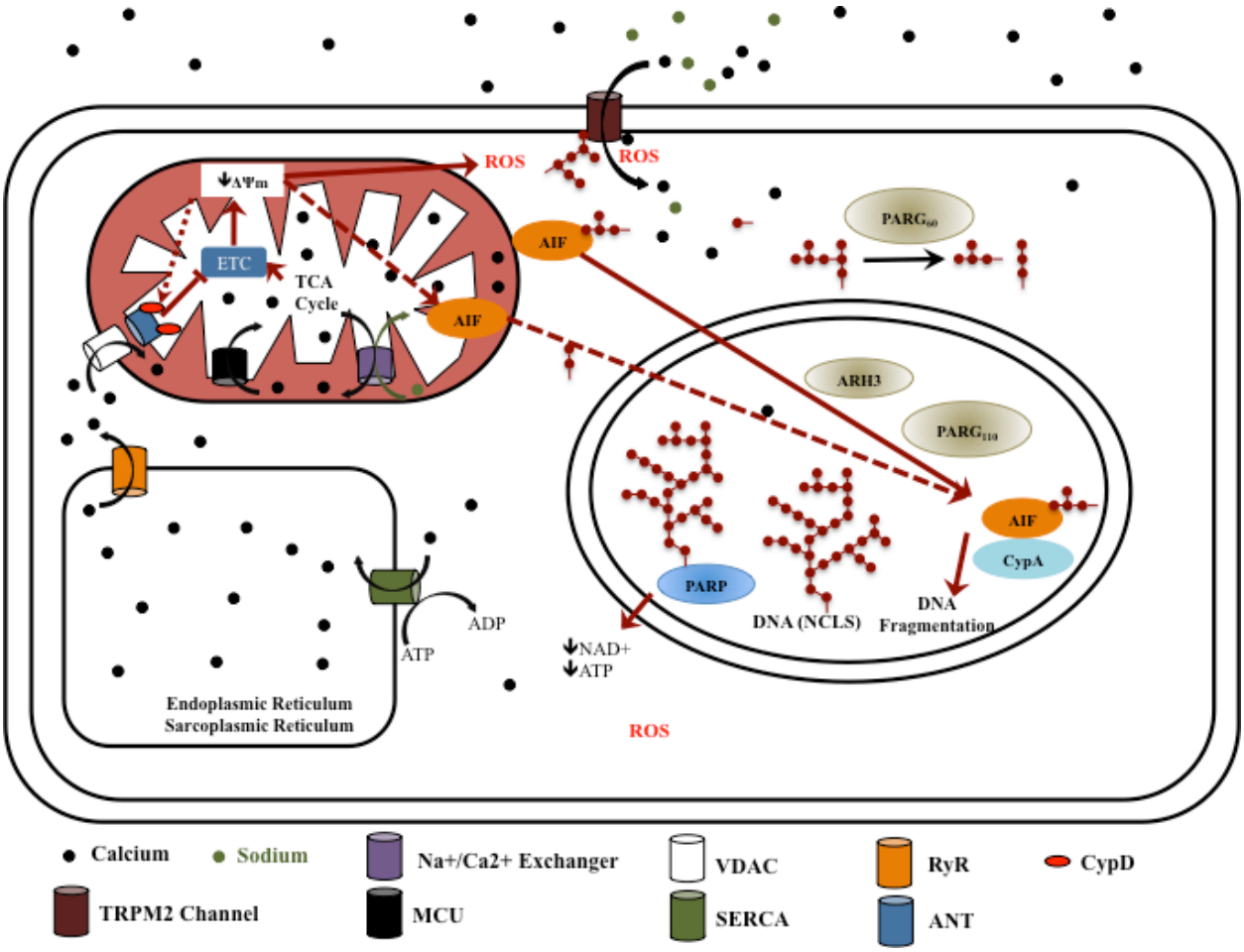

Figure A2. Overview of Parthanatos with Integrated Calcium Conductance Channels. Poly(ADP-ribose) polymerase overactivation from toxic insult results in adenine nucleotide depletion and excess ADP-ribose polymers (Red arbors). As DNA is repaired, PARG, and to a lesser extent ARH3, cleave ADPr polymers, which diffuse to the cytoplasm and, if in excess, can bind outer leaf-associated AIF and TRPM2 channels. AIF then mobilizes to the nucleus and initiates large-scale nuclear fragmentation and cell death (Parthanatos). Simultaneously, ADPr polymers, in conjunction with stress-mediated ROS, activate the TRPM2 channels, allowing conductance of extracellular cations sodium, potassium, and calcium. Calcium, if in high concentration intracellularly, can be shuttled within the intramembranous space of the mitochondria via VDAC channels, and finally within the matrix via MCU channels. Calcium overload within the matrix directly inhibits the ETC, reducing the proton drive necessary for ATP synthesis and mitochondrial membrane potential retention. Reduction in the $\Delta\Psi_m$ causes generation of ROS, which can, in turn, initiate or exacerbate TRPM2 calcium conductance. Similarly, reduction in $\Delta\Psi_m$ is associated with extrusion of intramembranous AIF in association with the mitochondrial membrane pore transition, leading to mitochondrial dysfunction and parthanatos. Abbreviations: adenine diphosphate (ADP); adenine nucleotide translocator (ANT); adenine triphosphate (ATP); ADP-ribosylhydrolase 3 (ARH3); apoptosis-inducing factor (AIF); cyclophilin A (CypA); cyclophilin D (CypD); electron transport chain (ETC); mitochondrial calcium uniporter (MCU); nicotinamide adenine dinucleotide, oxidized (NAD^+); poly(ADP-ribose) glycohydrolase (PARG); poly(ADP-ribose) polymerase (PARP); reactive oxygen species (ROS); sarco/endoplasmic reticulum Ca^{2+}-ATPase (SERCA); sodium/calcium exchanger (Na^+/Ca^{2+} Exchanger); transient receptor potential cation channel, subfamily M, member 2 (TRPM2); voltage-dependent anion channel (VDAC).

Appendix 2: Dulbecco's Modified Eagle's Medium

Table A1: Sigma-Aldrich Product Formulation for SKU: D5030

DMEM Composition (Stock Powder; Sigma-Aldrich Catalog Number: D5030)

Constituent	*Grams/Litre*	*Constituent*	*Grams/Litre*
Inorganic Salts		*Amino Acids*	
$CaCl_2$	0.2	L-Arginine•HCl	0.084
$Fe(NO_3)_3$•$9H_2O$	0.0001	L-Cystine•2HCl	0.0626
$MgSO_4$	0.09767	Glycine	0.03
KCl	0.4	L-Histidine•HCl•H_2O	0.042
NaCl	6.4	L-Isoleucine	0.105
NaH_2PO_4	0.109	L-Leucine	0.105
Vitamins		Lysine•HCl	0.146
Choline Chloride	0.004	Methionine	0.03
Folic Acid	0.004	L-Phenylalanine	0.066
myo-Inositol	0.0072	L-Serine	0.042
Niacinamide	0.004	L-Threonine	0.095
D-Pantothenic Acid•0.5Ca	0.004	L-Tryptophan	0.016
Pyridoxal•HCl	0.004	L-Tyrosine•2Na•$2H_2O$	0.10379
Riboflavin	0.0004	L-Valine	0.094
Thiamine•HCl	0.004		

Note: Composition of commercially available DMEM from powder utilized for experimentation. The powder composite presented formed the basis for which the pre-basal medium was later derived (See Methods). *Note: The information in this table is available free of charge and without disclaimer of credit on the manufacturer's website*.

Appendix 3: Acrylic Exposure Chamber

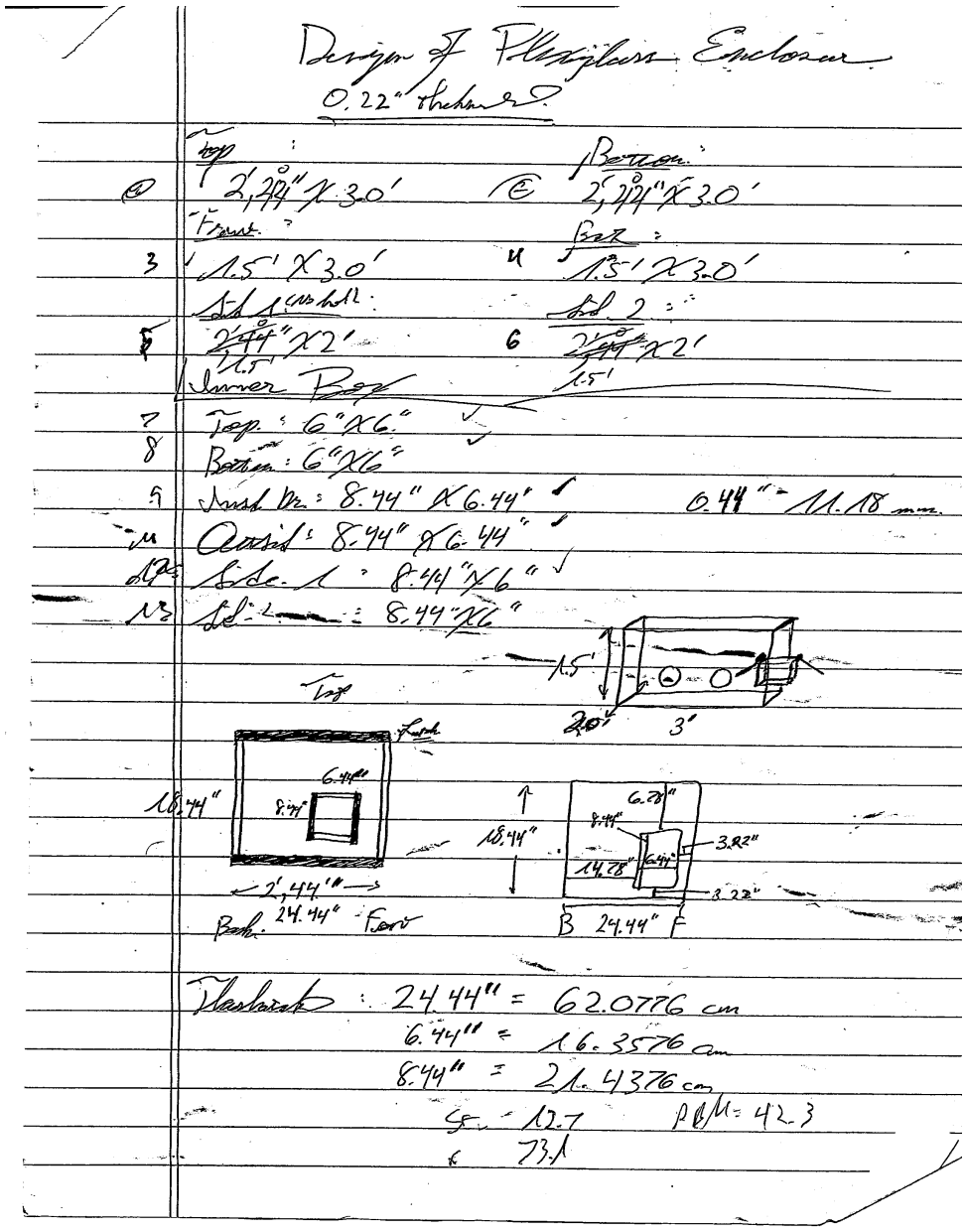

Figure A3. Initial Acrylic Exposure Chamber Construction Plans. The initial proposed dimensions of the acrylic exposure chamber are presented for comparison of final controlled volume calculation. The plans were modified during construction, especially with respect to the ante-chamber to accommodate ergonomic utilization with gloves installed *in situ* after completion.

Figure A4. Completed Exposure Chamber – Oxygen Retention Testing. (**Top**) Upon completion of the acrylic exposure chamber (Top), measurements of internal oxygen concentration were made with respect to time, as presented in *Figure 4* after reducing internal oxygen concentration to 5.4 % mol/mol with pure nitrogen. During testing, a handheld oximeter was utilized to monitor in real-time the oxygen concentration. (**Bottom**) The image shows the placement of the oximeter within the main chamber during measurements taken up to 99.5 hours after initial oxygen concentration reduction. At this time point, the internal oxygen concentration was 8.4 % at approximately 58 hour.

Appendix 4: Validation of the Poly(ADP-ribose) Polymerase Activity Assay

Preliminary validation included an inhibitor study with a compound of known PARP-1 kinetic data – 3-aminobenzamide (3-AB); the published 3-AB K_i value was reported to be 1.8 ± 0.2 μM[283]. Using the optimized detection system developed producing a strong, consistent PARP colorimetric signal, an experiment was conducted in order to experimentally derive the 3-AB K_i parameter for comparison against the aforementioned reported value. Purified PARP enzyme and a commercial source of 3-AB were purchased from Trevigen in order to conduct the experiment. Seven sets of triplicate wells were seeded with 5 IU of purified PARP enzyme per well, wherein each set was co-incubated with graded concentrations of 3-AB spanning seven orders of magnitude (20 nM to 20 mM) during the NAD^B incorporation step. Thereafter, the assay was conducted as per the method described above (See Methods). The results were normalized against the activity observed for the 20 nM 3-AB concentration triplicate set, which was denoted as 100 %. In order to derive the K_i value for the inhibitor experiment results, a three parameter log-logistic model with a fixed lower limit asymptote of 0 % was derived using the R statistical software program facilitated through the "drc" package. In order to include the fitted three-parameter log-logistic function to the observed data, the three parameter estimates produced by the statistical software were re-inserted into the general three-parameter log-logistic equation[284]:

$$f(x) = c + \frac{d - c}{1 + e^{(b(\log(x) - \log(e)))}}$$

Where:

b = Hill's slope coefficient

c = Lower limit asymptote; fixed at 0

d = Upper limit asymptote

e = Curve inflection point

The resultant model parameter derivations are presented in *Table A2*. Using the curve parameters derived, an inhibition curve was produced, wherein the observed PARP activity values were plotted against the base-10 logarithmic 3-AB concentration with the units of molar (M) and presented in *Figure A5*. Based on the model residua, the three-parameter log-logistic model aptly regressed against the observed data.

Table A2. Three-Parameter Log-Logistic Inhibition Curve Estimation

Model Parameters				
Parameter	**Symbol**	**Estimate**	**Estimate Standard Error**	**Note(s)**
Hill's slope coefficient	b	0.086582	0.063154	None
Lower limit asymptote	c	0	N/A	Fixed at Zero
Upper Limit Asymptote	d	100.18	2.0234	None
Point of Curve Inflection	e	0.0021995	0.00021693	None

Derived Parameter Estimate		
K_i Estimate ± SEM ($CI_{95\%}$)	**Theoretical Value**	**Note**
2.2 ± 0.2 μM (1.7-2.7 μM)	1.8 μM (1.6-2.0 μM)	95% Confidence Interval includes 1.8 μM

The concentration required to inhibit 50 % of PARP activity in the optimized detection system was approximated to be 2.2 ± 0.2 μM of 3-AB. Comparison to the theoretical K_i value of 1.8 ± 0.2 μM denoted that the observed estimate was not statistically significant than the theoretical, as the 95 % confidence interval of the point estimate around the derived K_i value includes 1.8 μM (1.7-2.7 μM). Therefore, the evidence suggests that the detection system developed for quantitating PARP activity does not alter the activation kinetics of PARP, and provides a method of measuring the specific activity of PARP, at least in simple sample matrices, i.e., a simple buffer.

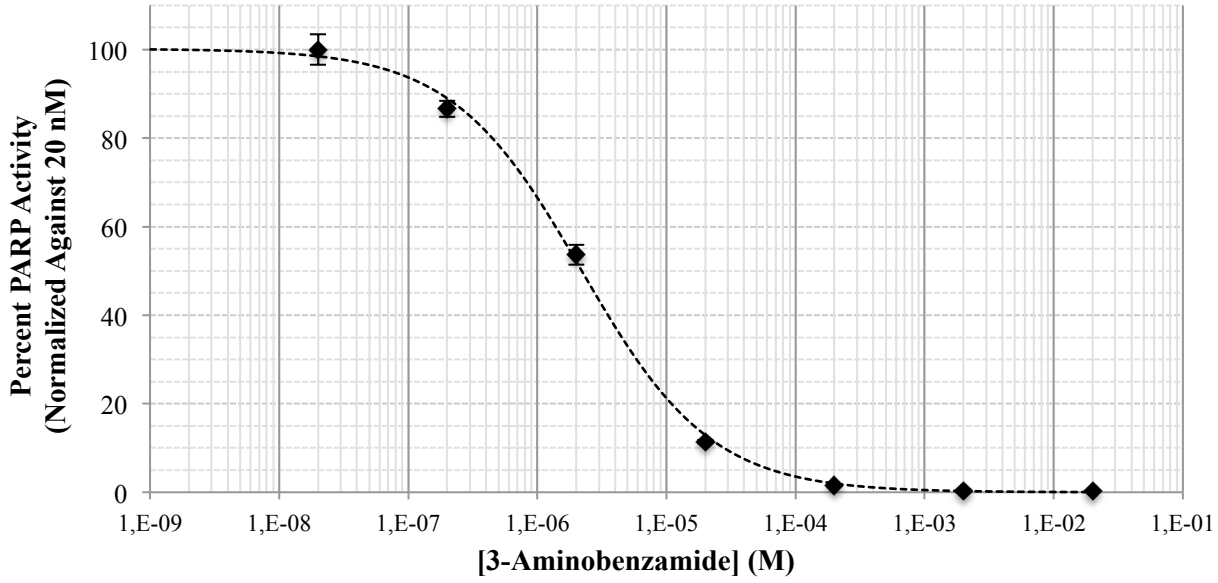

Figure A5. 3-AB K_i Derivation for PARP. Seven sets of triplicate wells containing 5 IU purified PARP were co-incubated with 3-AB at graded concentrations ranging from 20 nM to 20 mM. Over the 3-AB concentration range, a characteristic sigmoidal inhibition curve resulted. Derivation of the K_i estimate and associated 95 % confidence interval resulted in a value of 2.2 µM ($CI_{95\%}$: 1.7-2.7 µM), an interval which includes the value published by Purnell[283]. The regressed log-logistic model was overlain with the observed normalized PARP activity values obtained from experimentation. Each point estimate is the average of three technical replicates. Error bars denote SEM.

In optimizing the assay for use on biological samples, measuring activity of PARP in sample mouse liver was performed (Unpublished data, *Coyle et al*.). Differential fractionation of liver tissue homogenates via centrifugation into the nuclear and cytosolic fractions [Extraction buffer: 50 mM Tris-HCl, pH 8.0, 1.0 % Triton X-100, 400 mM NaCl, 2 mM $MgCl_2$, 100 ng/µL BSA, 1 mM D-*l*-1,4-dithiothreitol] were assayed for PARP activity in lysates containing 10 µg protein per 25 µL (One well volume). Baseline PARP activity in the nuclear and cytosolic fraction were 230 mU/10 µg protein and below the detection limit, respectively; concomitant incubation with 3 mM 3-AB resulted in both nuclear and cytosolic fraction PARP below the detection limit [*Figure A6*]. Therefore, the activity observed in the 3-AB deficient nuclear fraction, which disappeared with incubation with 3-AB, demonstrates successful isolation of

functional PARP enzyme. Moreover, demonstration of nuclear fraction PARP activity with negligible crossover to the cytosolic fraction, denotes attainment of assay specificity in assessing nucleic PARP activity, presuming the nuclear fraction did indeed isolate intact nuclei prior to envelope lysis and PARP stabilization. This is further evident since there were negligible cytosol-associated non-specific signals reported upon assessment via spectrophotometric measurement (Below detection limit).

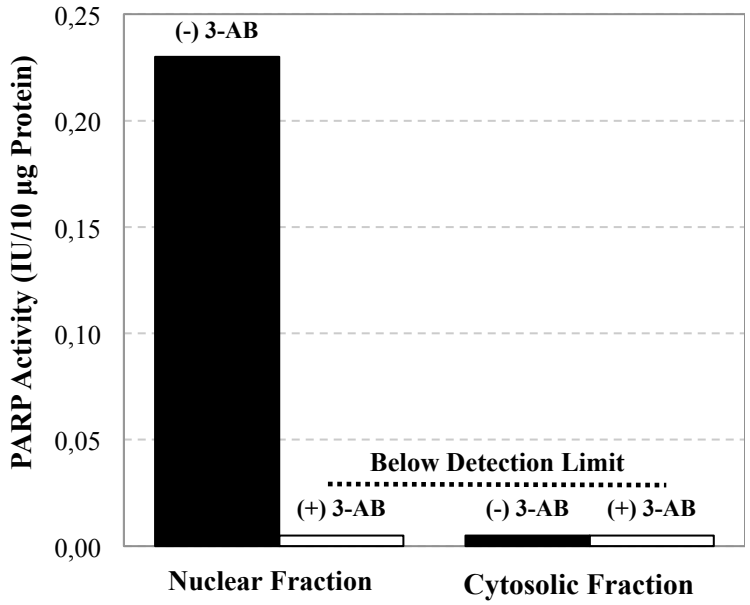

Figure A6. PARP Assay Specificity Verification. PARP activity in mouse liver tissue was determined using the developed assay to assess specificity. Assessment for PARP activity in the nuclear and cytosolic fractions after differential fractionation via centrifugation resulted in detectable PARP activity in the nuclear (Solid Black Bars), but not in the cytosolic (Clear White Bars), fraction in the absence of the PARPi, 3-AB. In the presence of 3 mM 3-AB, PARP activity in the nuclear fraction was reduced to below the detection limit, thus confirming specificity of PARP activity measurement. The bar labeled Below Detection Limit denotes underlying samples were indistinguishable from blank wells, thus unquantifiable.